A DESIGN AND DEVELOPMENT OF IRON ORE FISCHER TROPSCH CATALYST

by

SAMUEL MUBENESHA

A Dissertation submitted to the Department of Civil and Chemical Engineering in accordance with the requirements for the degree of

MASTER OF TECHNOLOGY IN CHEMICAL ENGINEERING

at the

UNIVERSITY OF SOUTH AFRICA

SUPERVISOR: **PROF XINYING LIU**

CO-SUPERVISOR: **DR MOYO MAHLULI**

(March 2020)

DECLARATION

Name: SAMUEL MUBENESHA

Student number: 61498858

Degree: Master of Technology (MTECH): ENGINEERING: CHEMICAL (98989)

A DESIGN AND DEVELOPMENT OF IRON ORE FISCHER TROPSCH CATALYST

I declare that the above dissertation is my own work and that all the sources that I have used or quoted have been indicated and acknowledged by means of complete references. I further declare that I submitted the dissertation to originality checking software and that it falls within the accepted requirements for originality. I further declare that I have not previously submitted this work, or part of it, for examination at Unisa for another qualification or at any other higher education institution.

DATE: 6/03/2020

ABSTRACT

The global community has accepted Fischer Tropsch synthesis as one of the sustainable pathways to transportation fuels and chemicals due to the ever-depleting reserves of fossil fuels and its detrimental impact on the environment. However, the high capital investment and operating expenses associated with this technology have hampered its ability to compete with conventional petrochemicals. Some of the operating costs emanate from the choice of catalyst precursors and operational problems, which could lead to plant shutdowns. In recent times, few efforts have been made to explore cheaper FT catalysts to reduce operational costs, but the mechanical strength of solid FT catalysts, especially for pilot-scale fixed bed operations is not well represented in open literature. As a result, there is a high prevalence of mechanical failure of solid FT catalysts in pilot fixed-bed applications. In this study, we propose a scalable, Fischer Tropsch iron ore catalyst that is mechanically suited for fixed bed reactors to help address this issue.

The catalyst development of the proposed iron ore catalyst involved the slurry phase impregnation of the precursor with copper and potassium and then shaping into spherical pellets with mass additions of 10%, 15% and 20% of bentonite(binder) on a rotating drum. There afterwards, the mechanical strength of each pelletized catalyst was tested using the single pellet crushing testing method (ASTM D 4179). These results were compared to the crushing strength of commercial spherical alumina to ascertain their suitability for fixed bed reactors. The most robust solid catalyst was the 10% binder iron ore pellets which recorded a single pellet crushing strength of 1833 kPa and was more than three times that of commercial spherical alumina and thus deemed apt for fixed bed reactors. A unique statistical approach was used to study the mechanical strength of the various binder combinations due to scattering in single pellet crushing strength data. The analysis revealed that the 10% binder iron ore pellets were most suited for laboratory FT runs and thus was tested for its catalytic performance. The FT runs revealed that the 10% binder iron ore catalyst had a CO conversion of 72.1 % and comparable to other similar iron-based FT catalysts reported in the literature. The proposed catalyst also showed a CH_{5+} selectivity of 83.2%, which was comparable the ones reported by other researchers. These findings provide a simple and cost- effect approach to upscale laboratory-scale FT catalyst designs to pre-emp its performance in pilot or industrial scenarios.

ACKNOWLEDGEMENTS

First and foremost, I would like to thank Jesus Christ for giving the strength to finish this degree. Secondly, my gratitude goes to the director of Institute for the development of sustainability in Africa (IDEAS), Professor Diane Hildebrandt and my supervisors Professor Xinying Liu and Dr Mahluli Moyo for their guidance, inspiration and sound advice throughout my study. It has been a privilege for me to study under their wing. I am also grateful to the staff and post-grad students at IDEAS, for providing a stimulating and fun environment in which to learn and grow. Especially, thanks to Dr Joshua Gorimbo, George Okeye- Chine, Nothando Shiba and Oliver Lenge, for their helpful advice and discussions.

I am incredibly thankful to Miss Rhandzu and the staff of CSIR for facilitating the characterization equipment needed to complete this work and not forgetting Miss Phindile Mbele and Anglo-American value in use staff for giving me the iron ore gratuitous and availing their facility for me to pelletize my catalyst.

I would also like to extend my gratitude to all my family, mainly my mum, dad and siblings, without their support, this work would not have been possible. Special thanks to my sister Marvellous for all her help in editing my grammar and scrutinizing my work

In closing, I would like to thank the National Research Foundation (NRF), the University of South Africa, the Department of Civil and Chemical Engineering, the Institute for the development of African Sustainability (IDEAS), for their financial support and Facilities.

CONFERENCES AND PUBLICATION

Some of the results of this dissertation were presented at various conferences (oral & postal) and are outlined in this section. Moreover, most of this data has also been included in a manuscript which will be submitted in peer reviewed journal.

Conference Presentations

- Mubenesha, S., Liu, X., Yao, Y., Mahluli, M.., D, Hildebrandt. An investigation of an iron ore Fischer Tropsch catalyst. Poster Presentation, Catalysis Society of South Africa (CATSA) annual conference, 18-21 November 2017, Atkwa Maritanebush Lodge, Pilanesburg, South Africa.

- Mubenesha, S., Liu, X., Mahluli, M. A design and development of an iron ore Fischer Tropsch catalyst. Poster Presentation, Catalysis Society of South Africa (CATSA) annual conference, 11-14 November 2018, Legends gold Resort & Spa, Mokopane, Limpopo, South Africa.

- Mubenesha, S., Liu, X., Mahluli, M. A design and development of an iron ore Fischer Tropsch catalyst mechanically suited for Fixed bed reactors. Poster Presentation, Catalysis Society of South Africa (CATSA) annual conference, 10-13 November 2019; Club Mykonos, Langebaan, Western Cape, South Africa.

- Mubenesha, S., Liu, X., Mahluli, M. A design and development of an iron ore Fischer Tropsch catalyst mechanically suited for Fixed Bed reactors. Oral presentation, 2nd International Symposium on Environment and Energy Science & Technology, 18-21 August 2019, Misty Hills, Johannesburg, South Africa.

Manuscript for Publication

Mubenesha, S., Liu, X., Mahluli, M., J, Gorimbo., K, Ramutsindela. Development of a Fischer Tropsch iron ore catalyst mechanically suited for upscale fixed bed reactors. Ready for submission.

TABLE OF CONTENTS

LIST OF FIGURES

LIST OF TABLES

LIST OF ABBREVIATIONS

Afrox	African Oxygen Limited
bbl/day	barrels per day
BET	Brunauer–Emmett–Teller
BTL	Biomass to liquid
CATSA	Catalysis Society of South Africa
CO	Carbon monoxide
CTL	Coal to liquid
Cu	Copper
FBR	Fixed bed reactor
Fe	Iron
FFD	Fixed fluidized bed reactor
FID	Flame ionisation detector
FR	Flow rate
FT	Fischer Tropsch
FTS	Fischer Tropsch synthesis
GC	Gas chromatograph
GHSV	Gas hourly space velocity
GTL	Gas to liquid
H2	Hydrogen
HTFT	High temperature Fischer Tropsch
ID	Internal diameter
K	Potassium
mL/min	Millilitre per minute
mol/min	Mole per minute
N2	Nitrogen
NL	Normal Litres
NTP	Normal temperature and pressure
OD	Outside diameter
Pre	Pressure
Syn	Syngas

TCD	Thermal conductivity detector
TEM	Transmission electron microscopy
TGA	Thermo gravimetric analysis
TOS	Time on stream
TPR	Temperature-programmed reduction
UHP	Ultra-high purity
XRD	X-ray diffraction
XRF	X-ray Fluoresce
TPR	Temperature Programmed Reduction
0(B)	Free binder promoted iron ore catalyst
10(B)	10 % by weight binder addition promoted iron ore catalyst
15(B)	15 % by weight binder addition promoted iron ore catalyst
20(B)	20 % by weight binder addition promoted iron ore catalyst

CHAPTER 1

INTRODUCTION

The rapid ongoing urbanization of the global economy is accelerating the demand for liquid transportation fuels and thereby necessitating the need for technologies to keep up with this trend [1, 2, 3]. Fischer Tropsch synthesis (FTS) has been widely accepted as the cleaner way of producing liquid transportation fuels from various carbonaceous feedstocks compared to the conventional hydrocracking of crude oil. Furthermore, the stringent legislature limiting green gas emissions coupled with the ever-depleting fossil reserves has instigated renewed interest in cleaner technologies such as Fischer Tropsch (FT) [1, 2, 3]. The most common FT catalysts commercially used are cobalt and iron due to their overall excellent catalytic performance validated by various FT practitioners in the literature [5, 10, 13]. However, for pilot-scale scenarios where the cost of catalyst precursor is crucial, iron is preferred over cobalt. It is also better suited for both low and high-temperature Fischer synthesis [7, 8, 11]. Iron-based catalysts are also responsive to the water gas shift reaction, which adjusts hydrogen deficient feedstock such as biomass and makes them an attractive option for BTL applications [4, 8, 11]. Figure 1.1 below depicts the various pathways to transportation fuels and chemicals to highlight the significance of FTS technology as a greener alternative to conventional hydrocracking of crude oil.

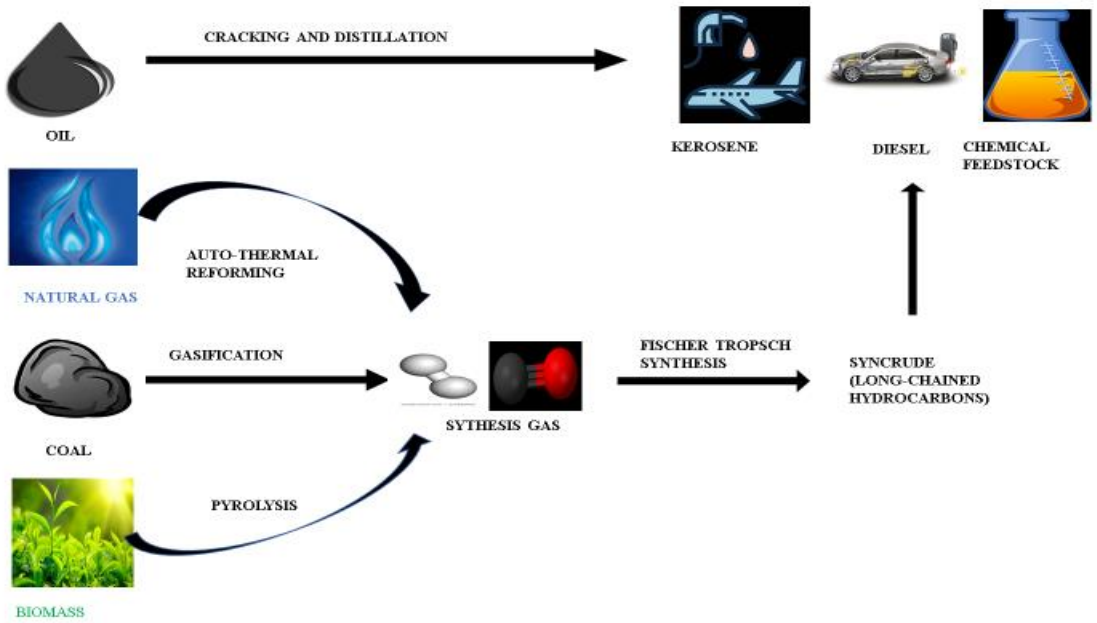

Figure 1. 1: Comparison between conventional and cleaner pathway to liquid transportation fuels [3]

Biomass-to-Liquid (BTL) via FTS is also accepted as one of the promising pathways to produce liquid hydrocarbons, and other chemical feedstocks from syngas derived from non-petroleum as shown in

Figure 1 [4, 5, 7]. BTL is considered as an attractive route to greener hydrocarbons because it yields transportation fuels and chemicals that have lower contents of sulphur, aromatics, and nitrogen in comparison to conventional petroleum derivatives [5, 7, 8]. Despite the merits of BTL mentioned above, the cost to upscale this technology is still very high compared to traditional refineries [20]. The BTL like its other compatriots (Coal-to-liquid, Gas-to-liquid) consists of gasification, gas cleaning and conditioning and Fischer Tropsch Synthesis (FTS) [3, 9]. This work focuses more on the FTS section of this technology and proposes a different approach to catalyst design and development.

The proposed catalyst development approach in this study provides a shorter route to the conventional one because it reduces the use of extra reagents and addition steps during catalyst preparation which is desirable for FT practitioners upscaling laboratory catalyst formulations with a limited budget. Most recently, Bae et al., 2018 proposed a promising iron ore FT catalyst approach alternative to conventional precipitated Fischer Tropsch iron-based with comparable FT activity to other traditional FT catalysts [12]. However, the study only focused on catalyst performance based on its chemistry, and no emphasis was made on the mechanical strength aspect, which is very important in upscaled fixed bed reactors (FBRs). In this project, we propose a more holistic catalyst development approach suited for upscaled FBRs which cover the mechanical strength aspect of solid catalysts for pilot or commercial scenarios.

The mechanical robustness of solid catalysts (pellets) is often not given the same attention than their chemistry gets as cited earlier despite the various contact, thermal, pressure and chemical stresses pellets experience during reactions which affect their overall performance [14, 15]. The mechanical failure of pellets due to weak mechanical strength during large scale fixed bed operations is more often the reason behind the frequent plant shutdowns than the chemistry of solid catalysts [15]. These shutdowns cost FT companies millions of dollars annually, which put a strain on their financial budgets [16]. Just to put things into perspective on average a typical manufacturing plant experiences 800 hours downtime due to plant shutdowns annually [16] and for an FT Plant with a production capacity of 25000 barrels of liquid fuels per day, the average hourly cost of production per barrel is US$4083 [17]. This suggests that this plant loses an average of US$ 3.3 Million in a year due to shutdowns. It is apparent to see that the costs of downtime due to shutdown impacts the economic viability of any plant and FT plants are no exception. This highlights the importance of developing not only mechanically robust catalysts but also reliability of catalyst systems and thus need special attention to ensure a prolonged lifespan of catalysts and minimize shutdowns. One of the operational challenges that arise from mechanical failure of solid catalysts in large-scale fixed reactors is the formation of fines that change its shape and size which instigates an excessive pressure drop, uneven flow of fluid, heat and

mass transfer limitations resulting in low catalyst activity [6, 15]. In Addition to that, the fragmentations of pellets subsequently plug units downstream [15, 18, 19] which stop operations altogether. Pellets that are not physically strong enough to withstand the mechanical stress before, during and after reaction studies makes the handling of the catalyst (during transportation and catalyst loading) and separation of products challenging [6].

This study used spherical pellets due to the availability of equipment and compatibility with our fixed bed at our pilot plant.

The main thrust of this work was to evaluate the mechanical strength of promoted iron ore pellets by using single pellet tests (ASTM D 4179) and then comparing its performance to commercial alumina spherical pellets. The mechanical evaluation involved statistical analysis of single pellet crushing data using Weibull distributions, Kruskal Wallis and Post hoc Dunn tests. The current study also evaluated the catalytic FT performance of the proposed catalyst and compared these findings to other researchers.

1.2 Structure of Dissertation

Chapter 2: gives a detailed description of Fischer Tropsch Synthesis process and the various factors to consider in the catalyst development of Iron-based Fischer Tropsch catalysts such as catalyst precursors, type of dopants, reaction conditions and both their physical and chemical properties. All these factors influenced the approach used to develop an alternative to the precipitated iron-based catalyst used in Fischer Tropsch Synthesis fixed bed operations. In addition to that, a unique statistical approach to mechanical evaluation of spherical pellets is also covered in this chapter and used to validate its application in this work.

Chapter 3: outlines the experimental procedure and materials used in this study which involved catalyst synthesis, characterization and then the evaluation of mechanical strength of developed catalysts and its performance during Fischer Tropsch reaction studies.

Chapter 4: presents the characterization findings and describes how it relates to the mechanical strength and reactivity of the solid catalysts. Moreover, this chapter discusses in depth the reactivity and selectivity of the proposed catalysts and compares it to other researchers in order to validate its suitability as a substitute to precipitated iron-based Fischer Tropsch catalyst. The mechanical strength using Weibull and post hoc statistics are also covered in this section and used to select the best catalyst system for this investigation.

Chapter 5: gives broad conclusions of this work.

Chapter 6: Outlines some of the recommendations to consider in the future.

REFERENCES

1. Wei, J., Wen, Z., Xu, H., Ge, Q (2017). Fischer-Tropsch synthesis over iron catalysts with corncob-derived promoters. *Journal of Energy Chemistry, 26(4), 632–638.* [Online] Available at DOI: 10.1016/j.jechem.2017.03.017.
2. Van de Loosdrecht, J., Ciobîcă, I. M., Gibson, P., Govender, N. S., Moodley, D. J., Saib, A. M., Niemantsverdriet, J. W (2016). Providing Fundamental and Applied Insights into Fischer–Tropsch Catalysis: Sasol–Eindhoven University of Technology Collaboration. *ACS Catalysis*, 6(6), 3840–3855. [Online] Available on: Doi:10.1021/acscatal.6b0059
3. Hensen, E.J., Wang, P., & Xu, W (2016). Research trends in Fischer-Tropsch catalysis for coal liquids technology. *Frontiers of Engineering*, 3(4), 321-330. [Online] Available at DOI:10.15302/FEM-2016051
4. Jahangiri, H,. Bennet, J., Mahjoubi, P,. Wilson, K., G, S (2014). A review of advanced catalyst development for Fischer-Tropsch synthesis of hydrocarbons from biomass derived syn-gas. *Catalysis Science & Technology*. [Online] Available at: DOI:10.1039/c4y00327f
5. De Smit, E., Weckhuysen, B.M (2008). The renaissance of iron-based Fischer Tropsch on multi-faceted catalyst deactivation behaviour. *Chemical Society Review.;* 37, pp 2758-2781. [Online]Available at: DOI:10.1039/b805427d
6. Badgoga, S., Vosough, V., Dalai, A.K(2018). Performance of promoted Iron/CNT for catalyst for Fischer Tropsch Synthesis: Influence of pellet shape and binding loading; *Energy Fuels 31*, 11, p 12633-12644[Online] Available on: DOI: 10.1021/acs.energyfuels.7b01318.
7. De Klerk, A (2011*).* Fischer Tropsch Synthesis: Fischer Tropsch Refining*;* Germany: Wiley-VCH Verlag GmbH; pp. 73-93.
8. Botes, F.G., Ciobica, I.M., Ferreira, A., Gibson, P., Moodley, D.J., Saib, A.M., Visagie, J.L., Westrate, C.J., Niemantsverdriet, J.W (2013). Fischer Tropsch Synthesis: Catalysts and Chemistry. *Comprehensive Inorganic Chemistry II*, p.p 531-537.[online] Available at: http://dx.doi.org/10.1016/B9978-0-08-097774-4-00729-4
9. Hunpinyo, P., Narataruksa, P., Tungkamani, S., Pana-Suppamassadu, K., Chollacoop, N., Sukkathanyawat, H., & Jiamrittiwong, P. (2017). A comprehensive small and pilot-scale fixed-bed reactor approach for testing Fischer–Tropsch catalyst activity and performance on a BTL route. *Arabian Journal of Chemistry*, 10, S2806–S2828. Available at: doi:10.1016/j.arabjc.2013.11.004

10. Zhang ,Q., Deng, W., Wang, Y (2013). Recent advances in understanding the key catalysts factors for Fischer Tropsch synthesis. '*Journal of Energy Chemistry*,22, pp 27-38.[online] Available at: https://doi.org/10.1016/S2095-4956(13)60003-0

11. Sharypov, V. I., Kuznetsov, B. N., Beregovtsova, N. G., Reshetnikov, O. L., Baryshnikov, S. V (1996). Modification of iron ore catalysts for lignite hydrogenation and hydrocracking of coal derived liquids, *Fuel 75*, 1, pp 39-42. [online] Available at: https://doi.org/10.1016/0016-2361(95)00194-8
12. Bae, J.-S., Hong, S. Y., Chan Park, J., Bae Rhim, G., Youn, M. H., Jeong, H., Chun, D. H. (2018). Eco-friendly prepared iron-ore-based catalysts for Fischer-Tropsch synthesis. *Applied Catalysis B: Environmental*. [Online] Available at: doi: 10.1016/j.apcatb.2018.11.082
13. Dry, E.M (2008). Handbook of Heterogenous Catalysis: Germany: Wiley-VCH-Verlag GmbH; pp 2965-2992
14. Li, Y., Wu, D ., Zhang, J (2000). Measurement and statistics of single pellet mechanical strength of differently shaped catalysts, *Powder Technology*, 113(1–2), pp. 176–184. doi: 10.1016/S0032-5910(00)00231-X.
15. David, E (2015).Mechanical strength and reliability of the porous materials used as adsorbents/ catalysts and the new development trends', *Archives of Materials Science and Engineering*, 73(1), pp. 5–17
16. Daisyme, P (2018). Understanding the financial cost downtime in manufacturing, Due 18 June. Available at: https://due.com/blog/understanding-the-financial-cost-of-downtime-in-manufacturing/
17. Mantripragada, H.C (2010). Techno-economical evaluation of coal to liquid (CTL) plants and their effect on the environment and resources. Available athttps://www.cmu.edu/ceic/assets/docs/publications/phd-dissertations/2010/hari-mantripragada-phd-thesis-2010.pdf
18. Wu, D., Zhou, J (2007). Mechanical Strength of Solid Catalysts: Recent Developments and Future Prospects. *Particle Technology and Fluidization*, 53, 10, pp. 2618-2629. [online] Available at: DOI 10.1002l aic.11291
19. Bertolacini, R.J(1989). In characterization and catalysts development, American chemical society; *Mechanical and physical of catalysts*. [online] Available at: DOI:10.1021/bk-1989-0411.ch034.
20. Luque, R., De la Olsa, A., Campelo, J.M., Romero, A.A., Valverde, J.L., Sanchez, P (2011). Design of development of catalysts for Biomass-to-liquid-Fischer-Tropsch (BTL-FT) process

for biofuels production, *Energy & Environmental Science*. 5, pp 5186-5202. Available on: DOI 10.1039/c1ee02238c

CHAPTER 2

LITERATURE REVIEW

2.1 Fischer Tropsch synthesis

Fischer-Tropsch Synthesis (FTS) is the conversion of carbon-based feedstocks into liquid (XTL) by the hydrogenation of CO occurs over transitional metal catalysts to produce an array of valuable products such as alkanes, alkenes and oxygenates [1, 2, 3,4]. The X denotes the carbon source of syngas which implies that FT can be classified as CTL (coal-to-liquid), GTL (gas-to-liquid) and BTL (biomass- to- liquid) [1, 2, 3]. Figure 1 below shows the overall process of Feed to liquid process;

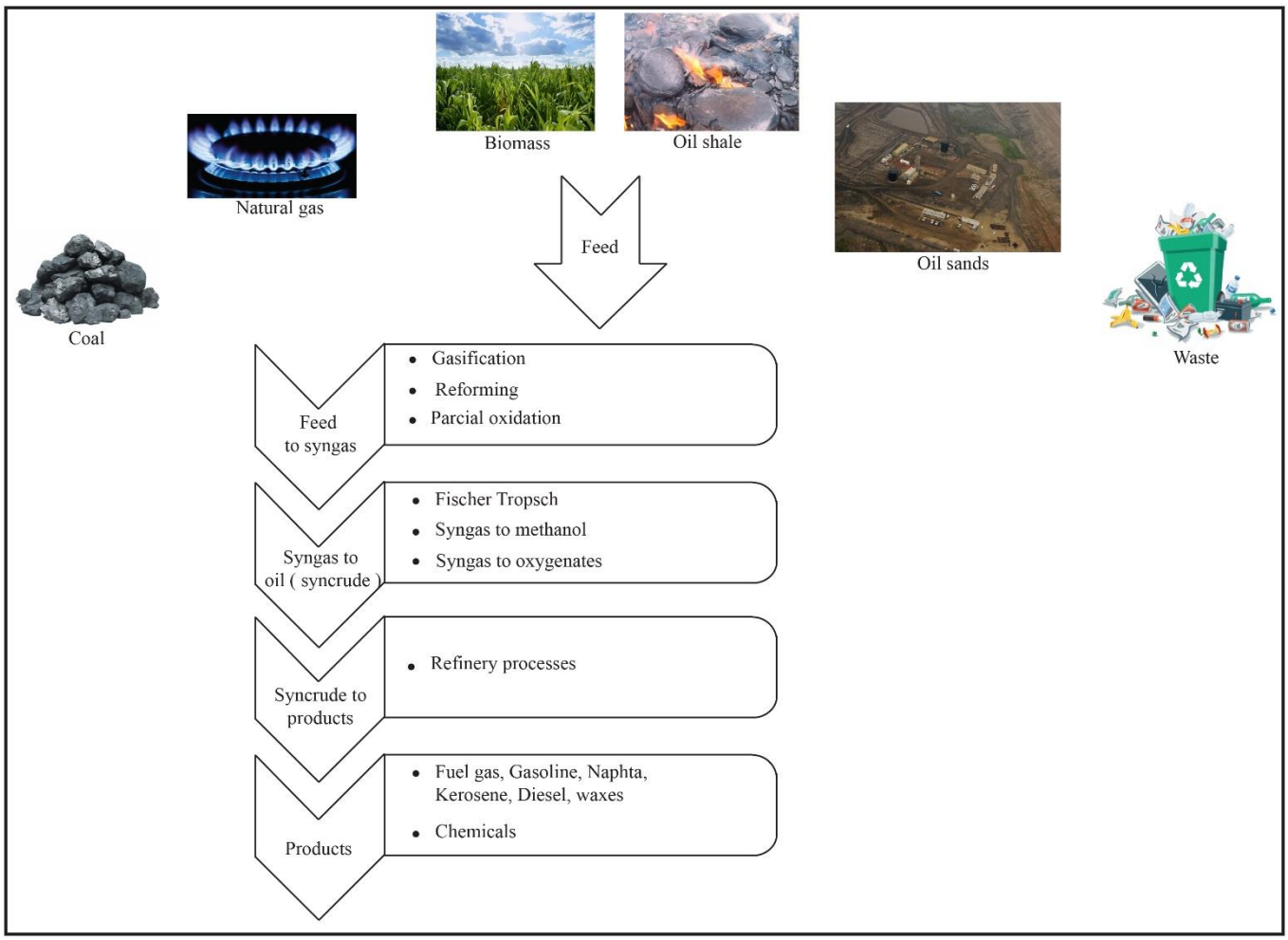

Figure 2.1: Summarized XTL Process [5]

The Fischer Tropsch Synthesis is governed by multiple reactions shown below;

Alkanes $nCO + 2nH_2 \rightarrow (CH_2)n + nH_2O$ (2.1)

Alkenes $nCO + (2n+1)H_2 \rightarrow H(CH_2)nH + nH_2O$ (2.2)

Alcohols $nCO + (2n)H_2 \rightarrow H(CH_2)nOH + (n-1)H_2O$ (2.3)

Water Gas Shift $CO + H_2O \rightarrow CO_2 + H_2$ (2.4)

FTS process via BTL is seen as a sustainable and greener pathway to transportation liquid fuels and chemicals [5, 7, 8] which is shown below;

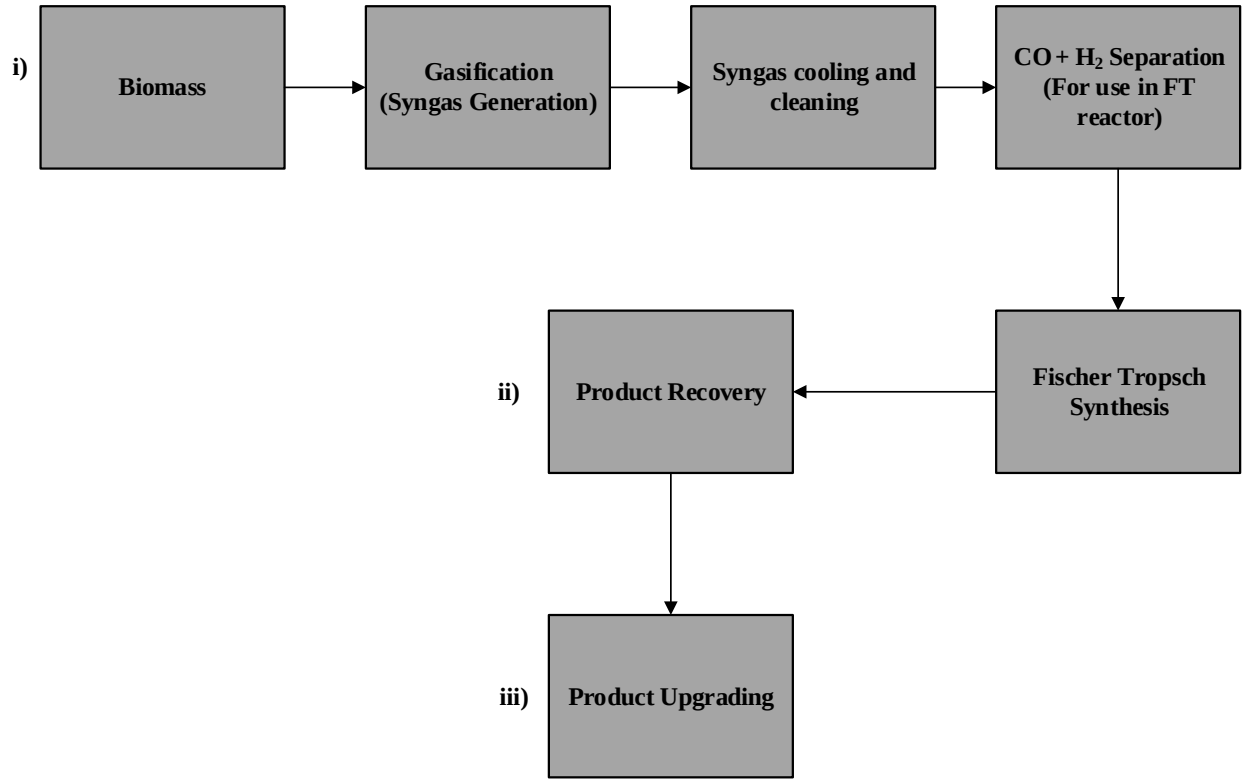

Figure 2.2: Summarized Description of the BTL Process [5]

The feedstock (biomass) for BTL shown in Figure 2.2 include vegetable oils, algae, municipal waste, wood, grass, non-edible oils and agriculture by-products [5, 8]. Biomass is a renewable source and consequently regarded as a sustainable source for transportation biofuels for the future via Fischer Tropsch synthesis [5, 8]. The conversion of biomass into biofuels via FTS is the same in terms of all the process the only difference will be the carbon source used to generate the syngas and thus the processes used in coal-to-liquid and Gas-to-liquid are still applied [8]. These processes include gasification which involves the conversion of the carbon source into synthesis gas either by auto-reforming, steam reforming, partial oxidation or partial catalytic oxidation and depends on to the nature of the feedstock being used. Syngas cooling and purification is also another process involved the BTL whereby after syngas is produced; it is conditioned to remove unwanted compounds such as chlorine and Sulphur which may poison the catalyst and affect its performance during FTS [1, 5, 12]. The FT process is the actual technology that converts the syngas into synthetic crude oil in the presence of a

catalyst at specific process conditions depending on the targeted hydrocarbons [1, 5,8, 12]. The synthetic crude oil is recovered and further refined into chemicals, diesel and gasoline products using hydrocracking, alkylation, isomerization and oligomerization [1, 5, 12].

The most popular FT catalysts are cobalt and iron [6,7,815]. However, in scenarios where the cost of the catalyst precursor was vital, iron is preferred. Another merit that iron- based catalysts has over cobalt is its responsiveness to the water gas shift reaction and thus preferred for syngas derived from biomass which have H_2/CO ratio less than 1.8 compared to the stochiometric value of 2 [6, 8]. Moreover, the water gas shift reaction produces hydrogen which adjusts this deficient syngas ratio [6,7, 8]. Iron-based catalyst are also less sensitive operating conditions (pressure and temperature) changes and less prone to sintering which makes them much more flexible in FTS [4, 8]. Iron based FT catalysts are also more selective to olefins and oxygenates in comparison to cobalt which have a higher affinity to paraffins [7, 8]. Nevertheless, the hydrocarbon selectivity is dependent on the temperature operating conditions. The high temperature FTS (280-340^{o}C) yields lower chain hydrocarbons C_1-C_{15} which is mainly used to produce gasoline and short-chained olefins. On the other hand, low temperature FTS (190-280^{o}C) is more directed towards longer chained paraffins and waxes [7, 8]. Some research has reported that iron catalysts are more susceptible to faster deactivation as compared to cobalt based catalysts and exhibit significant CO_2 selectivity [7, 8]. Conversely, cobalt based FTS has a higher affinity for paraffins, and long chained waxes compared to its counterpart and yield more hydrocarbon per unit mass of the catalyst. However, iron is cheaper, ubiquitous and more suitable for hydrogen lean syngas such as biomass thus more viable for Biomass to liquid FTS [4, 8].

2.1.1 Promotion of iron catalyst

Iron-based FTS catalysts formulations usually use large amounts of Fe coupled with alumina and silica as structural promoters to increase stability and mechanical strength [17]. The other promoters that enhance its structural properties are typically copper, potassium which will be discussed in this section. Alkali doping of iron- based catalysts with potassium (K) is widely believed to be the best because of high activity and selectivity to olefins apparently due to the increased adsorption of CO at the expense of the reduced adsorption of hydrogen on the surface of the catalyst [1, 2]. This is substantiated by other claims that K improves the carburization and reduction of iron oxides which in turn increasing nucleation sites leading to more formation of small crystallites of iron carbides believed to the active phase of the catalyst [2]. This in turn leads to higher selectivity to C_{5+} alkenes and lower selectivity to methane [4, 5, 10, 12].

Similarly, Cu has been reported to reduce the activation temperature and thus quicken the formation of the active phase of the catalyst [2, 4, 12]. This is because all iron-based FT catalysts are inactive and

varied oxide precursors and thus need conditioning using hydrogen, CO or syngas at specified reaction conditions [13]. Lowering the temperature is vital when hydrogen is used as activation gas due to the Fe metal formed which are prone to sintering at high temperatures. On the other hand, when CO or syngas is used sintering of the catalyst is not as crucial due to the formation of thermal stable iron carbides [2, 7]. Furthermore, the extent of reduction of the catalyst is dependent on some factors such as iron catalyst precursor, support material and its pre-treatment; pore diameter, pore volume and available surface area [2]. It is important to cite that combining the both promoters in a catalyst can have neutralization effect as K encourages CO chemisorption whilst Cu encourages H_2 chemisorption [2, 16, 17]. The critical aspect that dictates the catalyst behaviour is the ratio in which they are added to FT catalyst, the type of catalyst system(bulk/supported), preparation method just to mention a few [23].

2.1.2 Role of Iron phases in FTS

One of the main challenges with FT iron-based catalysts is formulating materials that are stable and active during Fischer Tropsch synthesis [5,17, 24]. FT iron-based undergo many structural changes during activation, reaction and deactivation reaction steps of FTS process and may be difficult to correlate these structural changes to their activity [5,17, 24]. The challenges stem from the co-existence of the various iron phases during the FT process [5, 17, 24]. The two main phases formed during this process are the iron oxides and carbides [5, 17, 24].

Iron oxides phases typically present in iron-based FT catalysts are hematite (α-Fe_2O_3), maghemite (γ-Fe_2O_3) goethite (FeOOH), ferrite (α-Fe), magnetite (Fe_3O_4), wustite (FeO) but hematite is usually the most common phase present in fresh iron catalysts [5]. The reduction of iron oxides under hydrogen (H_2) flow starts by α-Fe_2O_3 reducing into Fe_3O_4, FeO and metallic iron(α-Fe) respectively. The hematite(α-Fe_2O_3) transforms into magnetite with hydrogen flow at varying temperatures of 250-900^{o}C depending on the percentage of hydrogen used, the type of metal-interactions within the iron oxide source and catalyst pre-treatment[10, 16, 19].On the other hand, the magnetite(Fe_3O_4) transforms into Fe via the intermediate Wustite (FeO) at temperatures below 570^{o}C under irreversible thermodynamic conditions [8, 19]. Metallic iron particularly ferrite (α-Fe) cannot be found in nature due to its instability in air and is typically formed at temperatures lower 900^{o}C and thus also seen during the reduction of fresh hematite under FTS reaction conditions [5,16]. Ferrite(α-Fe) is renowned for its ability to disassociate CO by absorbing it on its surface-active sites which eventually leads to the formation of iron carbides [5]. However, its exact role during FTS is still ambiguous and often disputed by many FT researchers [4, 5]. In general, the reduction pathway of iron oxides during FT is believed to be $Fe_2O_3 \rightarrow Fe_3O_4 \rightarrow FeO \rightarrow Fe$, respectively [5,16].

2.2 Catalyst Design and Development

Catalyst development is at the heart of Fischer Tropsch Synthesis (FTS) and ongoing research is focalized on improving catalyst technology to make it more economical and efficient [6, 8, 13]. This can be achieved by promoting iron catalyst systems with suitable dopants and supports to improve overall catalyst performance. Catalyst performance can be defined as function of activity, selectivity, stability and mechanical strength [6, 13]. The figure below shows this concept;

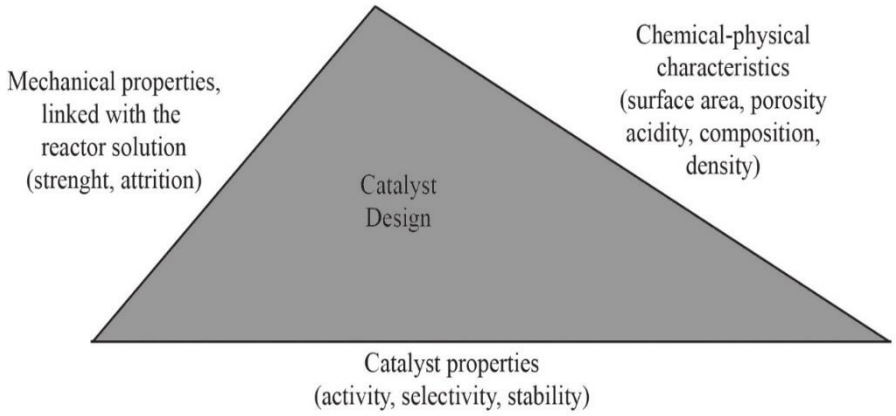

Figure 2.3: Triangular concept [13]

An in-depth analysis of the interplay between these properties is crucial for any catalyst development from the active phase identification to the choice of reactor (which determines the catalyst shape and size) and finally the catalyst formulation [12]. As already cited earlier, FT has a vast possibility of transitional metal catalysts to pick from, but cobalt and iron are the obvious ones for commercial purposes [2, 7, 12].

Another factor directly linked to catalyst design is the selection of the reactor which determines the catalyst size and its shape [3, 8]. Furthermore, the desired shape and size of pellets is dictated by the reactor being used which in turn affects the catalyst activity [20]. Moreover, some research by Zhang, (2010)) showed that larger pellet size exhibited higher CO conversion and C_5+ selectivity but a lower chain growth probability than a smaller pellet by ¼. This was attributed to more mass transfer limitations in the bigger pellet size [8]. The mass transfer limitation in larger pellet could influence the product selectivity of FTS; firstly, by increasing the H_2/CO ratio at the active sites of the catalyst

because hydrogen diffuses faster than CO and promote undesirable generation of methane [3]. Secondly, mass transfer limitation could hinder the transportation of heavy hydrocarbons products or encourage the re-adsorption of α-olefins resulting in higher selectivity to heavier paraffins [3]. Conversely, pressure drop is more prominent for smaller sized pellets and thus a compromise must be reached to optimize catalytic performance and depends on the dimensions of reactor [3, 8].

2.2.1 Relationship between Structural properties and catalyst performance

Industrial catalyst performance is related to textural properties such as BET surface area, porosity and other factors like mechanical strength and morphology of its structure [1, 2, 12, 13]. Moreover, commercial catalyst performance can be defined as a function of its selectivity, activity, stability and mechanical strength which are directly linked to the structural qualities of the catalyst as cited earlier [2,12]. The surface structure and pore size can improve the metal dispersion, mechanical strength of a catalysts, reducibility and diffusion coefficients of reacting species due to increased surface area [1, 2, 12]. This can be enhanced by adding structural promoters like silica, alumina, titania and its function is usually varies depending on the application [13, 23, 25, 26]. Supported catalysts are categorized as materials that have a weight percentage ≥50% of structural promoters such as silica, aluminium and titanium present. Conversely, unsupported catalysts typically have a maximum weight percentage of 25g per 100 g of the active metal and in this case, these structural promoters act as binders. Structural promoters in most instances are used to improve dispersion of active metal, enhance thermal stability and mechanical strength of solid catalysts [3, 17].

A low metal–support or binder interaction is required for easier reducibility of catalyst into its active phase which in turn dictates its overall performance [13, 27]. The synthesis route chosen promotes weak metal-support interactions compared to other methods due to the addition of silica source after doping of the catalyst. Other studies have shown that stage at which the binder is added affects its reducibility, carburization and activity of an FT catalysts [27]. The same research found that adding the binder after the catalyst is promoted yields weaker interaction between the active metal, the promoters and support which facilitates its reducibility and subsequent attainment of the active phase [27]. The choice of metal used for doping of the FT for this work was like classic ones used by FT practitioners which are potassium and copper. Their significance to FTS is discussed in detail later in this section. However, it important to note that the method of catalyst synthesis and doping used was different from the one used in this work.

2.3 Mechanical Testing of Solid Catalysts

Mechanical strength of catalysts, especially for pilot and industrial applications is vital and is often neglected or not given the same attention that activity, selectivity and stability of the catalyst are given [23, 25]. This is substantiated by the number of papers, patents and other research work available in the open literature [23, 25]. The compressive mechanical strength of catalysts is particularly vital in fixed beds in the initial stage of catalysts loading and during reactions conditions [23, 25, 26]. The mechanical failure of catalyst instigates significant pressure drop, gravity, thermal shock and chemical stress during reaction conditions [23, 25, 29]. Below is a schematic depicting a myriad of stresses that a catalyst pellet is subjected to;

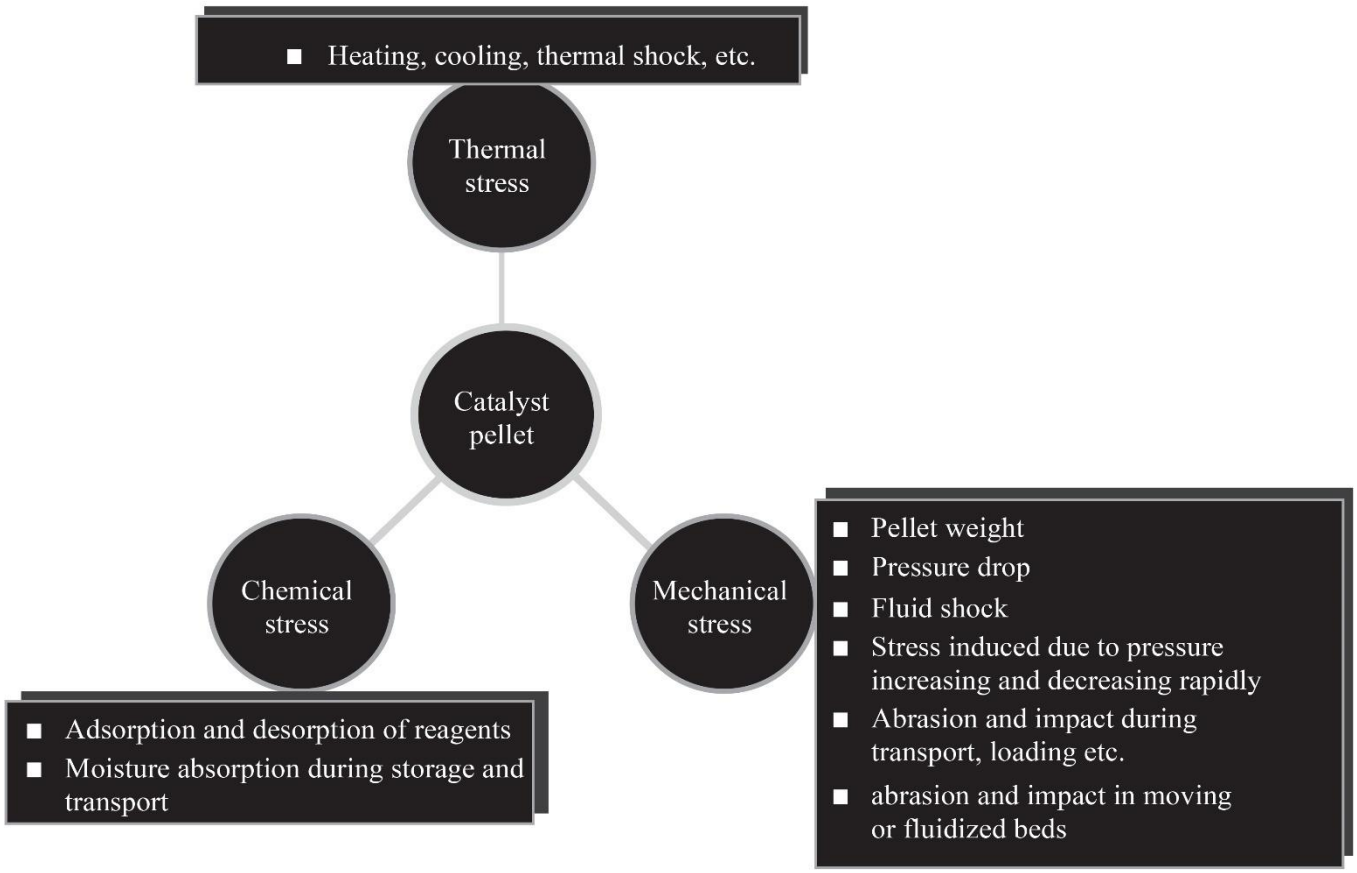

Figure 2. 4: Various Stresses that catalysts pellets may experience

Catalyst mechanical failure during reactions produce fines that change its shape and size and instigate excessive pressure drops, uneven flow of fluid, immense heat and mass transfer variations and subsequent plugging downstream [7,25, 26]. Consequently, many large-scale operations are shutdown to fix these problems [7,25, 26]. These shutdowns are costly and affect productivity during these periods. It is apparent to see that cause of shutdowns is often caused by catalyst mechanical failure more than catalytic activity and thus highlighting the need for mechanical testing of solid catalysts during the design phase [25, 26]. The most common compressive testing methods for solid catalysts

are bulk strength, impact test and single pellet crushing tests [19,23,25]. It is noteworthy to mention that single pellet crushing tests are deemed enough to quantify the mechanical strength of spherical pellets [22, 25, 29].

2.3.1 Compressive and Impact Tests

One of the standard methods of testing solid catalysts is single pellet crushing test which refers to amount external load in Newtons a single pellet can withstand before it fractures [8, 29] and is measured by a Force gauge (FG-5052 model) with maximum load measurement of 300N/pellet. It is worth mentioning that the FG-5052 model is equivalent to an Instron tester, but the only difference between Instron ad Force Gauge is that the latter can measure higher loads. The pellets strength before drying is called wet strength(N/pellet) and after drying is referred to as dry strength (N/pellet). The single pellet crushing strength can then be expressed in Pascals (Pa) using the following equation [20];

$$\tau_s = \frac{2.8 \times Force(N)}{\pi d^2} \qquad (2.5)$$

Where d is the diameter(m) of the spherical particles, Force is obtained from the Instron

The recommended single pellet crushing strength reported in literature is 660 kPa for fixed beds [20]. The single pellet crushing strength is also sometimes expressed in Kgf/pellet which is simply converted to N/pellet by multiplying by gravitational force of 10N. Additionally, measuring of single pellets allows for comparison between catalyst samples but parameters such as pellet size, loading mode, loading speed, temperature and humidity are fixed so that results are not biased [18].

Below is a schematic representation of single pellet crushing testing on spherical pellets;

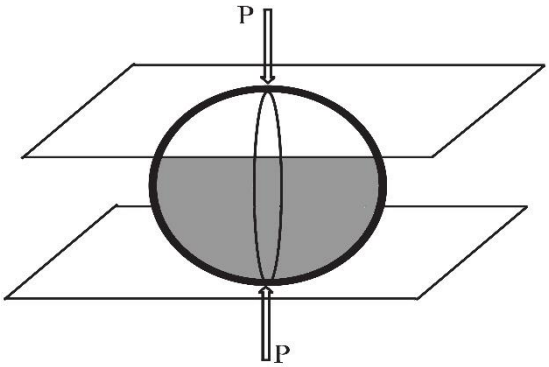

Figure 2. 5: Single Pellet Crushing test [8,23, 25]

2.3.2 Statistical Analysis of Mechanical Strengths

A hypothesis is a useful statistical tool used to rationalize experimental observations [31]. Moreover, a meaningful hypothesis will ensure that the independent variable determined by the researcher and the

dependent variable is measurable. Hypotheses can either be approached using the null hypothesis or alternative hypotheses. The null hypothesis (Ho) assumes that there is no difference between sampling groups, and the observed difference is simply due to variation in the observations [31]. On the other hand, the alternative hypothesis (H1, H2, …) gives possible reasons for the significant difference observed in sets of experiments [31]. A meaningful hypothesis has a rationale that explains the difference in an experiment and corresponds well with the background collected for that system [31]. The hypothesis test used for this study was the Kruskal-Wallis Test.

A central tendency characterizes the typical value of a group of samples and commonly expressed as arithmetic mean, median and mode to reflect the distribution of given experimental findings. The mean is simply the average of a set of results whilst the median ranks are given results and finds the median value. The mode is simply the frequency that a sample appears in the results. The mean is the most common parameter to describe results but has limitations when they are outliers within a given sample. This because mean values are sensitive to any skewed data points and not always accurate to compare the different set of results. Consequently, medians give a better comparative analysis between sets of results and thus commonly used for non-parametric statistics such as Kruskal -Wallis Test [31].

2.3.2.1 Kruksal- Wallis Test

The Kruskal Wallis test is the non-parametric alternative to the One Way ANOVA, which simply means that an abnormal distribution is observed in a particular population and thus; referred to as the one-way ANOVA on ranks [31]. Ranks are used instead of actual data points and are used to determine the overall difference across two or more sampling groups [31]. However, this test does not specify where the difference is located between groups [31]. The H test is valid when the assumptions for ANOVA are not satisfied, such as the assumption of normality [31]. Like other statistical tests, calculation of test statistic is performed and then compare it to a cut-off distribution point. The test statistic used in this test is called the H statistic [31]. A thorough statistical analysis of this experiment was simulated in R studio and single- pellet crushing strengths of each binder loadings were compared. The p-value is a probability that measures the evidence against the null hypothesis. Lower probabilities provide more substantial evidence against the null hypothesis [31]. The p-value is used to determine whether any of the differences between the medians are statistically significant [31]. The null hypothesis states in a set of results where medians are all equal [31, 32]; a significance level (denoted as α or alpha) of 0.05 works well [50]. A significance level of 0.05 indicates a 5% risk of concluding that a difference exists when there is no actual difference [31].

Null Hypothesis means P-value ≤ *α*: The differences between some of the medians are statistically significant

If the p-value is less than or equal to the significance level, the null hypothesis is rejected and conclude that not all the medians are equal.

Alternative Hypothesis means P-value > α: The differences between the medians are not statistically significant

If the p-value is greater than the significance level, then there is not have enough evidence to reject the null hypothesis that the population medians are all equal [31]. Verification of the test has enough power to detect a difference that is practically significant [31].

2.3.2.2 Post Hoc Dunn Test Results

The Post-Hoc Dunn Test Is a useful tool after the Kruksal test to compare groups against each other. It compensates for the Kruksal test by revealing which groups are different and not just the significant difference between them [31]. This is useful for this study in that it facilitates the comparative analysis between the different binder additions on the proposed iron ore catalyst in order to determine most suitable for our pilot scale fixed operation.

2.3.2.3 Weibull Statistics

The Weibull distribution is named after the Swedish physicist Waloddi Weibull; who used first used it in 1939 to describe the breaking strength of materials and extended its applications in other fields in 1951[32, 33]. The invention received much scepticism at the time. However, in the mid-50s, the discovery was improved by Dorian Shanin and Leonard Johnson prompting the American Air Force to fund research Weibull analysis until 1975[32]. Moreover, Dorian Shanin introduced the inventor to statistical engineering at the Hartford graduate centre and encouraged him and Pratt & Whitney Aircraft to use the improved Weibull analysis for their work [32]. This led to a Weibull analysis booklet and a movie production [32].

Furthermore, Leonard Johnson, whilst working at General Motors improved Weibull plotting methods by suggesting that instead of using mean ranks for representing data; median ranks are used [32]. He found that this was more accurate than the method that Weibull initially proposed [32]. Today Weibull statistics is widely accepted as a reliable tool for life data analysis in various fields [23, 25 32, 33].

There are three statistical distributions commonly used for describing mechanical strength data which are namely Weibull, normal and lognormal in various engineering applications [34]. However, the Weibull distribution is more accurate for describing strength data than the other two distributions, mainly due to the ability to estimate consecutive measurements which is desirable for engineering scenarios [35]. Furthermore, the Weibull statistics has proven to be a useful tool in various engineering applications to forecast the failure profile of materials with reasonable accuracy even with small sample sizes [22, 23, 25, 32]. Furthermore, small samples allow engineers to save costs and easily showcase analysis in a graphical way to management who do not always have in-depth technical knowledge [32].

Single crushing Strength tests for spherical pellets yield scattering of strength data which do not follow normal distributions and thus rendering them difficult to predict failure of solid catalysts [22, 23, 25, 32]. Weibull distributions provide a facile way of predicting the probability of failures and reliabilities of skewed strength data. The scattering of data recorded is attributed to the inherent defects found solid materials due to its brittleness, various porosities, shape and sizes contained in the bulk structure of the catalysts which results in subsequent crack propagation when stressed during testing [22, 23, 25, 32]. This phenomenon is based on the weakest link theory, which states that the most severe flaws will influence the strength of solid catalysts. However, the most severe flaw is not always the largest because its graveness is also dependent where it is in the bulk material [23, 25]. Moreover, in simple terms, this concept suggests that the structure of a solid material collapses when the link with the lowest mechanical strength breaks [36].

Comparative analysis between different solid catalysts to determine the optimum mechanical strength for a specific application using the standard deviations and mean are inaccurate to use as a barometer [23, 25]. The batch with the highest mean does not necessarily mean it is the best choice. However, it is mechanical reliability under specific loads is more significant for designing and manufacturing of solid catalysts. Reliability can be defined as the probability of that an equipment or material will perform within specific design constraints [37]. In our text, mechanical reliability is the probability that a catalyst system will continue to perform under specific process conditions. As a result, Mechanical reliability is obtained from probability distributions under specific loads by Weibull distribution statistics and is a better way to predict catalyst failures at various stresses [23, 25].

Moreover, the more samples are tested, the greater accuracy and confidence of the measurements, but most practitioners recommend at least 20 samples for this type of studies [38]. The most common form of Weibull statistics used for this type of measurements is the two-parameter Weibull distribution given by;

$$P_f(F) = 1-\exp[-(F/F_o)^m] \quad (2.6)$$

Where P_f is the probability of failure, F is the load at failure(Kgf), m Weibull modulus, F_o Weibull size parameter is a volume -dependent scale parameter which relates the fracture stress with a failure probability of 63.2%[23] . The Weibull two parameter distribution is valid when there is constant volumes for all tested pellets [23, 25, 34].

Linear regression is to estimate Weibull parameters in equation 2.11 and is linearized by taking logarithm twice which becomes [23, 25, 34];

$$Y=\ln\ln\left[\frac{1}{1-P_{f(F)}}\right] = mlnF - lnF_O \quad (2.7)$$

The expression becomes a straight line where the slope is m and the y-intercept is $\ln F_o$ with lnF and Y in the equation being the independent and depend variables; F is the crushing strength measured experimentally. The Weibull modulus, m is sometimes referred to as the shape parameter which determines the scattering extent of failure strength and F_o is simply the scaling parameter as previously cited obtained from either the probability of failure curve or equation 3.12[23, 25, 34]. The Weibull modulus is an indication of the defects present in solid material and the higher the modulus, the better but usually does not exceed 10 for brittle materials [36]. Moreover, the modulus (m) also describes the classes of failure present in catalysts as follows;

m< 1.0 signifies the source of catalyst mechanical failure is from product or processing of making the solid material

m=1.0 signifies random catalyst mechanical failures (Independent of time)

m> 1.0 signifies wear out catalyst mechanical failures

The first class in strength data (where modulus, m< 1.0) implies that they are various problems with the product such as overhaul problems, quality control problems, substantial state failures or even stress screening just to mention a few [32]. In cases where the modulus of is greater than 1 (m<1) of material or a solid catalyst is prevalent, it signifies that its mechanical failure will improve with time as hazard rate declines and in turn, its reliability will increase [32]. Consequently, overhauling a material at this point is not appropriate as these types of materials will get better with time and help save cost [32]. On the other hand, random failures (m=1) means that this type of failures are independent of time and could be due to human errors, maintenance errors, a mixture of data from different batches and intervals between failures, etc. This type of failure also overhauling is not recommended. Finally, the class (Wear out) with m greater than 4 have a high possibility of failure as soon as the strength data approaches that region due to the steepness of the slope. However, steeper Weibull modulus could be suitable for the manufactures because it means small variations in times of failures and thus more predictable life span of the material. Moreover, this type of failure is common in materials such as ceramics and other brittle materials which wear out with time which in turn decreases their reliability [32]. In this case, overhauling and inspecting components or materials with a high failure rate is cost-effective.

Below is an example of a Graphical form of equation 2.7 (Weibull plot);

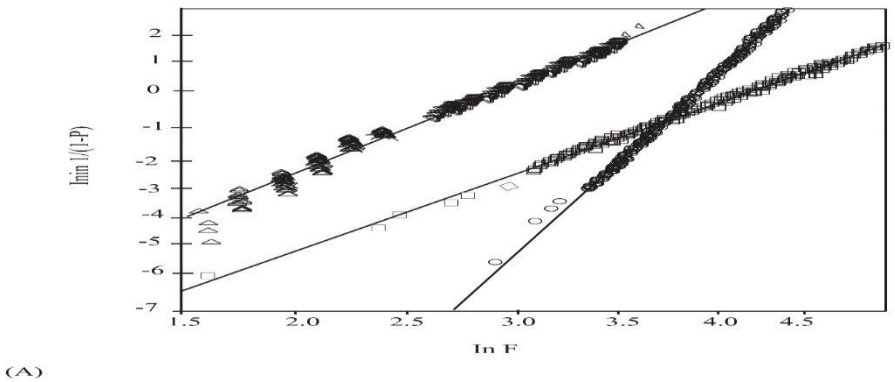

Figure 2. 6 Schematic representation of a Weibull plot of 3 different catalysts [23, 25]

From the example, Weibull plots in Figure 2.10 it is apparent to see which catalyst has a higher modulus (steeper gradient) and be useful to classify the materials and find out which has the least scatter in data and the most mechanically reliable [23, 25]. This highlights the significance of the Weibull plot in design and manufacturing solid materials [23, 32]. Estimation of the Weibull distributions parameters from experimentally measured strength data and the most frequent method is linear regression due to its simplicity [32,33]. The probability of failure (P_f) can be estimated by ranking the measured strength data are ranked in ascending order and P_f is assigned to each strength F_i. The P_f is unknown and computed using the median rank estimator given below;

$$P_f(F) = \frac{i-0.5}{n} \qquad (2.8)$$

Where P_f is the probability of failure for the ith ranked strength datum and n is the sample size being tested [22, 25]. Below is an example of probability failure curve;

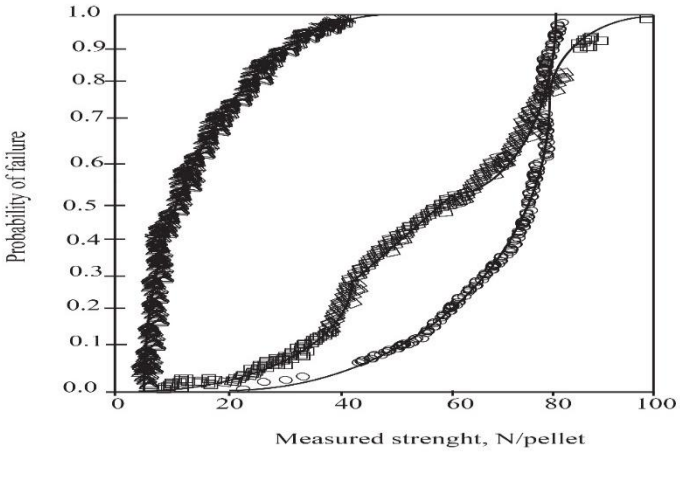

Figure 2. 7: Delineates the Weibull distribution curve of 3 different catalysts [25]

Weibull has many other applications in reliability studies, as mentioned earlier [33]. The significance of this model is particularly important in the design, development and manufacturing phase of any product [33] including solid catalysts before launching of the product. The model can help minimize

failures during operation and help optimize the manufacturing process by changing various factors in the pre-launch phase. The pre-launch phase involves the feasibility stage when studies are carried out using a targeted value for the catalyst. The importance of this model for failure forecasting various fields other than engineering is shown below;

Table 2. 1: Applications of Weibull statistics in other fields [31]

Discipline	Topic
Geophysics	Wind-speed data analysis
	Earthquake magnitude
	Volcanic Occurrence Data
	Low-flow analysis
	Regional flood frequency
Food science	Sterility in thermal preservation method
Social Science	Unemployment duration
Environment	Environmental radioactivity
Nature	Ecological application
Medical Service	Survival data

2.4 Impregnation method of catalyst preparation

Impregnation method of catalyst preparation is one of the techniques used to prepare FTS catalysts and will be discussed in this section. Impregnation can be classified into two categories according to their volume of solution added during their preparation, namely incipient wet impregnation and slurry phase impregnation. In this study, we will focus on the slurry phase impregnation method. This approach used the pore space of the support/material of interest is filled with the solution wet. However, the transfer of the solute from the precursor solution into the pores of the material of interest is governed by diffusion. The material of interest is submerged into a precursor solution to allow for mass transfer to take place. The first phase of saturation of the material interest follows that of incipient impregnation but progressively due to a loss of pressure inside the pores, diffusion of solute from the precursor into the pores becomes the driving force as mentioned earlier [34, 40, 41, 42]. The concentration gradient between the bulk solution and solution within the pores starts to dictate the impregnation and thus takes much more time than incipient impregnation [34, 40, 41, 42]. Slurry phase impregnation is not suitable for applications where the interaction between precursors and the material of interest is too weak to ensure deposition of the solute into its pores [34, 40, 41, 42].

The mechanism of slurry phase impregnation is governed by two principles;

- Diffusion of the solute within the pores described by Fick's law;

- Adsorption of the solute unto the material of interest which is dependent on the adsorption capacity of its surface and the adsorption equilibrium constant;

The distribution of the precursors within the material is reliant on the combination of the diffusion and adsorption principles.

Drying is one of the steps necessary during impregnation that eliminates the solvent inside the pores. Usually, the impregnated sample is dried in an oven in the presence of air or any other gas depending on the application [34, 40, 41,42]. The temperature is maintained slightly higher than that of the boiling point of the solvent e.g. 110^{o}C-120^{o}C for water [34, 40, 41,42]. The removal of solvent from the pores concentrates the precursors up to saturation and consequent crystallization [34, 40, 41,42]. Besides the temperature, the heating rate also influences the drying process [34, 40, 41,42].

The drying mechanism is governed by a conventional outward flow of the liquid towards the pore mouth of the solid catalyst surface where the solvent evaporations take place [43, 44]. The convective flow is described by Darcy's law whereby the outward flow of the precursors that are favored by low viscosity of the solution [34, 40, 41,42]. The outward flow onto the surface of the catalyst increases the precursor concentration with time [34, 40, 41,42]. On the other hand, there is inward back diffusion of precursors happening simultaneously which governed by Fick's law. Moreover, on top of these flows, the interaction between the precursor and catalyst surface needs to be considered [34, 40, 41,42]. The distribution of the precursor phase in the solid catalyst or its segregation at the outer surface depends on the combination of adsorption, convection and back-diffusion provided the flow of solvent is high [34, 40, 41,42]. This relates well with the constant rate period of drying described in Fig 15. Conversely, as the solvent recedes inside the pores, evaporation occurs within the pores relates well with the falling rate period of drying also depicted in Fig 15 [34, 40, 41,42]. The drying regime is deemed as slow when the constant rate period is dominant and considered fast when the falling rate period is pronounced.

The distribution of precursors within pores of materials is of interest depends on various conditions during impregnation and drying processes. The precursors distributions are categorized into three types as described in Table 2.2.

Table 2. 2: Distribution of precursors at different conditions of impregnation and drying

Precursor distribution	Conditions of Impregnation and drying
Egg shell distribution 	1. Strong adsorption of precursors during impregnation 2. High viscosity of impregnating solution 3. Slow drying regime for low concentration, low viscosity and weak adsorption conditions
Egg yolk distribution 	1. In presence of competitor ions that have stronger interaction with the supports 2. fast drying regime with predominant back diffusion
Uniform distribution 	1. Precursors and competitors interact equally with the surface. 2. Impregnating solution is concentrated and viscous 3. Room temperature drying with weakly adsorbing precursors

In the egg-shell distribution type of impregnation; precursors are accumulated and strongly adsorbed near the pore wall. The high viscosity of the solution precursor favors the egg-shell precursor distribution whilst slow drying leads to the low viscosity of the solvent, which in turn leads to weak adsorption of precursors on the pore walls. With the egg yolk distribution, the precursors accumulate in the interior core of pores because of competing ions present having a stronger interaction with the pore wall of the material of interest (Support). A fast-drying regime with predominant back diffusion equally contributes to an egg yolk type of precursor distribution. The Uniform precursor distribution type is a case where precursors are evenly dispersed across the pores. This regime occurs when adsorption of the solutes is weak, and impregnation is performed for extended periods. Moreover, uniform distribution also occurs when the precursors and competing ions interact equally with the surface of the impregnating solution is concentrated and viscous [34, 40, 41, 42]. Furthermore, room temperature drying with weakly adsorbing precursors also favors uniform precursor distribution such that for powders equilibrium is reached within minutes whilst for pellets, it takes several hours [34, 40, 41, 42].

Other parameters that affect the impregnation process are calcination and pH, which are interlinked to the structure of support or bulk catalyst, dopants. The pH of the solution determines the most abundant species in the solution to be deposited on the support or bulk catalyst. Nitric acid, carboxylic acids and ammonia are usually used to adjust the pH because these can decompose during thermal treatment. Moreover, the pH controls the nature of the surface charge and the number of charged sites which is commonly known as the zeta potential. During impregnation, the extent of interaction between the metal complex and the support (bulk catalyst) is controlled by factors like the isoelectric point of oxide

support (Bulk catalyst), temperature and nature of support and dopants as mention earlier. After the removal of pore liquid, further treatment is needed to convert the precipitate or dry gel to catalytically useful form and commonly called calcination. Calcination is usually performed in the presence of flowing air or oxygen to burn any residual organics or to oxidize the sample and this instigates various changes to sample discussed below;

- Active phase generation: The hydroxide form is converted to an oxide form;
- Stabilization of mechanical properties: The catalysts sample is subjected to a more severe heat treatment that what it will experience during reaction conditions. This ensures the stability of textual and structural properties during the reaction;
- Loss of chemically bound water: The chemically bound water is removed at a higher temperature;
- Changes in pore size distribution and surface area due to sintering: Exposing the sample to high temperatures over extended periods leads to sintering consequently reduces surface area;
- Changes in the phase distribution: Higher temperature cause material to crystalize into different structural forms;

The extent of changes in the physio-chemical properties of the final catalyst before the reaction is dependent on temperature, heating rate, heating time and gaseous environment it undergoes during its preparation stage. Therefore, careful consideration must be taken when preparing catalysts for FTS.

2.5 Proposed preparation method and development of catalyst

Iron ore in its raw form is not suited for LTFT because of its inferior structural properties such as low surface area, weak mechanical strength and small pore volumes [8,18]. Therefore, it needs to be modified to improve the structural properties and achieve high surface area, large pore volumes and good mechanical strength which have reported to favor LTFT [8,18,19]. Furthermore, intensive mechanical treatment of iron ore was reported to initiate some chemical transformation of the catalyst in question [12]. Furthermore, in this study the catalyst will be promoted via slurry phase impregnation method as discussed in section 2.4 for improved structural properties and thermal stability [9, 15, 16]. Powders are cumbersome to handle and cause a lot of operational problems such as pressure drops, uneven distribution of gases and subsequent shutdowns, so it necessary to agglomerate them [8, 23, 48]. They are many ways of agglomeration available, [34, 40, 41, 42, 45, 47, 48] but pelletizing was preferred for this work due to accessibility to the equipment and merits it has over other techniques. Additionally, pelletizing is the preferred option for iron ores in various fields of applications because there is the possibility of achieving spherical pellets with minimal energy input at a high rate [45, 47, 48].

2.5.1 Agglomeration of powders

Agglomeration of powders is a vital step in product manufacturing with applications in the mining, agriculture and pharmaceuticals to enhance product properties and process conditions [50]. Furthermore, this technique has some added merits such as;

- Drastic dust reduction/ elimination
- Mitigation of product lost to dust waste
- Improved handling and transportation
- Improved application and use

They are many other agglomeration methods used in industries but the emphasis in this section will be made on wet Pelletization. This technique has its merits and drawback depending on the application, costs and availability of equipment [48].

Wet Pelletization

Pelletizing is an agglomeration technique which involves the formation of pellets by mixing the ore with a binder and then tumbling on a rotating disc or drum using water as a dispersion medium [46, 47, 48]. This technology is a non-pressure technique which uses the binder and water to stick the power which eventually grows into balls and thus considered as a wet agglomeration process [50]. The agglomeration method involves, firstly, the addition of the fine material and binder in a mixer to achieve homogeneity and even distribution. Moreover, densification is also achieved during this step as the compactness may reduce the amount of binder needed and thus save some costs. The next is Pelletization which involves the formation of balls by tumbling action. The process occurs by feeding the pre-conditioned mixture unto the rotating pan whilst sprinkling water; as the fine material rubs against each other balling is then initiated. The pellets are then sieved on-site the desired size is put away, and the rest is re-fed on the rotating pan to repeat the process. The pellets with the desired size are then dried in an oven. Below is a schematic representation of the Pelletization process;

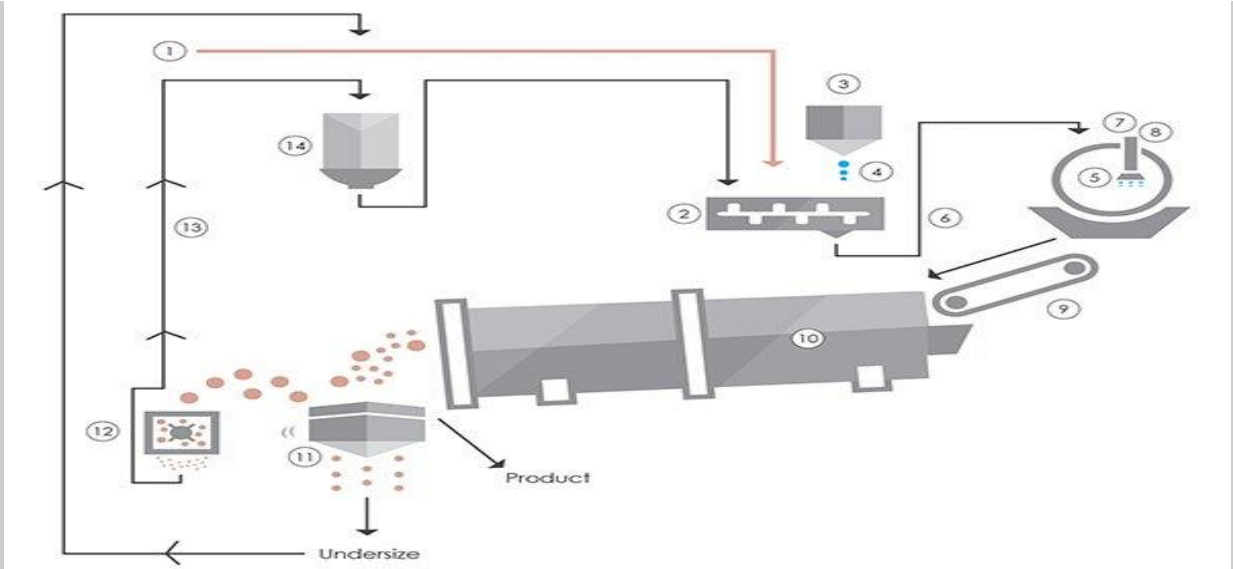

Figure 2. 8: Pelletization process [48]

Each unit is described below;

1. Raw Feed
2. Paddle/Pin Mixer
3. Binder Feed
4. Spray Rate
5. Disc Pelletizer
6. Feed onto Pelletizer
7. Binder Feed
8. Liquid Spray System
9. Transfer Conveyor
10. Rotaty Dryer
11. Vibrating Screen
12. Oversize Mill
13. Recycle
14. Surge Hopper

Pelletizing on a disc is art with various factors influencing the quality of the end-product. Consequently, an experienced operator needs to manage its operation. The most common factors that govern the process are as follows;

- Binder formulation
- Binder feed rate
- Material feed rate
- Pan speed
- Pan angle
- Liquid addition rate and location
- Particle size of fine material

These factors determine the size, uniformity and strength of pellets formed as already mentioned earlier [46, 47, 48].

Advantages of Pelletization

- The less dense pellets created in pelletizing can withstand handling, but can still quickly break down upon application, an ideal characteristic for soil amendments, fertilizers, and other applications that benefit from fast material breakdown [48];
- Less dust and fines are produced compared to compaction: Since pellets are round, there are no edges to break off and create dust [48];
- Binders can serve as beneficial additives – Pelletization offers the opportunity to control formulation, through the addition of specially formulated binders, to create optimum pellet characteristics [48];

Disadvantages of Pelletization

- Higher Processing Costs: The use of a binder, and the required drying step results in higher processing costs when compared to compaction granulation, though the Pelletization method often requires a lower capital investment;
- A Skilled Operator is Required: Pelletizing (on a disc pelletizer) requires a well-trained and skilled operator to produce a pellet with desired quality and characteristics, and to keep the process running smoothly;

It is noteworthy to cite that for a successful pelletizing the ore needs be have majority of its particle distribution as fine powder (52-150μm) [30]. This will improve interparticle interaction during Pelletization which enhances the compressive strength of the resulting pellets [30]. Additionally, the upper limit to discourage very strong interaction between the binder and the ore as this will impede its reduction and carburization. Thus, an interplay between the particle size and interaction needs to be considered to ensure that the bonding is not too strong but on the other hand, yields good compressive strengths suited for fixed bed operations. Furthermore, the recommended moisture of range of 8%-10% for particles together to stick but not too muddy and the binder most be able to hold the particle together

after drying [46,47]. It is obvious to see that the choice of the binder plays a vital role in achieving successful pelletizing[47].Moreover, the binder makes the moist ore plastic and able to nucleate into uniform-shaped seeds and helps the ore stick together after drying [46, 47].

Binder used for Pelletization in this work

The inorganic binders that can be used are kaolin, Alumina sol and Silica sol; organic binders that can be used are Methyl Cellulose and Polyvinyl alcohol [49]. All these alternatives were not considered due to very long waiting period to order the chemicals and other procurement difficulties.

Bentonite makes the moist ore plastic and able to nucleate into uniform-shaped seeds and helps the ore stick together after drying [46,47]. Moreover, bentonite can absorb more water than its weight which makes easier to control the free moisture content in the pellets formed by this technique. This is a significant attribute as the feed moisture content to pelletizer requires to be within a narrow range for good nucleation of green seeds to be achieved [46,47]. The unique feature of bentonite is associated with its moiety; the smectite mineral group which consists of sodium, calcium, magnesium, iron and lithium aluminium phyllosilicates both di-octahedral and tri-octahedral. Both of them maintain their two-dimensional crystallographic structure of this material even after contract or expansion [47]. Bentonite is a mixture of clays with the main constitute being montmorillonite of the following chemical composition [47];

$$M^{+}_{x+y}\,(Al, Fe^{3+})_{4-y}(Fe^{2+}, Mg)_y[Si_{8-x}Al_xO_{20}](OH)_4\ .nH_2O \qquad (3.10)$$

Where M represents absorbed alkali cation in the interlayer (especially Na^{+}); In cases where (Ca^{2+} and Mg^{2+} occur they are given by $M^{2+}_{x/2}$. It is basic structure is shown below [47];

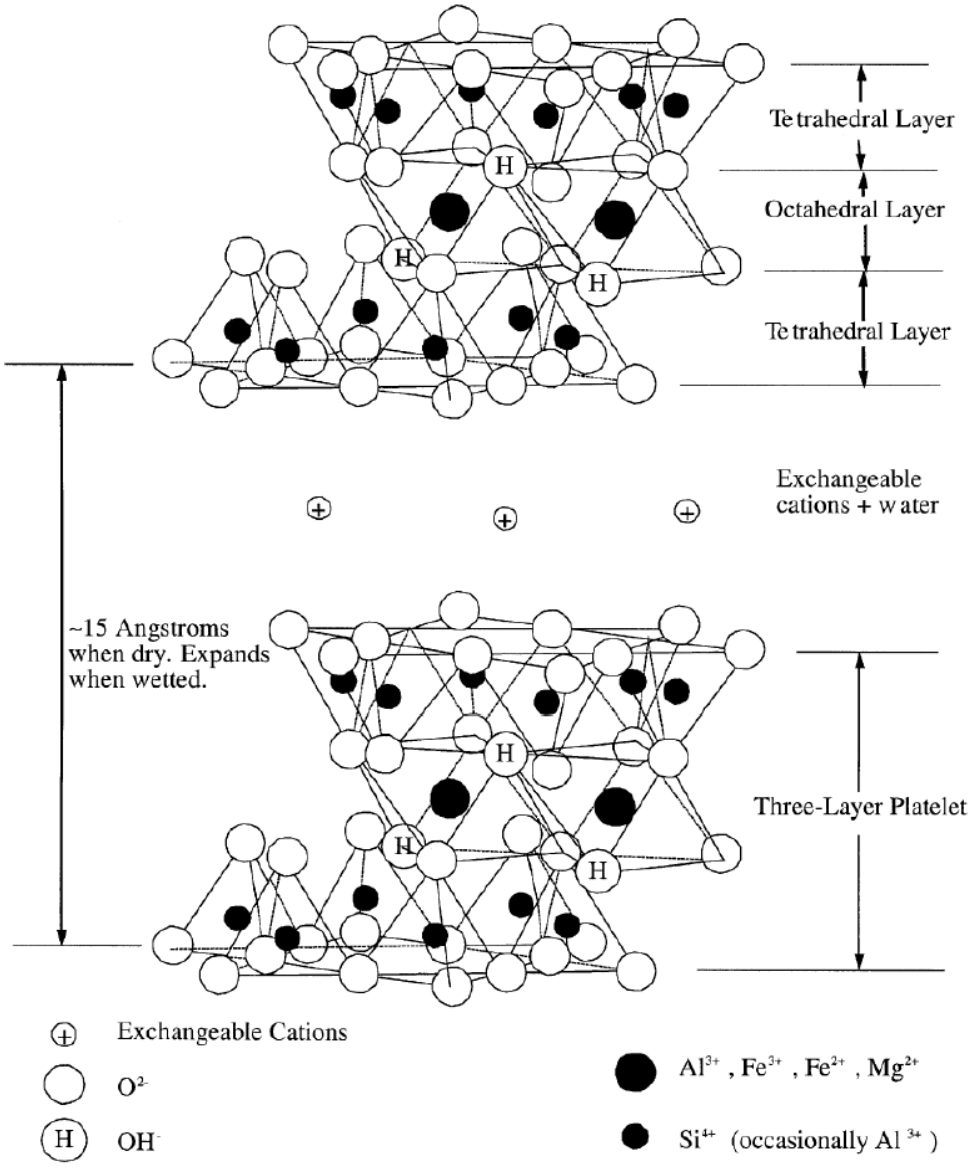

Figure 2. 9: Structure of smectite crystal [47]

The isomorphic substitution of Al^{3+} and Mg^{2+} into $[SIO_4]^{4-}$ tetrahedrons sheets disrupts the crystal charge balance necessitating the surface adsorption of exchangeable cations, usually Na^{+} and Ca^{2+}, to balance the charge. When water contacts smectite (Bentonite) hydration of these exchangeable cations leading to its swelling [47]. The type of exchangeable cation determines the swelling ability of montmorillonite (smectite). Ca^{2+} have a higher charge and smaller diameter than Na^{+}, and thus tend to interact more strongly with the aluminophyllosilicates platelets, rendering them less prone to hydration. Consequently, sodium bentonites hydrate and expand easily on contact with water compared to calcium bentonites [47]. Below is a schematic representation of this phenomena [47];

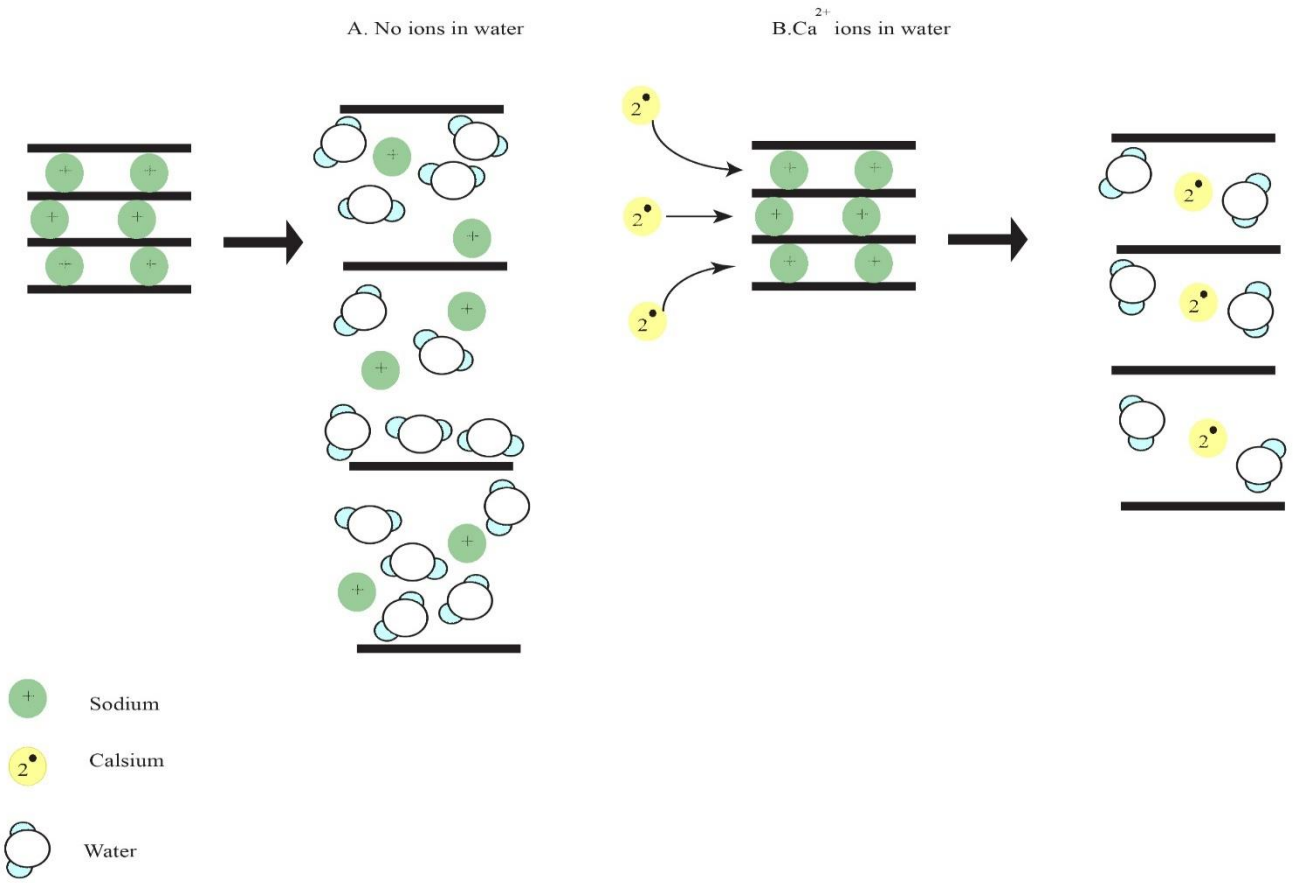

Figure 2. 10: Effect of Ca^{2+} ions in water on the expansion of sodium bentonite. (A) Water contains no ions, bentonite expands freely. (B) Calcium in the water can displace sodium and increase the bonding between bentonite platelets so that the expansion is reduced

In general, bentonite is a suitable binder, especially in applications where silica addition is merit as the case with this study due to its high adsorption capacity of water and being inexpensive as already cited above. Moreover, bentonite's impact on mechanical strength, textural properties and FTS activity of the catalyst in question will be under scrutiny. This will help validate the feasibility of iron ore as an alternative for precipitated iron-based catalyst in pilot-scale operations. The newly formulated catalyst will be deemed successful if an acceptable balance between its mechanical strength, an acceptable FT, conversion versus the ease of scale-up, operational costs and maintenance is achieved.

The decision on the best agglomeration is dependent on the application as some materials will respond well to a particular type, and others will not. Therefore, a careful analysis of both the type of material and costs of each technique must be taken into consideration before any agglomeration [48]. For our study, Pelletization was preferred because of easy access to Pelletization facility, which is in proximity to our laboratory. Dry granulator equipment is quite expensive and not manufactured locally, so the cost of the overall project would significantly increase.

2.6 Bentonite usage for FT Iron catalysts

Bentonite usage amongst FT practitioners is not well represented in the open literature, necessitating the need to close this gap. Sandeep el at studied bentonite as a binder for FT iron catalysts and his work involved developing promoted iron catalyst with copper, potassium and Molybdenum as dopants supported on Carbon nanotubes (CNT) and evaluating its effect on the mechanical strength and FT catalytic activity. The shaping of the powdered catalyst into spherical pellets was done by dry compression with varying loading of 10%, 15% and 20% respectively [8]. Furthermore, the mechanical strength tests were done to determine its suitability for application in fixed beds and compared with commercial alumina spherical catalysts. The FT reaction was performed at 270^{o}C and 21 bars respectively with syngas ratio of 2.0 in a fixed bed reactor [8]. A linear correlation between binder loading and mechanical strength is not always observed [50]. It depends on how the binder interacts with the catalysts, which in turn affect their textural properties. It is important to note that mechanical strength is related to how strongly the binder sticks to powder particles which in turn is related to the physio-chemical properties of the catalyst system [8,49, 50].

A comparative study of catalyst performance was also carried to ascertain which combination gave the optimum results for FTS. Experimental runs showed that the binder loading with 20% bentonite maintained the highest FT activity even after 70 hrs [8]. However, the powder with the binder still showed better CO conversion than all the materials with the binder additions [8]. The binder, in this case, reduced the overall CO conversion due to the reduction of iron present in the material. However, as the binder loading increased, it improved the CO conversions [8]. This trend was attributed to the growth in pore size of the material with an increase in binder loading, which in turn facilitates reducibility and thus produced more active sites for the FT reaction. On the other hand, a sharp decline in CO conversion for the pelletized catalyst with 10% and 15% loading was seen and related to change in textural properties such as high porosity and lower density [8]. It is clear to see that bentonite addition affects the mechanical strength and FT activity according to the inherent textural properties of the catalyst developed.

On the other hand, Seo et al., 2011 studied the effects of various binders on iron catalysts extrudates and evaluated their effects on catalyst performance [49]. Their catalyst preparation was into two steps; firstly, the promotion of Iron catalyst (using Iron nitrate as the precursor) with aluminium, and copper (Cu) using Co-precipitation. Then K_2CO_3 was impregnated unto the precipitate via slurry phase impregnation to produce a catalyst with following configuration 4K/ 100Fe-6Cu-16Al. Finally, the promoted catalyst was shaped using an extrusion screw to yield extrudates with a 3mm particle size. Each binder addition was 20 wt% and 80 wt% of the catalyst, respectively. The reduction was

performed with hydrogen at 450 ^{o}C at 1 bar for 12 hours whilst the FT reaction was undertaken at 280^{o}C with syngas and a pressure of 10 bar.

One of the comparisons was between solid kaolin and bentonite (solid inorganic binders) to ascertain their influence on the physicochemical properties of the extrudates and FT activity. The findings revealed that bentonite had a more significant effect on the physio-chemical properties of the catalysts such as porosity, reducibility and surface areas than kaolin [49]. A drastic reduction in surface area and porosity changes in the catalyst as bentonite increased. This was observation was ascribed to the clogging of small pores, and thus their average pore sizes increased [49]. These changes in textural properties of the catalysts, such as a reduction in surface area and porosity which influenced how the hydrogen gas was adsorbed during TPR analysis.

Furthermore, amongst the two binders, bentonite was the one that improved the reducibility of the catalysts the most. This could be related to the increase in the size of pore sizes that weaken the binder-metal interaction, thus making it easier to reduce. The FT results in this work revealed that the binders do not have a significant influence on the CO conversion and the selectivity to C5 or higher hydrocarbons were greatly affected after the addition of binders [49]. However, bentonite showed the lowest selectivity towards olefins than both the kaolin and the pure catalyst [49]. Overall the effect of these binders on catalyst performance was were not significant but mostly affected the textural properties of the catalyst as mentioned earlier.

.

The agglomeration technique used in both scenarios were dry granulation and screw extrusion respectively, which affected how the binder interacts with FT catalyst and thus influence their performance in terms of mechanical stability, activity and selectivity. Both studies used bentonite in FTS studies showed a similar trend; the addition of binder reduced the activity of the catalysts even though the first case experienced a more drastic reduction. These observations could be ascribed to the different reactions conditions and different agglomeration techniques used to shape the catalysts. Moreover, both studies showed that bentonite as binder promotes the reduction of solid FT catalysts due to agglomeration of the particles as a result of a weakened the metal-binder interactions. This is important for FTS as it facilitates the attainment of the active phase of iron FT catalysts and can improve the overall catalyst performance.

REFERENCES

1. .Dry E, M (2008). *Handbook of Heterogenous Catalysis*. [online] Available at: DOI: 10.1002/9783527610044.hetcat0150

2. Botes FG, Ciobica I.M, Ferreira A, Gibson P, Moodley D.J, Saib A.M, Visagie J.L, Westrate C.J, Niemantsverdriet J.W (2013). Fischer Tropsch Synthesis: Catalysts and Chemistry, *Comprehensive Inorganic Chemistry II*, p.p 531-537.[online] Available on: http://dx.doi.org/10.1016/B9978-0-08-097774-4-00729-4

3. Zhang Q, Kang J, Wang Y (2010). Development of Novel Catalysts for Fischer–Tropsch Synthesis: Tuning the Product Selectivity. *ChemCATChem,* 2, pp1010-1038. [online] Available on:DOI: 10.1002/cctc.201000071.

4. Van de Loosdrecht, J., Ciobîcă, I. M., Gibson, P., Govender, N. S., Moodley, D. J., Saib, A. M., … Niemantsverdriet, J. W. (2016). Providing Fundamental and Applied Insights into Fischer–Tropsch Catalysis: Sasol–Eindhoven University of Technology Collaboration. *ACS Catalysis*, 6(6), 3840–3855. doi:10.1021/acscatal.6b00595

5. Huve, J (2017). Highly selective, active and stable Fischer-Tropsch catalyst using entrapped ironnanoparticles in silicalite-1. *Catalysis*. Université de Lyon; English. <NNT: 2017LYSE1042>. <tel-01721319>

6. Jahangiri. H, Bennet. J, Mahjoubi.P, Wilson.K, Gu.S(2014). A review of advanced catalyst development for Fischer-Tropsch synthesis of hydocarbons from biomass derived syn-gas. *Catalysis Science & Technology'*. [Online] Available at: DOI:10.1039/c4y00327f

7. De Smit. E, Weckhuysen.B.M (2008). The renaissance of iron-based Fischer Tropsch on multi-faceted catalyst deactivation behaviour. *Chemical Society Review*.; 37, pp 2758-2781. [online] Available at: DOI:10.1039/b805427d

8. Badgoga S, Vosough V, Dalai A.K(2018). Performance of promoted Iron/CNT for catalyst for Fischer Tropsch Synthesis: Influence of pellet shape and binding loading; *Energy Fuels 31,* 11, p 12633-12644[Online] DOI: 10.1021/acs.energyfuels.7b01318.

9. Uberman**,** S. Žiković (2016). Gas Processing. *Evaluate GTL processes compared with conventional refining*. Available on : http://www.gasprocessingnews.com/features/201606/evaluate-gtl-processes-compared-with-conventional-refining.aspx (Accessed on 7 July 2017)

10. Dry, M. E(1990). Fischer-Tropsch process; Commercial aspects. *Catal. Today* 6, 183–206.

11. Sharypov V. I, Kuznetsov B. N, Beregovtsova N. G,.Reshetnikov O. L, Baryshnikov S. V (1996). 'Fuel 75'. *Modification of iron ore catalysts for lignite hydrogenation and hydrocracing of coal derived liquids*, 75, 1, pp 39-42. [online] Available on: https://doi.org/10.1016/0016-2361(95)00194-8

12. De Klerk. A (2011*).* Fischer Tropsch Synthesis; *Fischer Tropsch Refining;* Germany: Wiley-VCH Verlag GmbH; pp. 73-93.

13. Perrego C (2007).Development of a Fischer Tropsch catalyst: from laboratory to commercial scale demonstration,18;305-317.[Online] Available at: https://link.springer.com/content/pdf/10.1007/BF02934926.pdf.

14. van der Laan, G. P (1999).. Kinetics, Selectivity and Scale Up of the Fischer-Tropsch Synthesis. *Univ.Groningen* 1–251

15. Wei. J, Wen.Z, Xu.H, Ge.Q (2017). 'Journal of Energy Chemistry'. *Fischer-Tropsch synthesis over iron catalysts with corncob-derived promoters*. Available at: doi: 10.1016/j.jechem.2017.03.017

16. Davis, BH (1999). Technology development for Iron and cobalt catalysts: University of Kentucky research Foundation. [online] https://www.osti.gov/servlets/purl/8961

17. Hensen, E.J., Wang, P., & Xu, W. (2016). Research trends in Fischer-Tropsch catalysis for coal liquids technology. Frontiers of Engineering, 3(4), 321-330.DOI:10.15302/FEM-2016051

18. Hong. S.Y, Park. J.C, Lee.H.T, Yang. J-II, Hong. S.J, Jung.H, Chun D.H (2016). 'Journal of Nanoscience and nanotechnology'. *Nanocrystalline Iron-Ore-Based Catalysts for Fischer Tropsch Synthesis* 16,2, pp 2014-2018.Available at:DOI:10.1166/jnn.2016.12002

19. Pineau, A., Kanari, N., & Gaballah, I. (2006). Kinetics of reduction of iron oxides by H2. Thermochimica Acta, *447(1), 89–100.* DOI:10.1016/j.tca.2005.10.004

20. Cubeiro M. L, Goldwasser M. R, Perez Zurita M. J, Franco C,González-Jiménz F, Jaimes E (1994).' Hyperfine Interact 93'. *Mossbauer study of evolution of a laterite iron mineral based catalyst: Effect of the activation treatment*,pp -1831-1835.[online] Available at: DOI: 10.1007/bf02072954

21. Bae, J.-S., Hong, S. Y., Chan Park, J., Bae Rhim, G., Youn, M. H., Jeong, H., … Chun, D. H. (2018). Eco-friendly prepared iron-ore-based catalysts for Fischer-Tropsch synthesis. Applied Catalysis B: Environmental. DOI:10.1016/j.apcatb.2018.11.082

22. Y. Li, D Wu, J Zhang (2000). 'Measurement and statistics of single pellet mechanical strength of differently shaped catalysts', *Powder Technology*, 113(1–2), pp. 176–184. DOI: 10.1016/S0032-5910(00)00231-X.

23. E.David (2015).Mechanical strength and reliability of the porous materials used as adsorbents/ catalysts and the new development trends', *Archives of Materials Science and Engineering*, 73(1), pp. 5–17.

24. Wang, P., Chen, W., Chiang, F.-K., Dugulan, A. I., Song, Y., Pestman, R., … Hensen, E. J. M. (2018). Synthesis of stable and low-CO2 selective ε-iron carbide Fischer-Tropsch catalysts. *Science Advances, 4(10), eaau2947.* DOI:10.1126/sciadv.aau2947

25. Wu D, Zhou J (2007). Particle Technology and Fluidization; *Mechanical Strength of Solid Catalysts: Recent Developments and Future Prospects*;53, 10, 2618-2629. [online] DOI 10.1002l aic.11291

26. Bertolacini R.J(1989). In characterization and catalysts development, American chemical society; *Mechanical and physical of catalysts*. [online] Available at: DOI:10.1021/bk-1989-0411.ch034.

27. D. Burkur, X. Lang, D Mukesh (1990).Binder / Support Effects on the Activity and Selectivity of Iron Catalysts in the Fischer-Tropsch Synthesis, *Industrial & Engineering Chemistry Research*, 29, pp. 1588–1599. DOI: 10.1021/ie00104a003

28. H.Wan, B.Wu, X. An (2007) 'Effect of the ratio of precipitated SiO_2 to binder SiO_2 on iron-based catalysts for fischer-tropsch synthesis, *Catalysis Letters*, 119(3–4), pp. 353–360. doi: 10.1007/s10562-007-9244-0.

29. Huazhang, L (2013). *Ammonia Synthesis Catalysts: Innovation and Practice*. Singapore: World Scientific Publishing Co. Pte. Ltd. and Chemical Industry Press. pp 712-716

30. S Patra#, A. Kumar, R. Venugopal (2017). The Effect of particle size on the green pellets properties of iron ore; *Journal of Mining and Metallurgy*, 53 A (1) (2017) pp 31 – 41.

31. Weaver, K.F; Morales, V.C; Dunn. S.L; Godde, K; Weaker, P.F(2018). An Introduction to Statistical Analysis in Research: With Applications in the Biological and Life Sciences; John Wiley & Sons, *First Edition;* NW, USA; pg 353-392. DOI:10.1002/9781119454205

32. Abernethy, R. B (2006).The New Weibull Handbook- Reliability and Statistical Analysis for Predicting Life, Safety, Supportability, Risk, Cost and Warranty Claims. 5 th ed. Abernethy, R. B .North Palm Beach, Florida , pp 1.1-4.25.

33. Pham, H (2006). Springer Handbook of Engineering Statistics; *Springer*-Verlag, London; pp 3-75

34. de Jong, K.P.,(2009). Synthesis of solid catalysts, Wiley –VCH, 10.1002/9783527626854

35. Datsiou, K. C., Overend, M. (2018). Weibull parameter estimation and goodness-of-fit for glass strength data. Structural Safety, *73, 29–41*.doi: 10.1016/j.strusafe.2018.02.002

36. Hristopulos, D., Petrakis, M., & Kaniadakis, G. (2015). *Weakest-Link Scaling and Extreme Events in Finite-Sized Systems. Entropy, 17(3), 1103–1122*.doi:10.3390/e17031103

37. Van de Loosdrecht, J., Botes, F. G., Ciobica, I. M., Ferreira, A., Gibson, P., Moodley, D. J., … Niemantsverdriet, J. W. (2013). *Fischer–Tropsch Synthesis: Catalysts and Chemistry. Comprehensive Inorganic Chemistry II, 525–557*.doi:10.1016/b978-0-08-097774-4.00729-4

38. Daisyme, P (2018).'*Understanding the financial cost downtime in manufacturing*', Due 18 June. Available on:https://due.com/blog/understanding-the-financial-cost-of-downtime-in-manufacturing/

39. Geankoplis, C.J.(2008). *Transport Processes and Separation Process Principles*. (2008). 4th ed. Upper Saddle River, NJ: Prentice Hall, Pearson Education, pp.125-130.

40. Richardson, J.T., (1989). Principle of catalysts development, Plenum Press,

41. Ertl, G., Knozinger, H., Weitkamp, J., (1997). Handbook of Heterogeneous Catalysis Vol 1, Wiley – VCH,

42. Farrauto, R.J., Bartholomew, C.H., (1997). Fundamentals of Industrial Catalytic Processes, *Blackie Academic & Professional*,

43. Gorimbo J, Muleja A.A, Liu X, Hildebrandt D (2018). Fischer-Tropsch: product distribution, operating conditions, iron catalyst deactivation and catalyst speciation. International Journal of Industrial Chemistry.[Online] Available on: https://doi.org/10.1007/s40090-018-0161-4

44. Luque. R, De la Olsa. A, Campelo. J.M, Romero A.A, Valverde.J.L, Sanchez. P (2011). Design of development of catalysts for Biomass-to-liquid-Fischer-Tropsch (BTL-FT) process for biofuels production. *Energy & Environmental Science*, 5, pp 5186-5202. [Online] Available on: DOI 10.1039/c1ee02238c

45. Eisele T.C, Kawatra, S.K (2003): A review of binders in iron ore pelletization, Mineral Processing and Extractive Metallurgy Review,, 24:1, pp1-90 [Online] Available on: http://dx.doi.org/10.1080/08827500306896.

46. Nikai, I (2015). The Use of Iron Ore Fines in Cold-Bonded Self- Reducing Composite Pellets. *Mineral Processing and extraction metallurgy Review*, 37, pp 42-48[online] Available on: https://doi.org/10.1080/08827508.2015.1104506

47. Carrison, C; Kozicki, C. '*Pelleization vs Compaction Granulation'*, FEECO International Inc. Available on: https://feeco.com/pelletization-vs-compaction/

48. Seo, J.H., Chae, H.J., Tae, W.K., Kwang-Eun, J., Chul-Ung, K., Sang-Bong, L., Soon-Yong, J., (2011). Influence of Binder on Fe-based Extrudate as Fischer-Tropsch Catalysts. Korean Chem. Eng. Res., Vol. 49, No. 6, December, 2011, pp. 726-731

49. Ail, S. S., & Dasappa, S. (2016). Biomass to liquid transportation fuel via Fischer Tropsch synthesis – Technology review and current scenario. *Renewable and Sustainable Energy Reviews*, 58, 267–286. doi:10.1016/j.rser.2015.12.143

50. Zakeri, M., Samimi, A., Shafiee Afarani, M., & Salehirad, A. (2016). Effects of porosity and pore size distribution on mechanical strength reliability of industrial-scale catalyst during preparation and catalytic test steps. *Particulate Science and Technology*, 36(1), 96–103. doi:10.1080/02726351.2016.1220437

CHAPTER 3

EXPERIMENTAL

3.1 Materials

Iron ore powder (Fe_2O_3) was supplied by Anglo American from their Sishen tailing Dams based in Northern Cape, South Africa. Copper (II) nitrate trihydrate ($Cu(NO_3)_2.3H_2O$) and Potassium Carbonate(K_2CO_3) were purchased from Sigma-Aldrich, South Africa, Bentonite Binder was purchased from Gw mineral Resources, Johannesburg, South Africa.

Table 3.1: Materials and Safety data sheet of Bentonite binder supplied by Gw mineral Resources

SiO_2	Al_2O_3	Fe_2O_3	TiO_2	CaO	MgO	K_2O	Na_2O
67.50%	20.20%	3.80%	0.22%	0.87%	4.01%	0.76%	2.60%

3.2 Catalyst Preparation

The catalyst was synthesized according to the slurry phase impregnation method reported in the literature [1]. In this method 1 kg iron ore powder (Fe_2O_3) with particle size range of 60 to 80 microns was mixed with water and turned into a slurry in a 5L beaker. Then 42.64 g of copper (II) nitrate trihydrate was added; followed by 84.36 g of Potassium Carbonate. These additions yielded a catalyst with an atomic ratio percent relative to elemental iron of 100Fe/3.8Cu/9.6K. The subsequent slurry was stirred for 2 hours and then dried in an oven at 120^oC for 24 hours and then calcined for 4 hours in atmospheric air at 400^oC in a muffle furnace.

3.3 Pelletization of Promoted ore

The first batch for Pelletization was prepared first by weighing 300 g of bentonite (10 % binder addition) and then adding to 3kg of catalyst Powder labelled 100Fe/3.8Cu/9.6K. The mixture was thoroughly mixed and then fed to the pelletizing disk. The same procedure was followed for the preparation of the catalysts containing 15 % binder (450g of bentonite addition) and 20 % binder (600g of bentonite addition). The powder 100Fe/3.8Cu/9.6K was pelletized in a rotating disk using bentonite as the binder. The binding additions were varied by 10, 15 and 20 wt.% to determine the optimum catalyst-binder combination for the highest mechanical strength. This involved weighing of powder

and binder in the specified ratio, followed by thoroughly agitating the mixture. The mixture was then loaded to the pelletizer (rotating drum). Water was sprinkled to initiate sticking of fine particles and subsequent coalesce of seeds. The formed pellets were then sieved, and the undesired particle size range was re-loaded to the pelletizer to achieve the designed particle size range (2mm to 3mm). For convenience, the samples have been denoted as 10B for the catalyst containing 10% bentonite binder ,15B for the catalyst containing 15% bentonite binder and 20B for that containing 20% bentonite binder Fig 3.1 depicts the overall schematic representation of the catalyst development for this work.

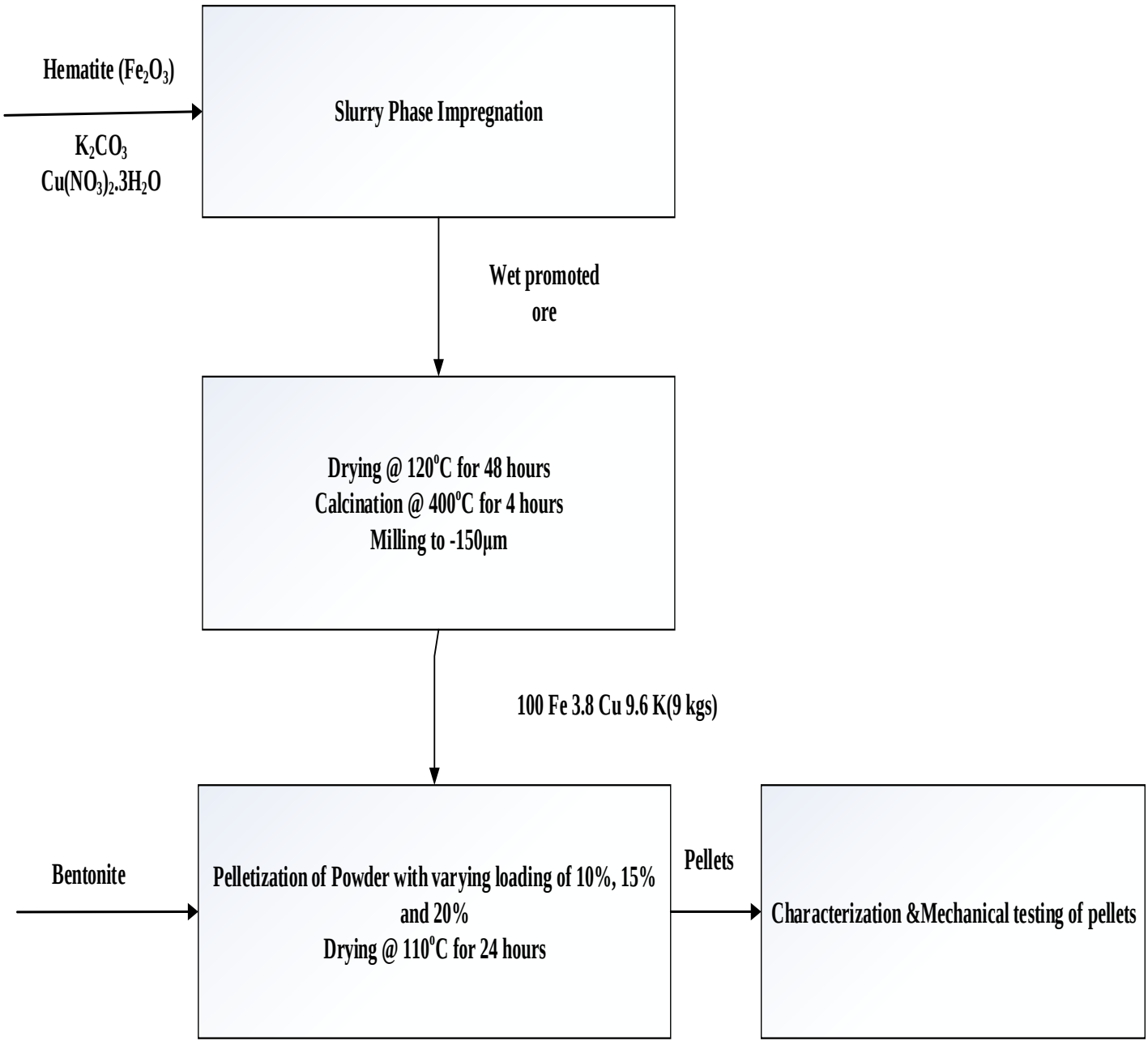

Figure 3. 1: Overall catalyst design of this study

3.4 Mechanical testing of Pellets

The single pellet crushing testing method (ASTM D 4179) was the standard used to assess the compressive strength of each solid catalyst [2]. A Force gauge (FG-5052 model) with a maximum load measurement of 300N/pellet was used to evaluate the mechanical strength of the pellets in work. Testing of the mechanical strength of solid catalysts involved the placement of a pellet in between the anvil of the transducer and movable piston of the strength tester which crushed the pellet. The force required to break the solid catalyst was then displayed on the computer connected to the Force Gauge. A total of 20 pellets from 10B, 15B and 20B batches were tested using this method and then analysed statistically to determine which was the best option for this work.

3.5 Characterization of catalyst

3.5.1. BET

The formulated catalysts and binder's surface area, pore volume and pore diameter were measured by N2 physisorption at -196^{o}C using the Brunauer-Emmett-Teller (BET) method using the Micrometrics ASAP 2460 instrument. N_2 gas was used for degassing the samples at 190^{o}C for 8hrs before the actual measurement of the textural properties. The BJH (Barrett, Joyner and Halenda) technique to estimate the pore volume and pore diameter of the samples while the BET technique was used to estimate the surface areas.

3.5.2 TPR

Temperature Programmed Reduction (TPR) of the samples was performed using Micrometrics Auto-ChemII chemisorption analyser to determine their reducibility. This analysis was undertaken by weighing approximately 0.1g of the samples and placing into the instrument under a flow of 10%H_2/90%Ar at a volumetric flow rate of 50mL/min. A ramping temperature of 10 ^{o}C/min was used during this analysis, and the TRR temperatures ranged from 100 ^{o}C and 900^{o}C. The consumption of H_2 was quantified by the TCD signal and automatically recorded on the computer linked to the instrument.

3.5.3 XRD

The pulverized catalyst samples were loaded into sample holders and placed into the PANalytical X'pert Pro powder diffractometer to measure their crystallinity. The diffractometer used a Bragg-Brentano geometry with Cu Kα radiation (λ=0.15405 nm) at 40 kV and 40mA between a range of 2θ angle from 4 to 90 degrees. The X'Celerator detector was attached to diffractor beam monochromator

to reduce high fluorescence background caused by iron mineral phases. The raw P-XRD patterns were predicted using ICDD PDF-4+2015 and High score (Plus) software.

3.5.4 XRF

The catalyst samples chemical composition was measured by the PANalyticall Axios Fast 1 MagiX PRO X-Ray Fluorescence Spectrometer. The catalyst samples were crushed before analysis and loaded into XRF cups. The XRF cups with samples were then placed into XRF sample tray of Spectrometer for analysis. The samples were then excited by photons in the instrument and produced some peaks which were recorded on the personal computer (PC) connected to the instrument. The software on the PC automatically gave a quantitative and qualitative report of each element present in samples.

3.6 Fischer Tropsch Synthesis

Catalyst evaluation was carried out in a fixed bed reactor (FBR) of 204 mm length and 8mm internal diameter. All experiments were carried out at a gas hourly space velocity (GHSV) of 3.6 NL/g-cat-h, pressure of 20.85 bar (abs), reaction temperature of 270^{o}C and feed H_2/CO ratio of 2.0. The catalyst was activated for 12 hours at 350^{o}C with syngas (H_2/CO=2.0, 1.8 NL/g-cat-h) at 1.85 bar (abs). All products were analysed by an online Gas Chromatography (GC) equipped with a Flame ionization detector (FID) and two thermal detectors (TCDs). The Flame ionization detector enabled the detection of C_1-C_5 organic compounds whereas gaseous inorganic compounds CO, H_2, N_2, CO_2, were analysed using TCDs. The integrated peak areas from these chromatograms were used to quantify the amount CO/H_2 conversion into hydrocarbons. The catalyst with the strongest mechanical strength was chosen for testing in the FT reaction. The GC was equipped with three multiple sampling valves which were heated at 150°C and the detectors at 220°C. To accurately quantify the amounts of hydrocarbons formed, calibration was done with premixed gas with knows molar ratios which is presented in Table 3.2. The amounts of the products will then be given by determining the relationship between the size of a peak for a known amount of analyte in a standard against the amount of that analyte in a sample of unknown concentration [4, 8]. The quantities of C_1 and C_2 hydrocarbons were determined directly and the remaining hydrocarbons in the gas phase were calculated using the calibration for C_2 and the corresponding response factors [8].

Table 3. 2 Response factors for hydrocarbons products [8]

Carbon number	Olefin	Paraffin
2	1	1
3	0.7	0.74
4	0.55	0.55
5	0.47	0.47
6	0.4	0.4
7	0.35	0.35
8	0.32	0.32
9	0.28	0.28
10	0.24	0.24
11	0.21	0.21
12	0.19	0.19
13	0.18	0.18
14	0.17	0.17
15	0.15	0.15

The data collected from the on-line GC was quantitatively processed. Nitrogen (10 vol % of N_2) contained in syngas feed of FT experiments was used as the internal standard for the measurements of TCD data.

Typical chromatograms from the TCDs and FID are given in Figures 3.2 to 3.4 , respectively.

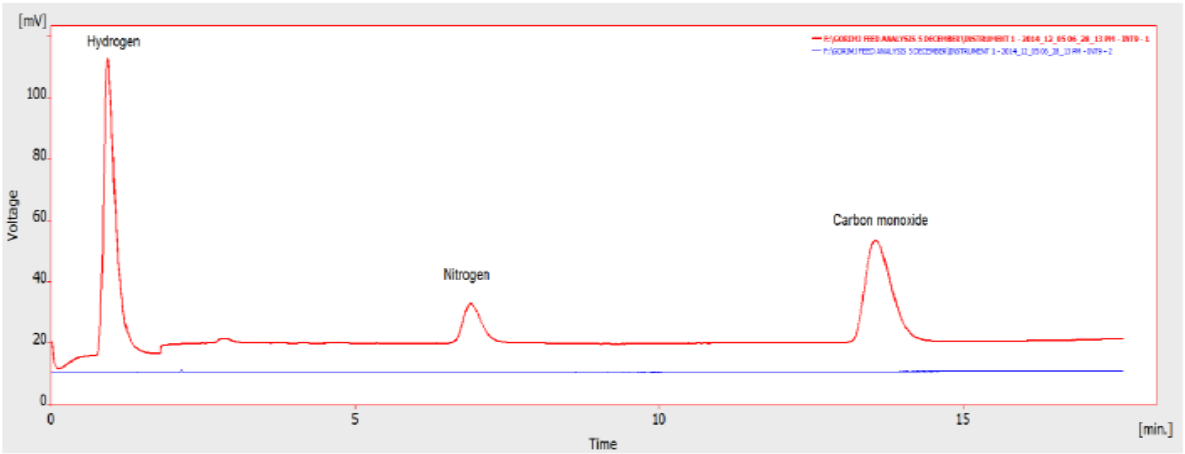

Figure 3. 2: Typical online analysis of the syngas (red line from TCD detector and blue line from that of FID).[8

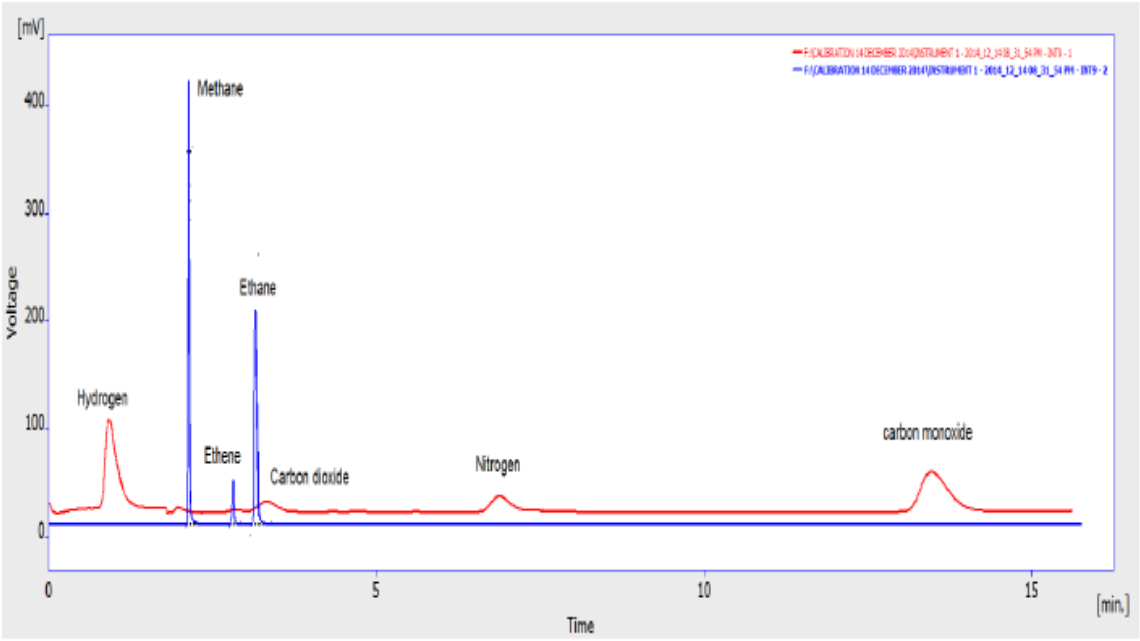

Figure 3. 3: Typical online analysis of the calibration gas (red line from TCD detector and blue line from FID) [8]

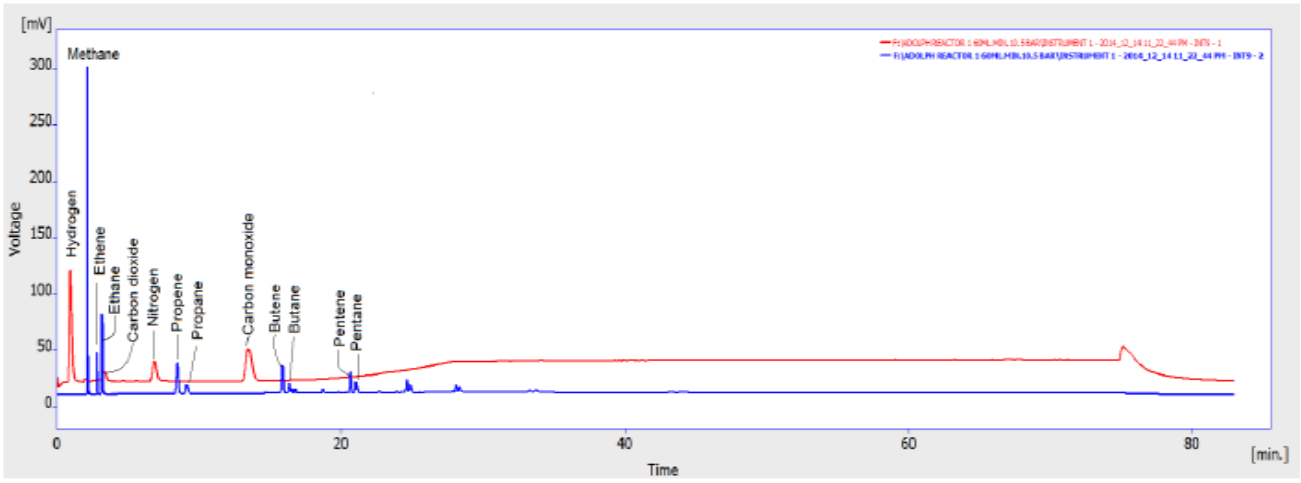

Figure 3. 4: Typical online analysis of the tail gas (red line from TCD detector and blue line from FID) [4]

Once the molar flow rates of the various reactants and products were determined, then conversions and mass balance calculations were calculated [4, 8]. Mass balance calculations including the conversion of reactants CO and H_2 were determined using the equations below [4, 8];

$$\% \boldsymbol{CO} = \frac{\boldsymbol{F_{in}X_{co,in} - F_{out}X_{co,out}}}{\boldsymbol{F_{in}X_{co,in}}} \quad (3.1)$$

Where $X_{co,\,in}$ and $X_{co,\,out}$ are the molar fractions of CO in the reactor inlet and outlet, whilst F_{in} and F_{out} are the molar flow rates of gas in and out of the reactor[4]. The CO consumption rate, (mol/(min g-cat), was calculated using the following equation[4];

$$\boldsymbol{r_{CO}} = \frac{\boldsymbol{F_{in}X_{co,in} - F_{out}X_{co,out}}}{\boldsymbol{m_{cat}}} \quad (3.2)$$

Where m_{cat} is the mass of the catalyst used in the reaction, in grams

The rate of formation of product θ_i, mol/(min.g.cat) mathematical represented as [4, 6];

$$\boldsymbol{r_{\theta_i}} = \frac{F_{out}X_{\theta_i,out}}{m_{cat}} \quad (3.3)$$

Where $X_{\theta i,\,out}$ is the molar fraction of θ_i in the reactor outlet gas stream. The product selectivity for species θ_i, Sel (θ_i) is calculated on a moles of carbon basis , as follows[4, 6]:

$$\boldsymbol{Sel}(\theta_i) = \frac{[nC]_{\theta_i}}{-r_{CO}\,X\,t\,X\,m_{cat}} \quad (3.4)$$

Where $[nC]_{\theta_i}$are the moles of carbon in species θ_i contained in a sample of the exit of the reactor collected over time.

$$\boldsymbol{r_{FT}} = \boldsymbol{r_{CO_2}} - r_{CO} \quad (3.5)$$

Where $r_{CO}$is the rate of consumption of Carbon monoxide, r_{CO_2} is the rate of formation of carbon dioxide; $\boldsymbol{r_{FT}}$ is the Fischer Tropsch (FT) rate of formation

$$\boldsymbol{FT\ selectivity} = \frac{\boldsymbol{r_{CO} - rCO_2}}{r_{CO}} = \frac{-r_{FT}}{r_{CO}} \quad (3.6)$$

REFERENCES

1. Bae, J.-S., Hong, S. Y., Chan Park, J., Bae Rhim, G., Youn, M. H., Jeong, H., Chun, D. H. (2018). Eco-friendly prepared iron-ore-based catalysts for Fischer-Tropsch synthesis. *Applied Catalysis B: Environmental*. [Online] Available at: DOI: 10.1016/j.apcatb.2018.11.082
2. Badgoga, S., Vosough, V., Dalai, A.K(2018). Performance of promoted Iron/CNT for catalyst for Fischer Tropsch Synthesis: Influence of pellet shape and binding loading; *Energy Fuels 31*, 11, pp12633-12644[Online] Available on: DOI: 10.1021/acs.energyfuels.7b01318.
3. Davis, BH (1999). Technology development for Iron and cobalt catalysts: University of Kentucky research Foundation. [online] Available on: https://www.osti.gov/servlets/purl/8961
4. Gorimbo, J., Muleja, A.A., Liu, X., Hildebrandt D (2018). Fischer-Tropsch: product distribution, operating conditions, iron catalyst deactivation and catalyst speciation. *International Journal of Industrial Chemistry*. [Online] Available at: https://doi.org/10.1007/s40090-018-0161-4
5. Okeye-Chine, C.G., Mbuya, C.O.L., Ntelane, T.S., Moyo, M., Hildebrandt, D (2019). The effect of silanol groups on the metal-support interactions in silica supported cobalt Fischer Tropsch Catalysts. A temperature programmed surface reaction; *Journal of Catalysis*, 381, pp121-129.
6. Lu, X (2012). Fischer-Tropsch Synthesis: Towards Understanding. PhD thesis. University of Witwatersrand, South Africa. Available at: http://mobile.wiredspace.wits.ac.za/handle/10539/11175.
7. Nilsson, A (2016). Wet Granulation of carbonized bio-ash. Master's thesis. Lulea University of Technology, Sweden. Available at: https://www.semanticscholar.org/paper/MASTER'S-THESIS-Wet-Granulation-of-, Carbonised-Nilsson/262beb2bc0b0b6d784cef844f118cd97691d9a41
8. Gorimbo, J (2016). An Experimental and Thermodynamic study of iron catalyst activation and deactivation during Fischer Tropsch Synthesis. PhD thesis. University of Witwatersrand, South Africa.[Online] Available at: https://pdfs.semanticscholar.org/5ca0/3004a9a57bbdffc37ed573d580ef626fc769.pdf

CHAPTER 4

4.RESULTS AND DISCUSSIONS

4.1 Characterization results related to FT Catalysts Performance

The physio-chemical properties of the proposed catalyst are discussed in this section and correlated to their mechanical and catalytic performance.

The chemical contents of the Binder (Bentonite) are presented in Table 4.1 to determine how it affected the elemental composition of the proposed catalyst. The binder is mainly composed of aluminium and silica, as shown below and influenced the physio-chemical properties of the catalysts.

Table 4. 1: Depicts the chemical composition of bentonite (binder)

Chemical	Weight percentage (wt %)
TiO_2	0.23
CaO	0.91
Fe_2O_3	3.96
K_2O	0.79
Na_2O	2.71
Al_2O_3	21.05
SiO_2	70.35

The elemental analysis of all the developed catalysts was analysed by XRF to ascertain their chemical composition and study how the binder addition affected its chemical compositions and confirm the presence of promoters in the catalysts.

Table 4. 2: XRF results of promoted iron ore(0B), 10 wt% Binder(10B), 15 wt% Binder(15B), 20 wt% Binder(20B) catalysts

Chemical	Weight percentage (wt %)				
	Raw iron ore	**0% binder Catalyst**	**10% binder catalysts**	**15% binder catalysts**	**20% binder catalyst**
Fe_2O_3	95.16	89.62	85.00	83.39	79.76
K_2O	0.042	6.41	5.23	4.78	4.87
Na_2O	0.091	0.032	0.22	0.35	0.42
Al_2O_3	1.36	0.55	2.08	2.59	3.51
SiO_2	3.29	1.42	5.32	6.60	9.01
MgO	0.054	0.036	0.30	0.44	0.61
CuO	0.088	1.93	1.92	1.85	1.83

Table 4.2 shows that the addition of the binders diluted the iron ore content in the catalyst from 89.6 wt % in the 0B catalyst to 79.76 wt% in the 20B catalysts, these results were as expected. Besides, the potassium oxide(K_2O) and CuO content also decreased from 6.41 and 1.93 wt% to 4.87 wt% and 1.83 wt% with an increase in binder loading. This was also expected because the binder addition was diluting the promoters present in the modified iron ore. On the other hand, an increase in both alumina and silica is clearly seen in Table 3 whereby the aluminium and silica weight composition increased from 1.42% wt and 3.29 % wt to 3.51 wt% and 9.01 wt% respectively. This trend was attributed to the alumina and silica that was present in the binder (Table 4.1). A similar trend is also seen in the sodium (Na) content and Copper which increased from 0.033 wt% to 0.43wt % as the binder addition increased. These XRF findings show that 10B has the least amount silica and aluminium content compared to the 15B and 20B which desirable because it would entail their Fe-Al and Fe-Si metal interactions in catalyst 10B would be relatively weaker than in its counterparts. Moreover, weaker metal interactions would favor the attainment of active phase during FT reactions, and thus 10B was a favor for this work more than the other pelletized catalysts. Temperature Programmed Reduction (TPR) analysis was done to bolster this assertion.

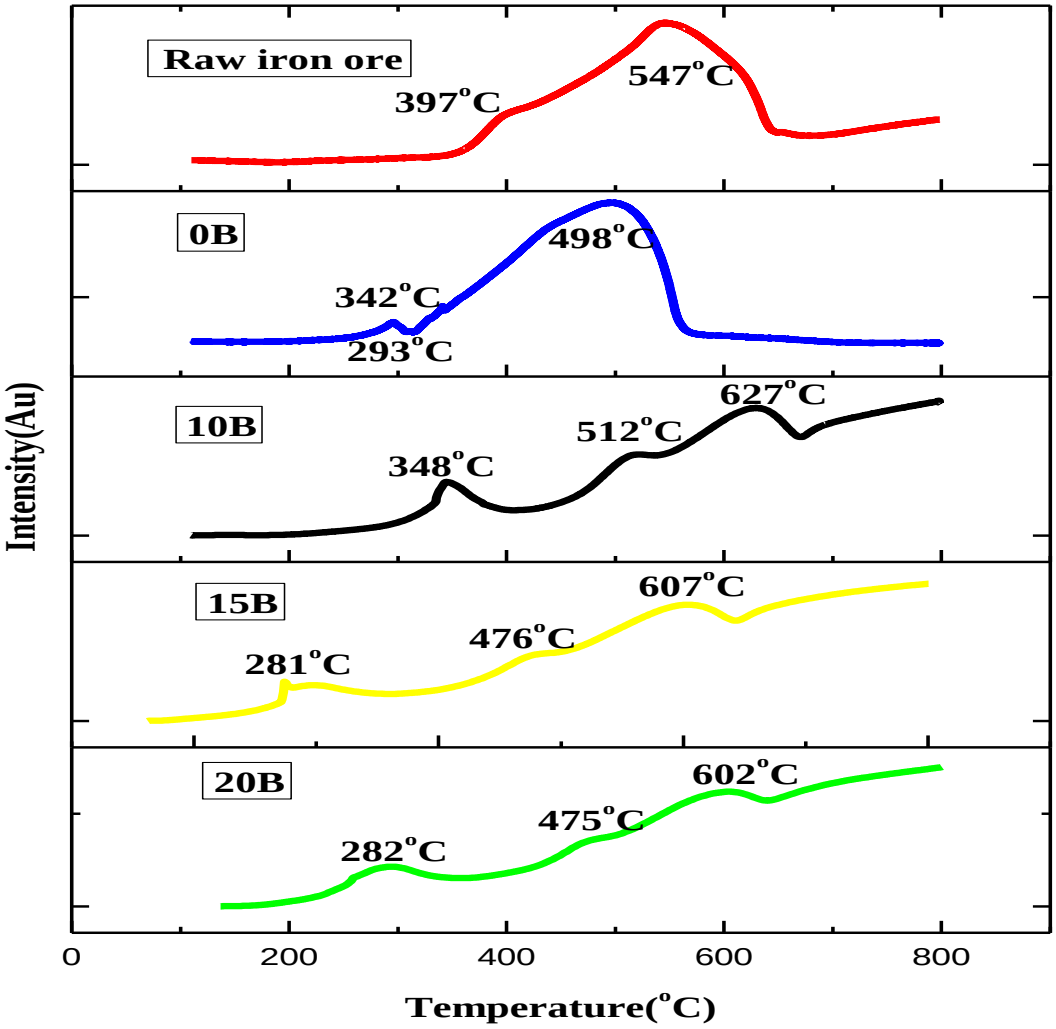

Figure 4. 1: Comparison of H_2-TPR profiles of the catalyst starting from the fresh ore up to the pelletized ore

A two-step reduction profile of the hematite raw iron ore (Fe_2O_3) was observed, as shown in Fig. 4.1. The first reduction step occurs at a temperature of ~380°C; this peak relates to the reduction of hematite (Fe_2O_3) phases to Magnetite (Fe_3O_4) phases. The second peak that appears at ~550°C is ascribed to the reduction of Magnetite (Fe_3O_4) phases to metallic iron (Fe) phases. These reduction temperatures are slightly higher than the previous work on raw ore that reported temperatures of ~325°C [3] instead of ~380°C and could be characteristic of the source of fresh ore with a different elemental composition of the current one, which in turn influences their metal-interactions. Furthermore, these TPR profiles are consistent with Fe/SiO_2 or Fe/Al_2O_3 catalysts, which could suggest that silica and aluminium present in the raw ore (Table 4.2) could be responsible for this trend [3].

The promoted iron ore showed a similar two-peak profile like the fresh iron ore. However, its peaks were observed to occur at lower temperatures in comparison to the fresh iron ore catalyst. The first reduction peak at ~280^{o}C was ascribed to the reduction of CuO to Cu [5] and confirmed that the addition of Cu promotes the reduction of iron ore phases. This was bolstered by the peak shift of the hematite phase change in the raw iron ore from ~380^{o}C to ~350^{o}C in the promoted ore (0B). This small shoulder peak at ~350^{o}C was 30^{o}C lower in comparison to the raw iron ore and confirming the positive effect of copper addition. The shoulder peak is thought to have been due to the particle size distribution of the promoted iron ore. These findings are comparable to studies in the literature for bulk iron extrudates [3, 4].

The presence of 10% wt/wt bentonite binder on the promoted (10B) resulted in an additional temperature-programmed reduction (TPR) profile comparison to raw iron ore and the promoted catalyst (OB), this result has also reported in the literature [5]. The 10B catalyst showed three distinct reduction steps; these correspond to the change of hematite (Fe_2O_3) to magnetite (Fe_3O_4) then magnetite (Fe_3O_4) to Wustite (FeO) and finally into metallic iron (Fe). The reduction peak of the hematite into magnetite was like the promoted ore(0B) and occurred at ~350^{o}C. However, a slight shift of reduction to the right by ~12 ^{o}C (~522 ^{o}C) was observed for the magnetite phase change into metallic iron in after the binder addition. As the binder addition by wt/wt in 15% and 20 %, binder catalysts increased, their reducibility decreased such that the hematite phase change into magnetite occurred at ~476 ^{o}C and ~477 ^{o}C respectively. The difficulty in reducibility was attributed to increasing in silica and aluminium content in which in turn led to stronger metal-binder interactions in the 15B and 20B catalysts which was supported by the increase Si and Al elemental content reported Table 4.2. This assertion was confirmed in the literature where extruded bulk iron catalyst that used bentonite as a binder for FT [5]. In general, these reducing temperatures are relatively high in comparison to the typical iron catalysts [3, 4, 5], which implies that the addition of binder decreases the ease of reducibility. 350^{o}C was found to be a suitable temperature to activate the 10Bcatalyst, as confirmed by TPR. As a result, 10B was most favoured for this work out of all the pelletized catalyst since it was easier to reduce compared to 15B and 20B. The ascending order of reducibility as the binder increases is attributed to its high silica and aluminium content, which strengthens metal-binder interactions. This assertion was bolstered by the XRF results whereby the silica and aluminium increased as the binder addition increased and contributing to the ascending order in reducibility as observed in the TPR profiles above. Other researchers also reported similar results in the literature [3.4,5].

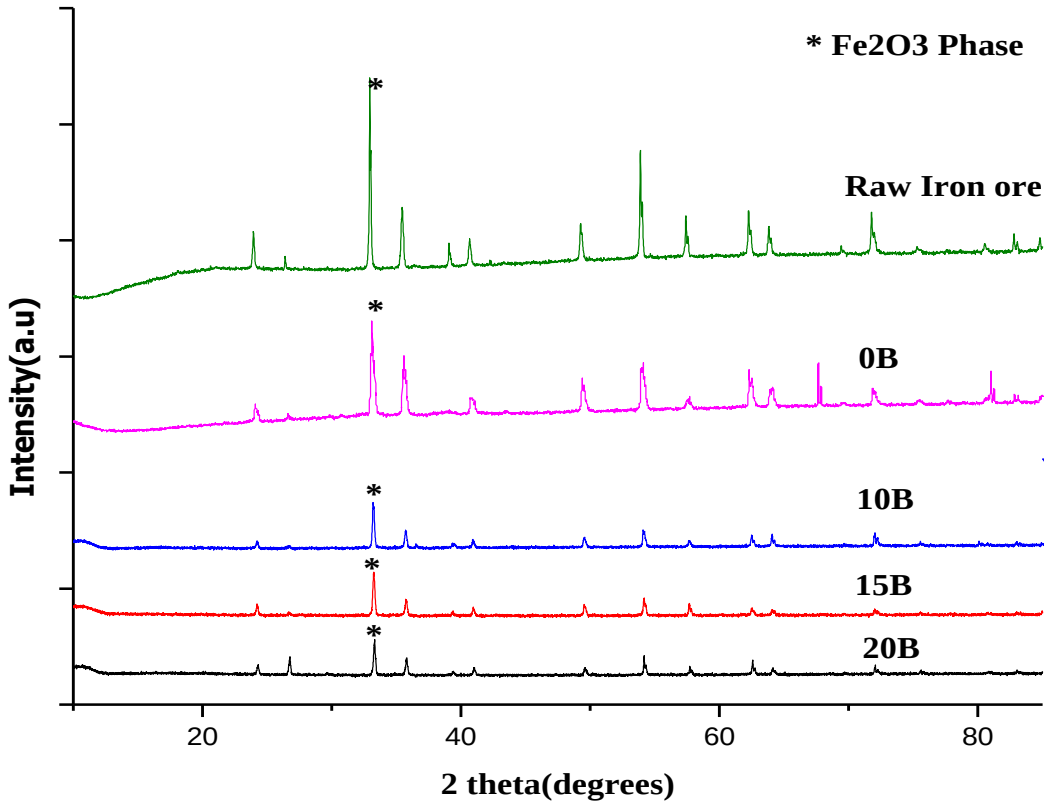

Figure 4. 2: The diffraction patterns of raw iron ore, Binder free promoted iron ore catalyst (0B), 10 wt % binder addition catalyst (10B), 15wt % binder addition catalyst (15B) and 20wt % binder addition catalyst (20B)

Table 4. 3: Crystalline and phase determination of pelletized catalyst as determined by XRD

Catalyst	Phase name	Crystallite size (nm)
Raw iron ore	Hematite	41.19
0B	Hematite	41.63
10B	Hematite	46.23
15B	Hematite	46.60
20B	Hematite	43.80

A thorough analysis of the crystallinity of catalyst systems before and after binder addition was performed with X-ray diffraction (XRD). The XRD patterns generated by powder diffractor using Cu Kα radiations is delineated in Figure 4.2, together with phase determination. The crystallite size of oxides present in the selected catalyst systems was also determined by Scherer's equation and presented in this section as well. The XRD patterns displayed show various intensities and occurrences at different peaks angles, which suggest a myriad of phases present in the samples. The prominent peaks occurring at $2\theta = 34.4^{o}$ and 40.0^{o}, confirm the presence of hematite (Fe_2O_3) in all samples and

corresponds well with the ones in literature which are reported to occur at 33º and 40.8º respectively [4]. The Tenorite (CuO) occurring at 2θ of about 39.0º and for Potassium Aluminium Silicate 2 theta of about 32.5º were identified via XRD analysis and confirmed the successful deposition of dopants unto the catalyst's surface for shaped materials. The crystallite size of the active phase(hematite) in each sample was calculated and displayed in Table 4.2. The crystallite of hematite phase in raw iron ore sample was measured to be 41.2 nm and was like the 47 nm in the literature [6]. It is clear to see that there is a crystallite size of the hematite phase in the 0B remained the same after calcination and was expected. It is also clear to see that as the binder addition did not change crystallite size of the iron ore catalysts supported by them ranging between 41 and 46.6 nm after pelletising. The XRD spectra also reveal that the increase in binder addition did not change the crystallinity of the proposed catalyst, as shown in Figure 4.2. Thus, the crystallinity of pelletised catalysts did not influence, which was the best choice.

Table 4.3 depicts the textural properties of the proposed catalyst at each stage of its development to show how the binder affected its porosity and surface area.

Table 4. 4: Summarized textural properties of all catalysts and Binder

Catalyst	**BET surface area (m^2/g)**	**Pore volume (cm^3/g)**	**Average pore diameter (nm)**
Raw iron ore	2.07	0.0023	9.72
0B	0.44	0.00018	7.147
10B	1.22	0.0033	43.85
15B	1.46	0.0044	40.51
20 B	1.49	0.0045	37.70
Binder	73.79	0.073	8.30

The figure below shows how the binder addition affected the porosity distribution of through out the catalyst synthesis.

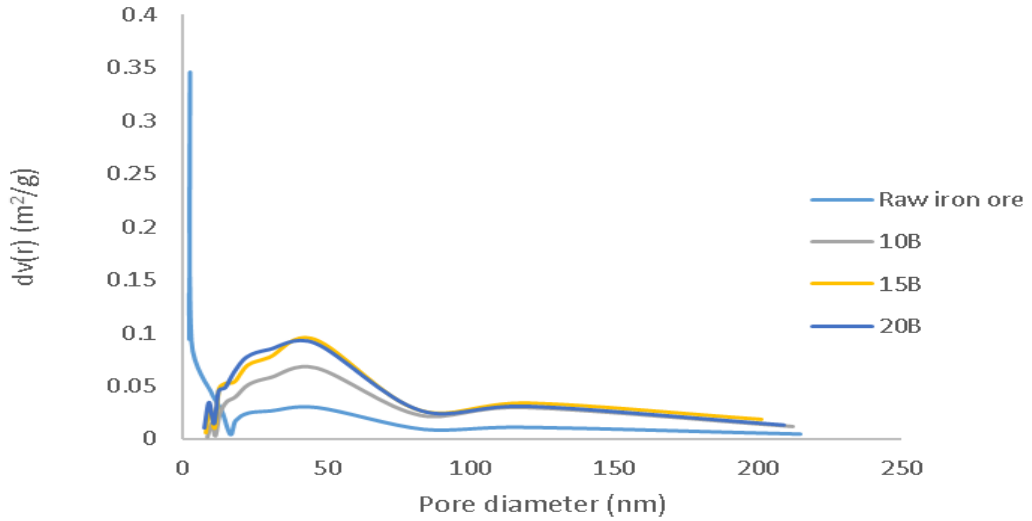

Figure 4. 3: Pore size distributions of catalysts during synthesis

The fresh powder iron ore sample shows a smaller pore size distribution compared to the solid catalysts with the binder additions, as shown in Figure 4.3. However, the catalyst without the binder incremental pore areas and pore diameters data points were not enough to plot a line graph. The blocking pores of the powder catalyst were believed to have caused this trend. Conversely, solid catalysts 10 B, 15B and 20B pattern in Figure 4.5 reveal that the was particle agglomeration and unblocking of their pores by the binder addition. Additionally, the pore size distribution of pelletized catalyst was mostly around 40-50 nm(mesoporous) confirmed by the peaks at those areas in Fig 4.3.

Table 4. 5: A comparison of chemical composition, textural properties, average crystallite size of 10% binder promoted iron ore versus similar catalyst systems in the Literature

Catalyst	Chemical Composition (g/100 Fe) [a]			Textural Properties [b]			Average crystallite Size (nm) [c]	Category (Literature or Present work) [d]
	Fe	K	Cu	BET Surface Area (m^2/g)	Pore volume (cm^3/g)	Average Pore Size (nm)		
10 B CAT	100	9.62	3.83	1.22	0.0033	43.85	46.2	Present Work
IO-CAT	100	5.28	5.43	84.7	0.312	14.7	21.5	Literature [2]
PFe-CAT	100	5.25	5.09	135	0.326	10.8	12.5	Literature [2]

[a] Analysed by XRF; [b] Analysed by N_2 Adsorption; [c] XRD Average crystallite size; [d] Category; 10B CAT denotes the promoted 10% binder pelletized ore whilst is IO-CAT promoted ore without any binder and PFe-CAT iron catalysts prepared by precipitation by the same researchers.

The textural properties of the catalyst synthesis at each step were studied to track any physical changes it undergoes the catalyst development to help relate it to the reaction studies and is summarized in Table 4.3. It is evident see from the summarized results that there was a drastic drop in BET surface area and pore volume of the precursor by 79% and 92% respectively; which was attributed to the blocking of pores during the promotion of the raw ore and thus needed enhancement before its application for FT. On the other hand, a comparison between the promoted ore and the 10% as revealed in the summarized results indicate an improvement in the BET surface area and pore volume respectively which was credited to milling before Pelletization process [3, 7]; unblocking the pores of its precursor. The improvement in surface area and pore volume can be ascribed to the addition of the binder as seen Table 4.3; the binder has a very high surface area of 73.79 m^2/g and 0.073 cm^3/g so when it combines with 0B catalyst the increment in these two textural properties is apparent.. Moreover, this trend continues as the binder increases and is showed by an increase of both BET surface of 15B and 20B catalyst from 0.44-1.22 m^2/g and 0.00018-0.0033 cm^3/g, respectively. It is noteworthy to cite that the binder additions to the promoted iron ore catalyst increased their pore sizes from 9.72 to 43.5 nm but the still mesoporous range (2 -5 0 nm pore sizes) and thereby deemed suitable for surface reactions including FTS. The 15% and 20% binder catalysts' textural properties were comparable to the 10 Binder catalyst, so a statistical analysis of mechanical strength of pelletized materials was used to decide which catalyst was suited for micro-scale studies and the ones for upscaled operations. On the contrary, the textural properties of the 10B CAT in Table 4.4 showed inferior properties compared analogous work reported in the literature, owing to the difference in raw iron ore sources. Raw iron ore was sourced locally from Sischen Mines, South Africa, while the one reported in the literature was from South America [3]. The raw iron ore utilized in this work already from the onset had very low surface areas compared as discussed earlier, which was carried over throughout the synthesis process, as shown in Table 4.3. The surface area and pore volume of the promoted pelletized ore were measured to be 1.22 m^2/g and 0.033 cm^3/g which much lower compared to 84.7 m^2/g and 0.312 cm^3/g to the promoted iron ore in the literature delineated in Table 4.4 [3]. Furthermore, the pore size between the pelleted ore in this study was 43.5nm compared to 14.7 nm reported in the literature [3] was more than three-fold and confirmed the particle agglomeration ascribed to the binder addition. These textural properties were also not comparable to precipitated iron catalysts reported in the literature [3] but exhibited comparable FT activity to both catalyst systems and justified its application for this type of work.

4.2 Statistical Analysis of Mechanical Strength Results

4. 2.1 Single Pellet Crushing Tests results

The single pellet crushing strength mostly accounts for the compressive stresses that a catalyst undergoes before and during the reaction; which plays a vital role in catalyst manufacturing. Moreover, single pellet crushing strength is a strong function of how the starting material bonded during the shaping of the catalysts. As a result, a depend on the binder (Bentonite) addition and many other factors which will be discussed later in this section. This investigation varied the binder additions by 10, 15, and 20 % respectively. It is noteworthy to cite that the single pellet testing was done using a pellet size of 2-3mm for all three batches.

Table 4. 6: Physical properties of catalyst (Fe/K/Cu) with binder(B) before Reduction

Catalyst	Density (Kg/m^3)	Force measurement by Force gauge(N)	Average Single pellet Crushing Strength (kPa)	Porosity (%)
10B	4329	32.9±10.43	1833± 581.00	1.43
15B	4210	19.19± 5.01	1069± 279.08	1.85
20 B	4133	21.78±4.30	1213± 239.53	1.86

N.B 0B single crushing strength of 0B could not be determined because the promoted ore(0B) could not make a pellet without binder addition.

Based on the results depicted in Table 4.5, 10% binder addition yielded the strongest the single pellet crushing strength of 1833 Kpa, which is more than three-fold the recommended strength of commercial alumina spherical pellets [4]. Moreover, both 15% and 20% binder additions exceeded the recommended single pellet crushing strength of alumina commercial spherical pellets [4], which is a good indication that all pelletized iron ore catalysts in this study are suitable for fixed-bed applications. Both 15% and 20% binder catalysts single pellet crushing of 19.19 N and 21.78 N are statistically equal due to the uncertainties depicted in Table 4.5 which means that it is challenging to state which is mechanically more robust between them. This assertion is bolstered by their porosities being 1.85% and 1.86% respectively. Furthermore, there is an inverse proportionality relationship between porosities and single pellet crushing strength, which is congruent with the literature [4,6, 8]. This phenomenon can be attributed to how the binder interacts with the solid catalyst; suggesting that higher porosity means the weaker binder and solid catalyst interaction and on the other hand the lower porosity means a stronger bond between the two. The average single pellet crushing strengths of comparable

catalysts is not enough to predict the reliability of each batch [10, 11], especially in large scale scenarios so Weibull statistics, Kruskal Wallis and Post hoc Dunn tests will help tackle this problem.

4.2.2 Kruksal- Wallis Test Results

Table 4. 7: Kruskal Wallis Test results

Kruskal Wallis Test results		
Chi Squared	**Df**	**P-value**
29.1	2	4.835 e^-07

The skew single scattered pellet crushing strengths data presented in this work were statistically analysed using the Kruskal Wallis test to determine if the batches are significantly different [9]. Moreover, Kruskal Wallis test is an alternative to the one-way ANOVA statistical tool and suitable with data that have independent variables that are ordinal(ranked) and cannot be analysed using the one-way ANOVA test [9]. The Chi-squared of 29.0844, df=2 and P-value < 0.05 from Table 4.6 means we can reject the null hypothesis and conclude that a single pellet crushing test from each batch have a significant difference.

4.2.3 Post hoc Dunn Test results

Table 4. 8: Post hoc Dunn Test Results

Post hoc Dunn Test Results	
Group comparison	**P-value**
10% binder SPCS versus 15% binder SPCS	0.00
10% binder SPCS versus 20% binder SPCS	0.00
15% binder SPCS versus 20% binder SPCS	0.12

After the Kruskal test reveals that the groups are significantly different, there is a need to perform a Post hoc Dunn test to determine which amongst the sampling groups is different [9]. Based on the results presented in Table 4.7 after performing the test above; the null hypothesis for a comparison between 10% binder loading with both 15% and 20% loadings were invalid because the p-value is less than the estimation one of 0.05. Therefore, the 10% binder addition is significantly different from the rest based on the p-values, and we can conclude it gave the best mechanical strength. We have not only considered the means but are medians by performing these two hypothesis tests.

4.2.4 Weibull Statistics

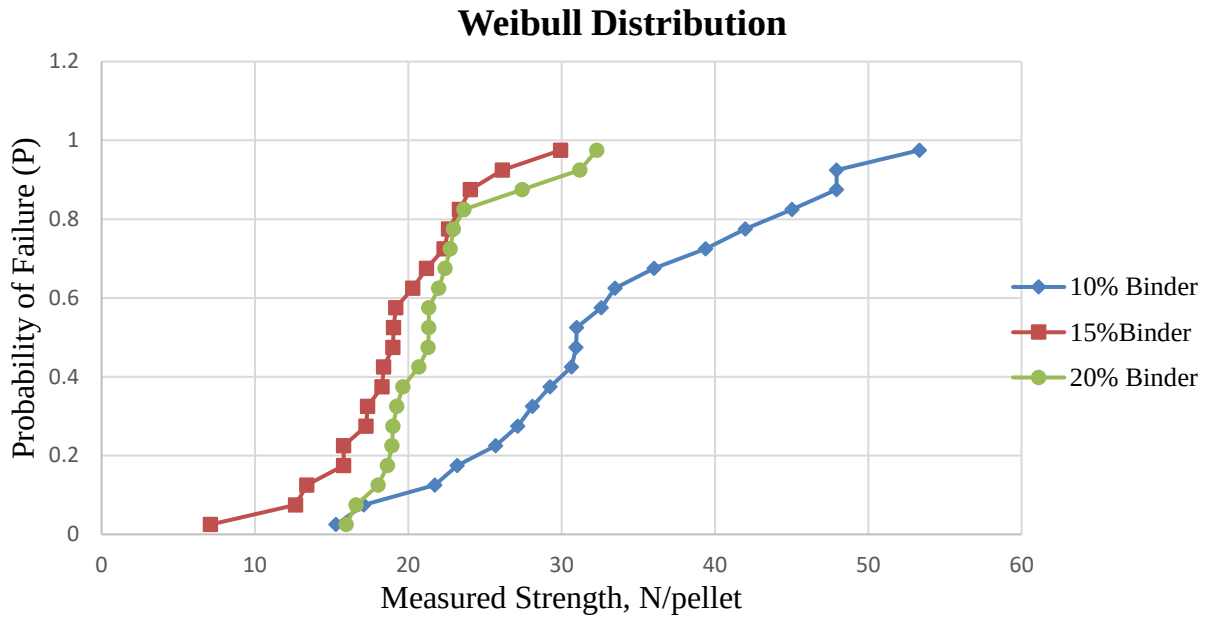

Figure 4. 4: Weibull Distribution curve for pelletized catalysts

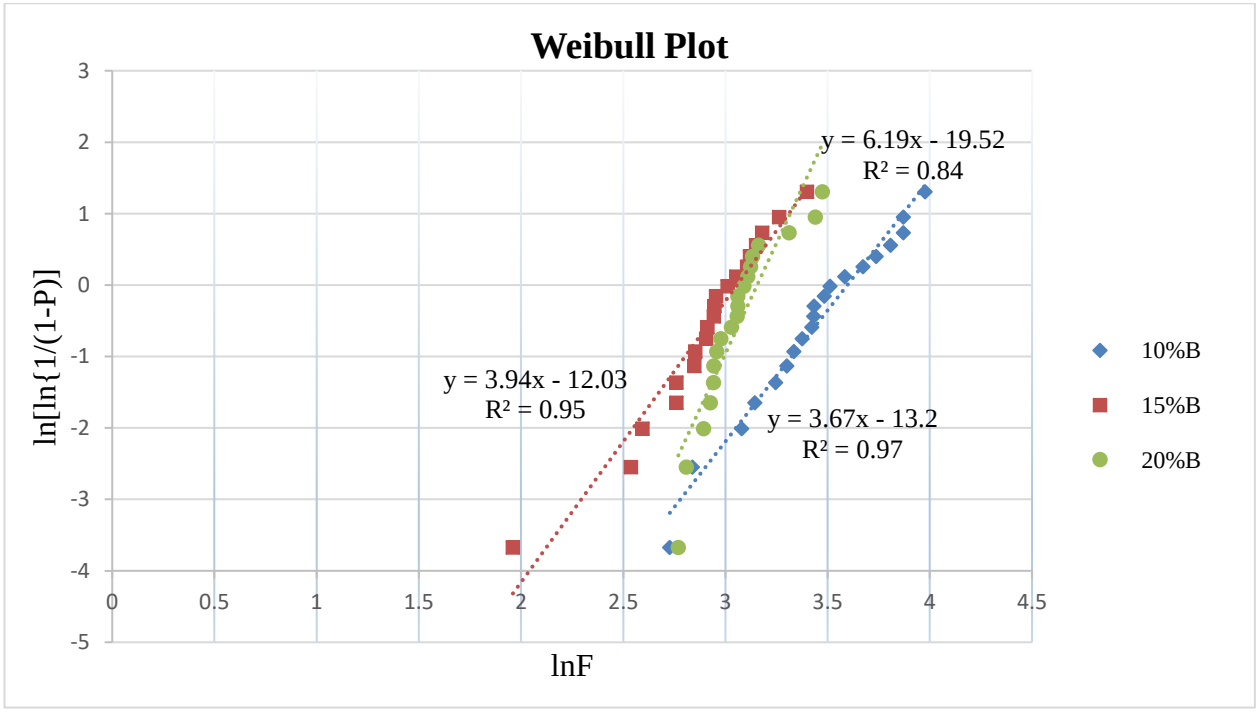

Figure 4. 5: Weibull Plots of all pelletized catalyst systems

Table 4. 9: depicts the calculation of the size parameters of each binder loading

10%Binder	**15%Binder**	**20%Binder**
-3.67 ln (F_O) = -13.2	-3.94 ln(Fo) = -12.03	-6.19 ln(Fo) = -19.52
Fo= e^[(-13.2)/(-3.67)]	Fo = e^[(-12.03)/(-3.94)]	Fo = e^[(-19.52)/(-6.19)]
= **40.68 N(2266.04 kPa**)	= **21.19 N (1180.37 kPa)**	= **23.42 N(1304.59 kPa)**

Table 4. 10: Summary of Mechanical strength testing Parameters

Binder Additions by Weight percentage (%)	**Crushing Strength**		**Weibull Modulus**	**R^2**	**Weibull Size Parameter, F_O(kPa)**
	Mean (kPa)	**Standard Deviation** (kPa)			
10B Fe/K/Cu	1832.67	581.00	3.67	0.97	2266.04
15B Fe/K/Cu	1068.96	279.08	3.94	0.95	1180.37
20 B Fe/K/Cu	1213.24	239.53	6.19	0.84	1304.59

Fig 4.4 is a graphical representation of the probability failures curve of all the shaped catalysts for this work and depicts that 10 % binder pellets(10B) can withstand a wide range of compressive strengths compared to its counterparts which agree with the Post hoc Dunn test. To put things into perspective, when a compressive force of 33.0 N is applied to 15% (15B) and 20%(20B) binder pellets, the high possibility that they fail entirely but 10% binder pellets would survive by more than 30%. Although this useful but a closer look at Weibull modulus (mechanical reliability factor) of each batch in Table 4.10 and Fig 4.5 shows that 10B has the lowest Weibull modulus which indicates that its single pellet crushing strengths are widely distributed and least reliable mechanically. Furthermore, a lower modulus signifies that this catalyst system has the most defects in the structure; such as variance in pores and dislocations with a much more complicated catalyst system [10]. This bolsters the claims made earlier that average single pellet crushing strengths is not enough to classify a catalyst system as suitable for an industrial application. However, Weibull statistics is more accurate in comparative studies of catalyst systems because it addresses the mechanical reliability aspect too. It is worth citing that all modulus of catalyst systems was within the recommended range of brittle solid materials of less 10 [10]. Weibull statistics provided relevant information to compare all three catalyst systems and facilitate the selection of the catalyst that will be the most reliable in an industrial set up.

Moreover, the mechanical reliability from an industrial standpoint favours the 20 % binder pellets compared to its counterparts. However, the FT catalytic performance will also have to be considered in selecting the best catalyst system for future upscaled fixed bed reactions. In our context, we chose 10% binder catalysts for laboratory FT reaction studies to test its applicability based on the post hoc and Weibull distribution curve as the best catalyst for reaction studies without considering the mechanical reliability aspect. This decision was made because in scenarios where FT runs were for short periods, and thus reliability of the catalysts was not as crucial. However, for future pilot-scale studies, the mechanical reliability parameter given by the modulus will be considered when applying the various catalysts with binder variations on an upscaled Fixed Bed Reactors and linked to functionality for FTS. Additionally, the Weibull reliability parameters provide relevant data for the varying binder additions of the present iron ore catalyst to be scaled-up at our pilot plant fixed beds. Moreover, Table 4.10 depicts that the two-parameter Weibull statistics was a good fit for scattered single pellet crushing strengths substantiated by the Pearson's coefficients being all very close to 1 and 10% binder catalysts was the most robust catalysts but not necessarily the most mechanically reliable.

4.3 Catalyst Performance

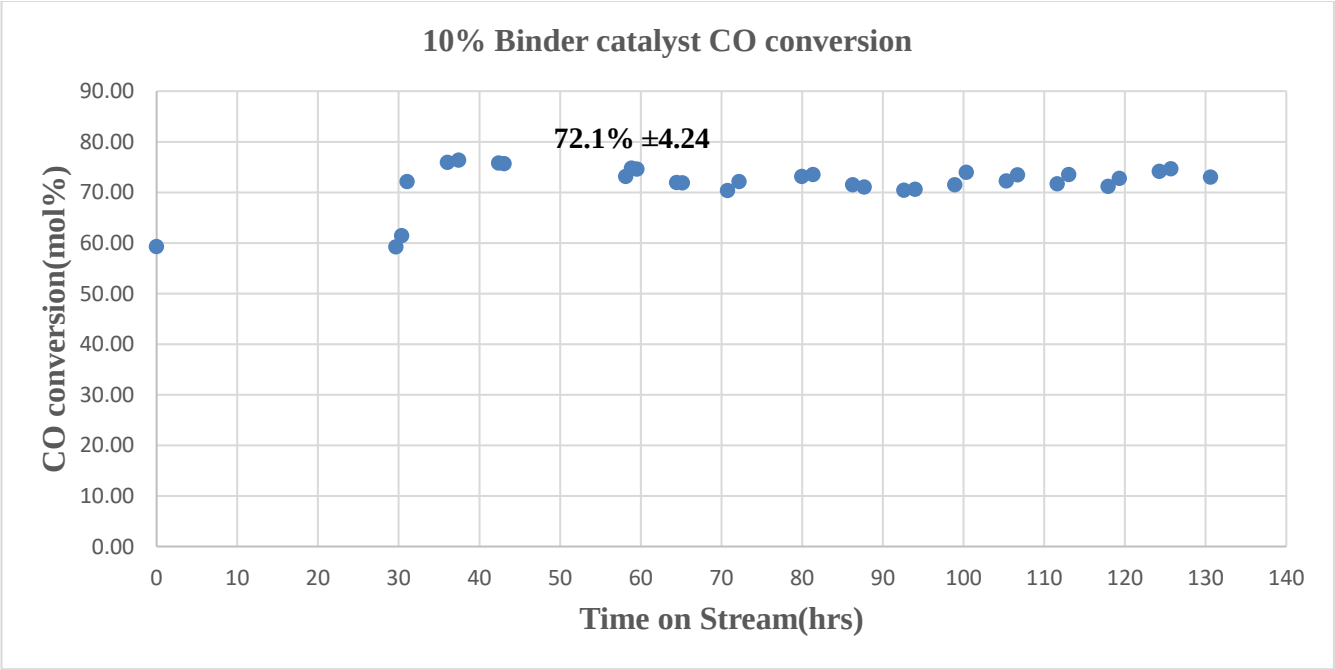

Figure 4. 6: CO conversion of 10% binder catalyst after 131h time on stream. Reaction conditions: 270ºC, 20 bar, Reduction done for 12 hours at 350 ºC, GHSV of 3.6 NL/g-cat/h (H2/CO=2.0)

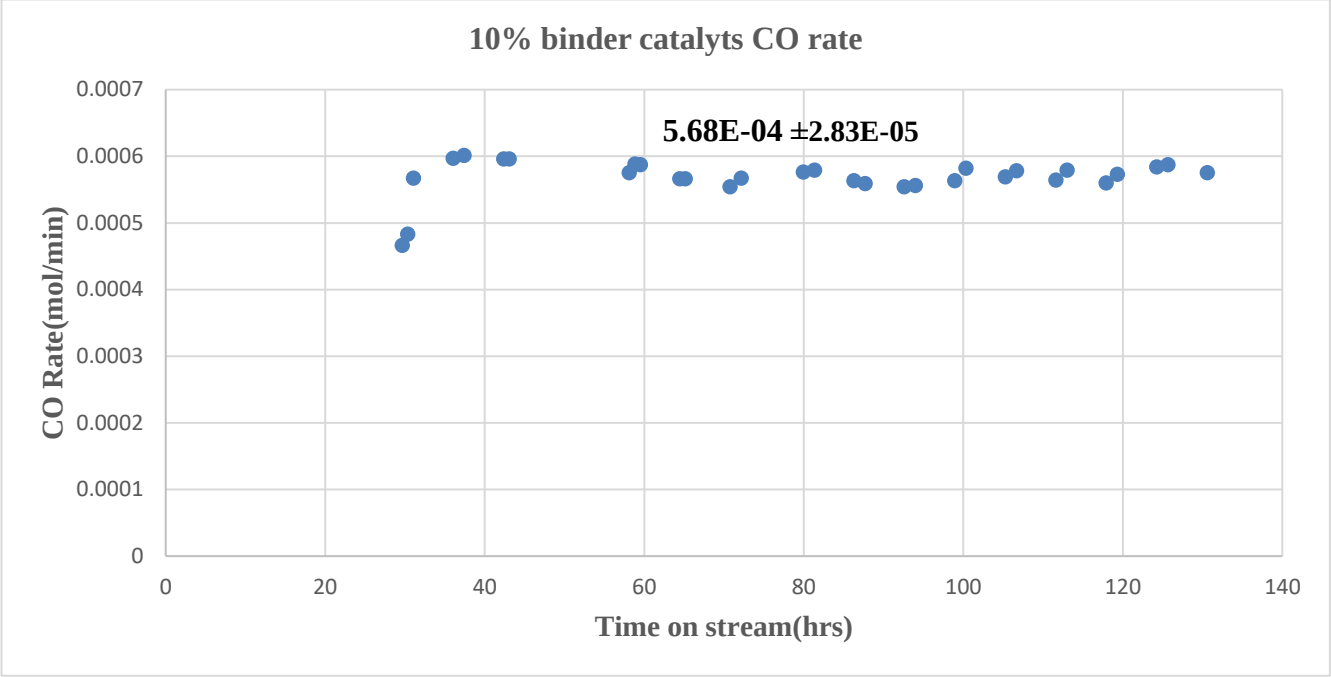

Figure 4. 7: CO rate of 10% binder catalyst after 131h time on stream. Reaction conditions: 270ºC, 20 bar, Reduction done for 12 hours at 350ºC, GHSV of 3.6 NL/g-cat/h (H_2/CO=2.0)

The catalyst evaluation of the 10% binder pellets was performed by looking at the CO conversions, selectivity, rates and other FT results. These parameters were then discussed thoroughly in this section.

The CO conversion and consumption rate of the 10% binder catalysts showed similar trends in that they both start to reach stabilize at a TOS of about 65 hrs and maintains this steady state for the rest of the experiment. This is attractive because it shows that the proposed catalyst is stable for most the time on stream and beneficial for this study where upscaling existing laboratory catalyst formulations is the main objective. The average CO conversion and rate yielded by this catalyst were 72.1% and 5.68E-06 mol/min respectively.

The 10B CAT's CO conversion of 72.1% was very close to the 75.5% reported in the literature where promoted iron ore was also used but the only difference was that the latter had no binder addition. Moreover, the 10% binder catalyst still yielded showed good CO conversion despite having inferior textural properties than other iron-based catalysts. In addition to that, the 10% binder catalyst's performance is comparable to the promoted iron ore reported by Bae et al., 2018 despite the present study has Gas Hourly Space Velocity (GHSV) of 3.6 NL/ g-cat. h compared to the 2.8 NL/ g-cat. h which means that the latter has a longer space-time (792 h) in reactor than its counterpart (351h) and thereby more reactant-catalyst time [12]. The CO conversion of 72.1% was lower to a conventional precipitated iron-based FTS catalyst (PFe-1) in the literature by the same author but they also used a

slower GHSV of 2.8 NL/g-cat.h. However, the 72.1% was still considered a good CO conversion due to its similarities with other precipitated iron catalysts (Table 4.11) which were in the range 70-81% [3].

Sandeep et al. reported a conversion of 42.4% after 70h time on stream with identical operating condition, spherical pellets [4] as the present study with also 10% binder addition by weight but the main difference was that the catalyst system was supported on carbon nanotubes and the proposed catalyst was an unsupported iron ore catalyst. The 42.4% conversion is lower than the 70.35% one of the 10B CAT after 70h time on stream, but CO rate of the same author was 1.60E-02 mol/min which much better than the 5.54E-06 mol/min reported in this work after 70h time on stream.

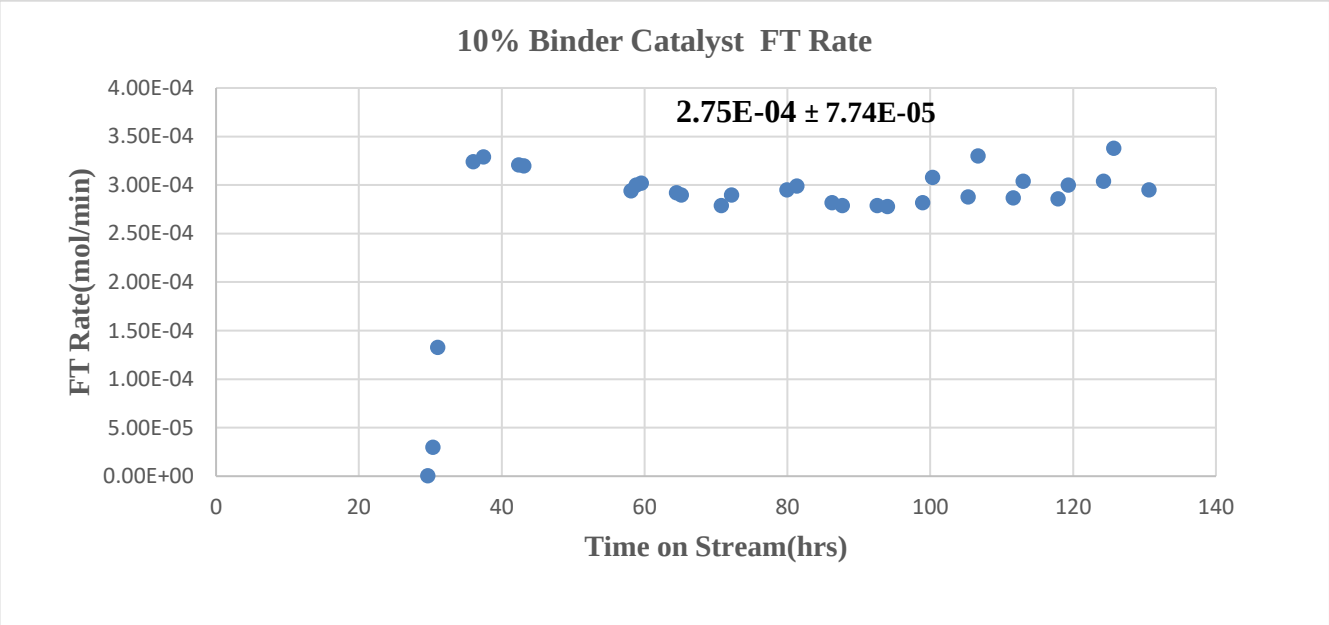

Figure 4. 8: FT rate of 10% binder catalyst after 131h time on stream. Reaction conditions: 270ºC, 20 bar, Reduction done for 12 hours at 350ºC, GHSV of 3.6 NL/g-cat/h (H_2/CO=2.0)

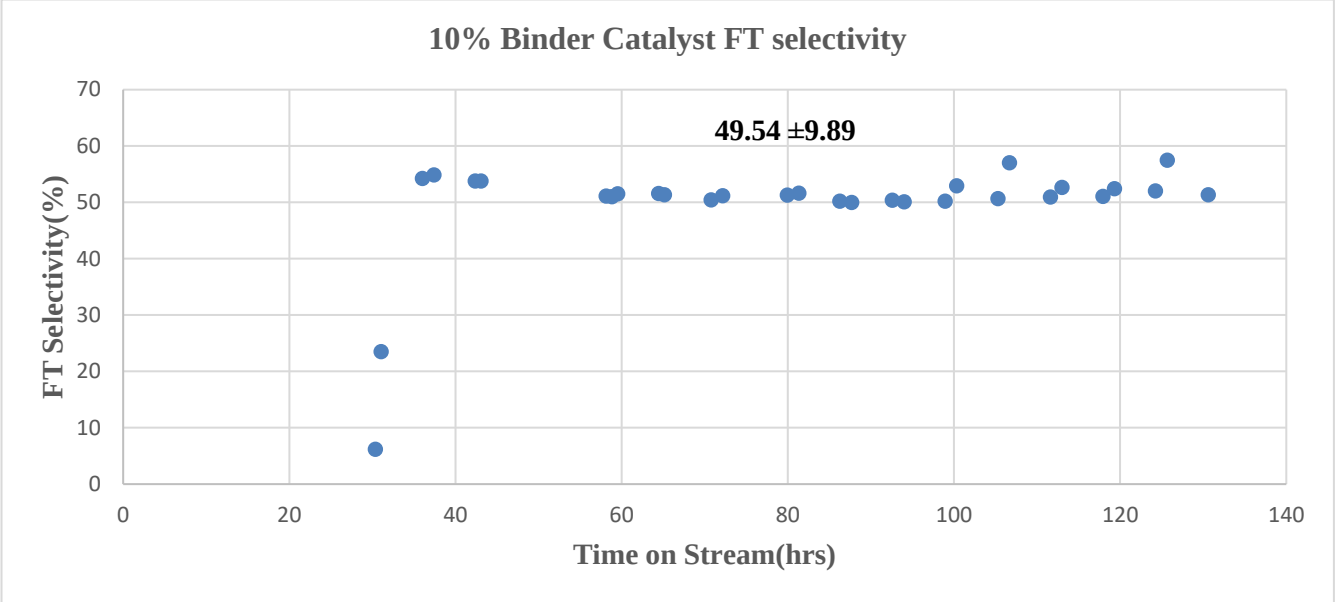

Figure 4. 9: 10% binder catalyst 's FT Selectivity after 131h time on stream. Reaction conditions: 270°C, 20 bar, Reduction done for 12 hours at 350°C, GHSV of 3.6 NL/g-cat/h (H_2/CO=2.0)

The FT rate and selectivity of 10% binder catalyst are presented in Figure 4.8 and 4.9, respectively and displayed a similar pattern. From about 30h TOS, both FT rate and selectivity start gradually increase until it starts to stabilize at about 60 h time on stream and both remain stable through the rest of the experiment. The average recorded FT rate and selectivity were 2.75E-04mol/min and 49.54% respectively. It is also apparent to see that they seem to be a correlation between the CO conversion and CO rate and the FT rate and selectivity because the latter is a function of them [6]. This implies that as the CO consumption rate changes the FT rate and selectivity responds proportionally.

The figure below shows the calculated methane rate formation of 10B CAT and discussed in this section.

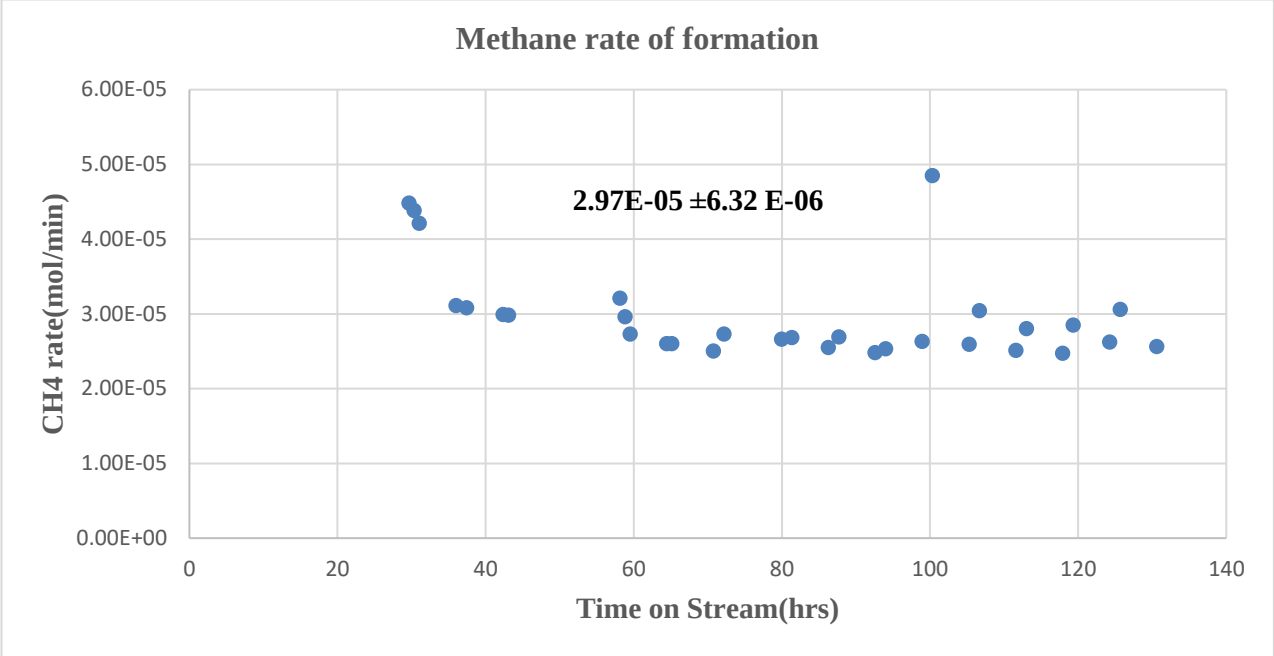

Figure 4. 10: 10% binder catalyst's methane rate after 131h time on stream. Reaction conditions: 270ºC, 20 bar, Reduction done for 12 hours at 350 ºC, GHSV of 3.6 NL/g-cat/h (H_2/CO=2.0)

The methane formation rate shows a gradual decrease from about 30h time on stream and then generally stabilized at about 60 h time on stream for the rest of the experiment and is analogous to the FT and CO consumption rates pattern reported earlier. It is apparent to see that as the CO and FT rate increase with decreasing methane rate, which is desirable for iron FT catalysts. This may imply that the rest of the reactants are being converted to higher carbon compounds and will be verified in the later section of the study.

Carbon dioxide formation rate was calculated and presented in the figure below to access the catalytic performance of the 10% binder catalyst.

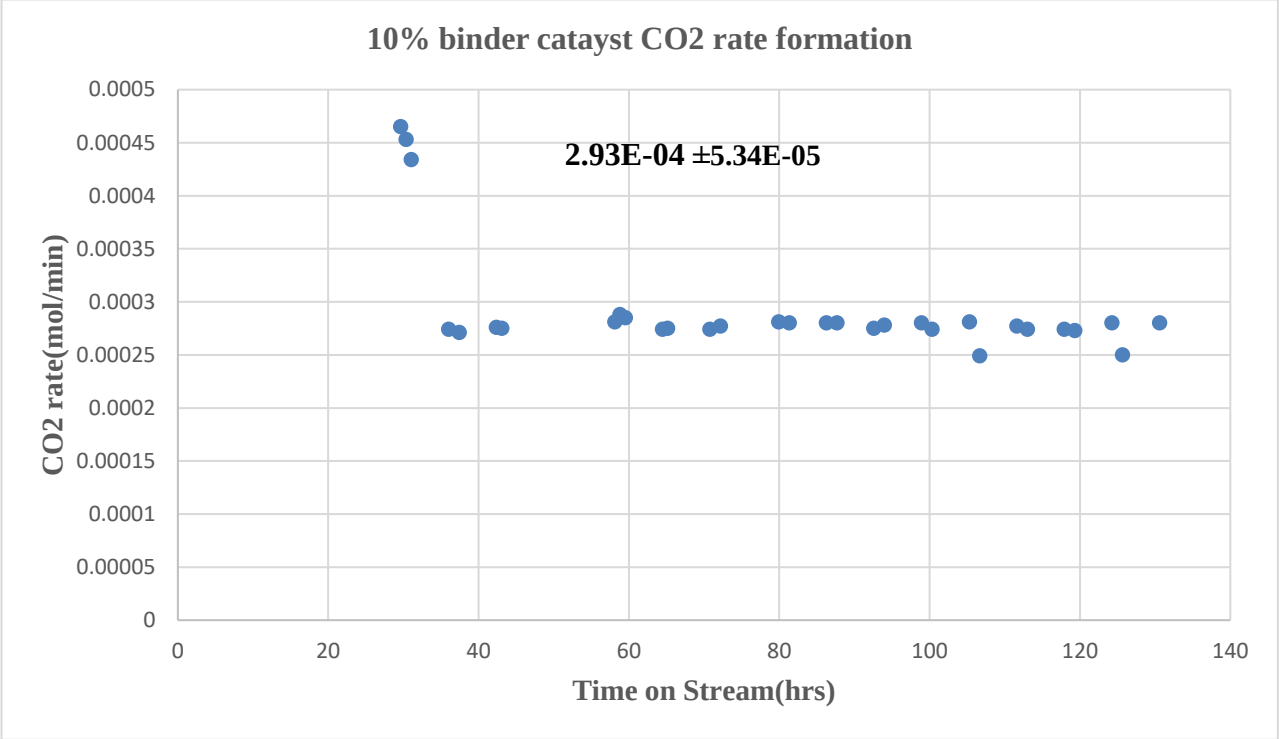

Figure 4. 11: CO_2 rate of 10% binder catalyst after 131h time on stream. Reaction conditions: 270ºC, 20 bar, Reduction done for 12 hours at 350 ºC, GHSV of 3.6 NL/g-cat/h (H_2/CO=2.0)

The CO_2 rate presented in Figure 4.11 showed a similar pattern to the methane rate where there is a sharp decrease from about 30h time on stream and started stabilizing at about 44 h time on stream. CO_2 formation rate was reported to be 2.93E-04 mol/min and stabilized for the rest of the FT run. The CO_2 selectivity will give a better indication of how this catalyst measures up against like other FT iron catalysts which will be discussed later in this chapter.

Figures 4.12-4.15 below represents the calculated rates of olefins and paraffins from C2-C5 hydrocarbons and will give insights on is more dominant in each class of hydrocarbons covered in this study.

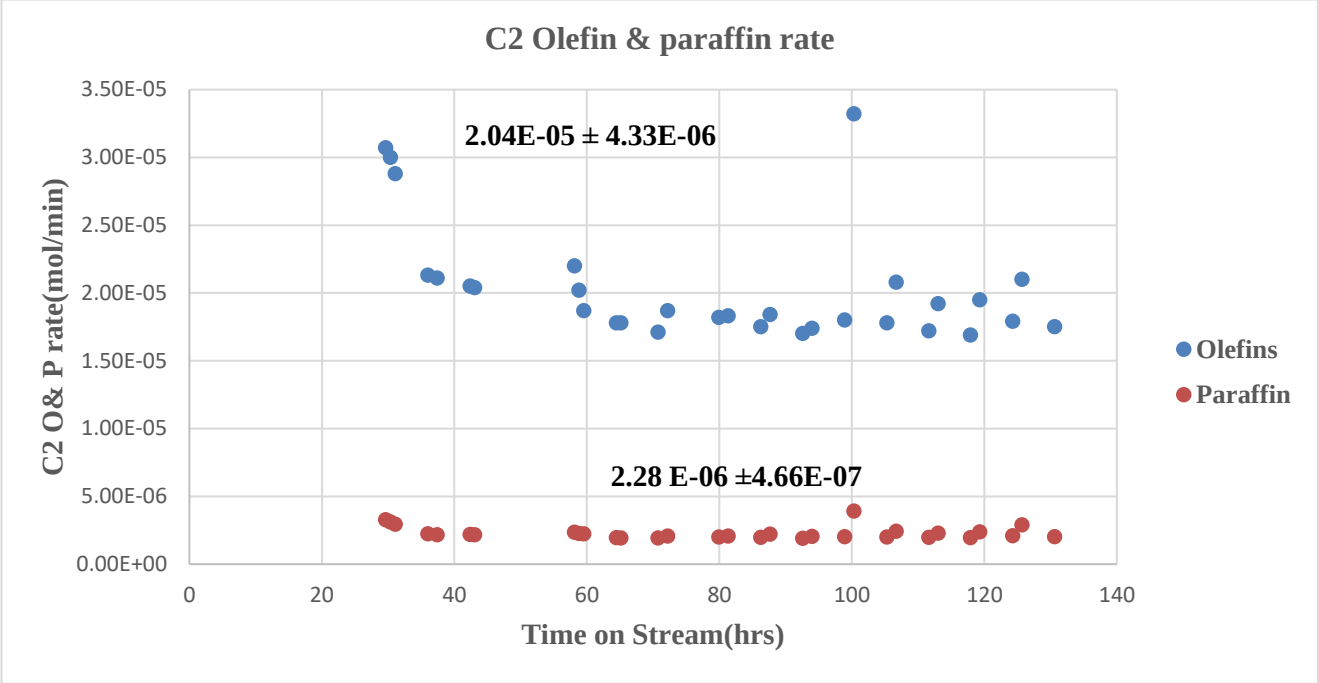

Figure 4. 12: C2 Hydrocarbon rate of 10% binder catalyst rate after 131h time on stream. Reaction conditions: 270ºC, 20 bar, Reduction done for 12 hours at 350 ºC, GHSV of 3.6 NL/g-cat/h (H_2/CO=2.0)

The formation rate of ethane displayed in Figure 4.12 shows that it is relatively stable for most of the FT run and recorded an average rate of 2.28E-06 mol/min. On the other hand, the formation rate of ethene showed a slight few spikes but was also stable for most of the experiment. It is obvious to see that the rate of ethylene is higher than ethane shown in the graph above where the mean ethylene rate was 2.04E-05 mol/min and the ethane rate was 2.28 E-06 mol/min. This suggests that the proposed catalyst produces more olefins than alkanes for the C2 hydrocarbons.

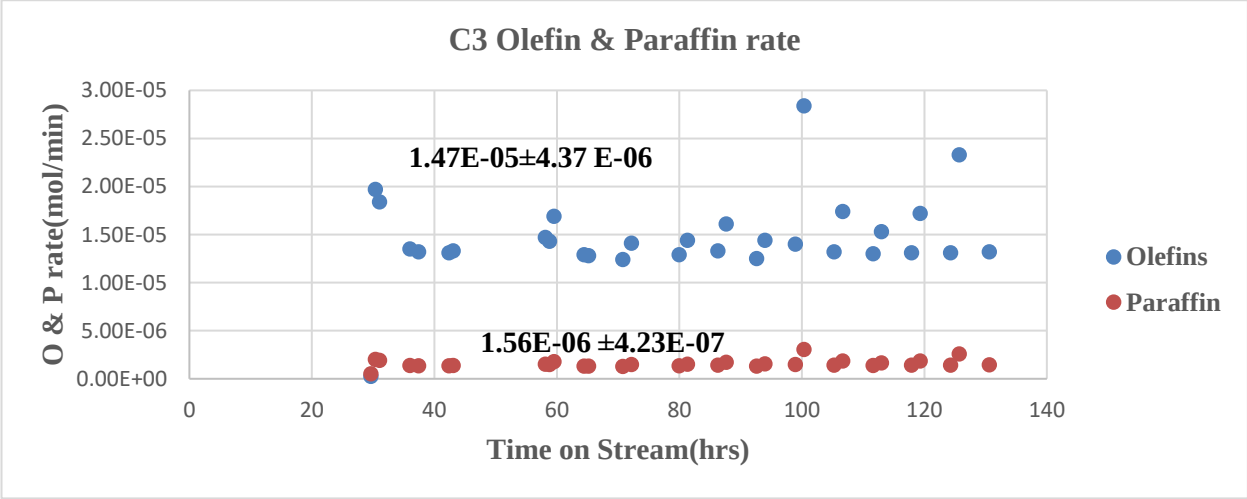

Figure 4. 13: C3 Hydrocarbon rate of 10% binder catalyst rate after 131h time on stream. Reaction conditions: 270ºC, 20 bar, Reduction done for 12 hours at 350 ºC, GHSV of 3.6 NL/g-cat/h (H_2/CO=2.0)

A similar trend is also observed in Figure 4.13 for C3 hydrocarbons as it was for the C2 hydrocarbons; whereby the propane formation rate is stable for most of the run, but the propylene formation showed a few spikes but mostly stable throughout the experiment. The olefin rate as was for the C2 hydrocarbons was also higher than that of the paraffin rate of formation with the mean propylene rate of formation found to be 1.47E06 mol/min while the propane was recorded as 1.56E07 mol/min. The proposed catalyst also favoured the formation of olefins over paraffin.

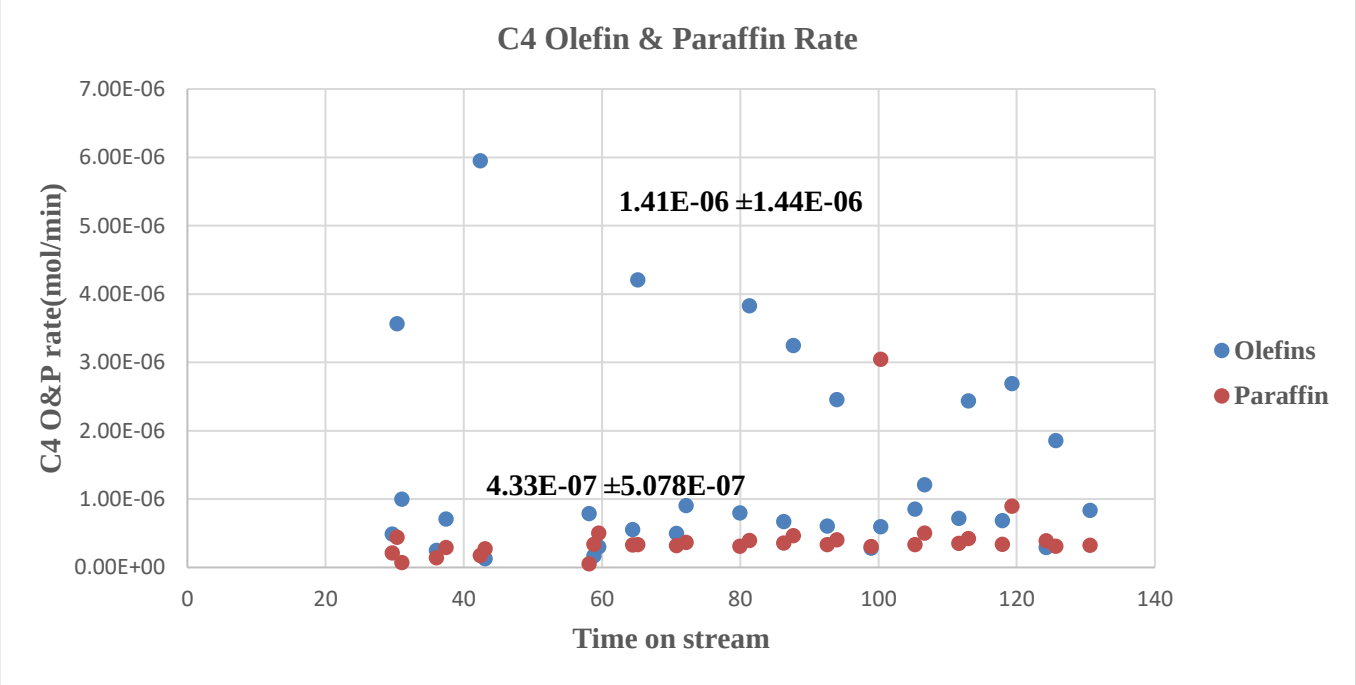

Figure 4. 14: C4 Hydrocarbon rate of 10% binder catalyst rate after 131h time on stream. Reaction conditions: 270ºC, 20 bar, Reduction done for 12 hours at 350ºC, GHSV of 3.6 NL/g-cat/h (H_2/CO=2.0)

The graph above shows the same patterns observed in C2 & C3, where the paraffin formation rate was much more stable than the olefins formation rate. The mean formation rate of 1.41E06 mol/min for butene was higher than the one of butane which was 4.33E-07 mol/min. This is congruent with the previous findings in Figure 4.12 and 4.13, where olefins formation rate dominated the paraffin one. It is clear to see that this catalyst favours more olefins over paraffin for C4 hydrocarbons.

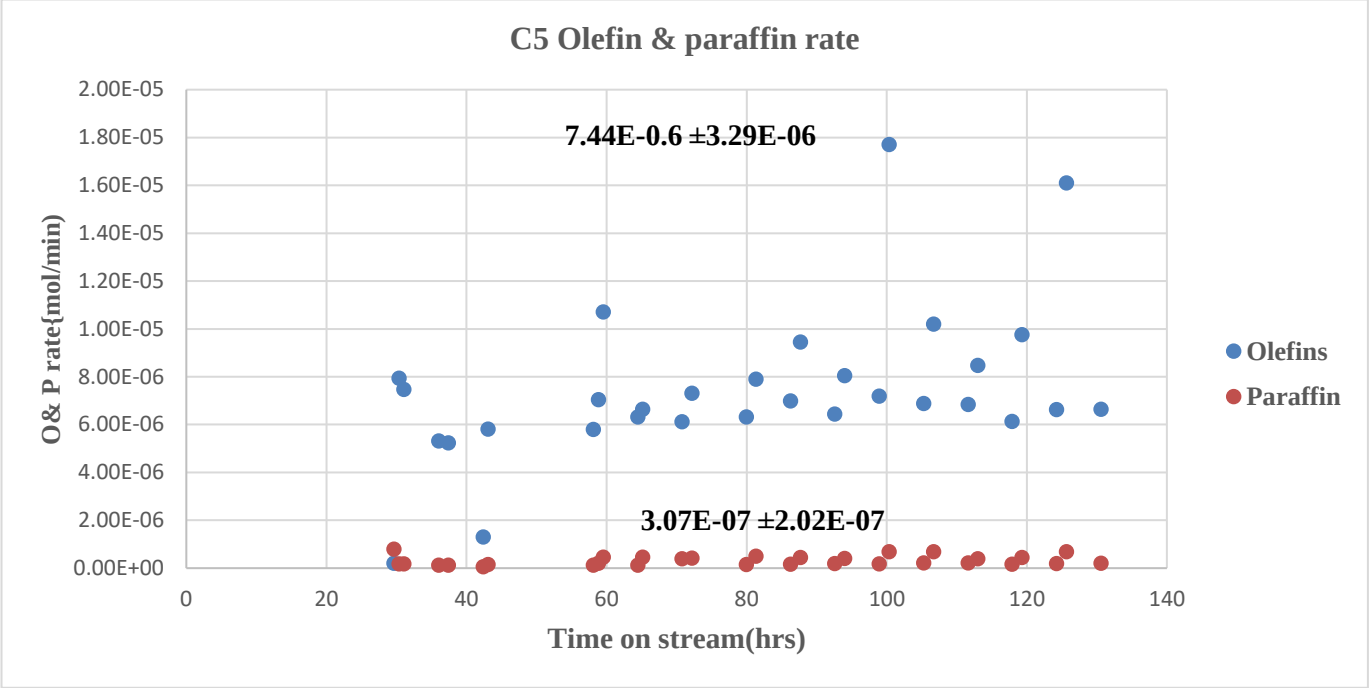

Figure 4.15: C5 Hydrocarbon rate of 10% binder catalyst rate after 131h time on stream. Reaction conditions: 270ºC, 20 bar, Reduction done for 12 hours at 350ºC, GHSV of 3.6 NL/g-cat/h (H_2/CO=2.0)

As expected, Figure 4.15 also follows a similar pattern to the rest of the formation rates of the other hydrocarbons discussed earlier. The average pentane formation rate of 3.07E07 mol/min was much lower than the formation rate of pentene, which was 7.44 E-06 mol/min. The 10B catalyst overall favours the production of olefins over paraffin and is a trend that it is maintained through each class of hydrocarbon covered in this study.

The 10B CAT Olefin to paraffin ratio is displayed in the figure and discussed in this section.

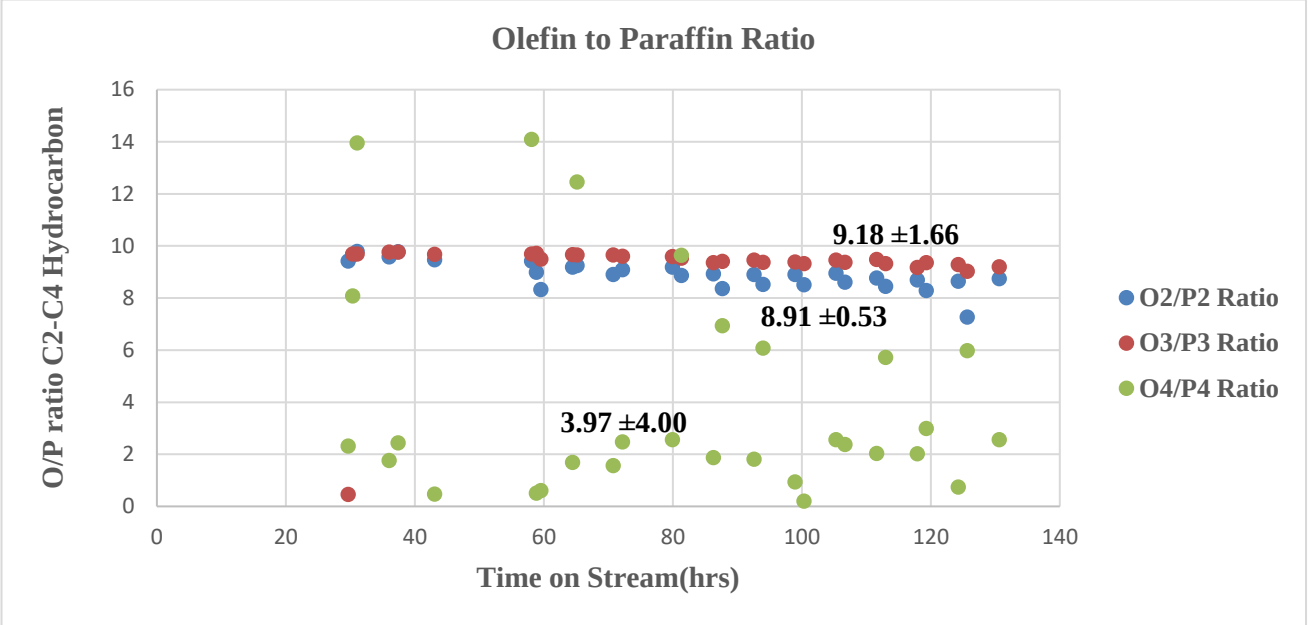

Figure 4. 16: Olefin to Paraffin ratio of 10% binder catalyst after 131h time on stream. Reaction conditions: 270ºC, 20 bar, Reduction done for 12 hours at 350 ºC, GHSV of 3.6 NL/g-cat/h (H_2/CO=2.0)

Figure 4.16 displays the olefin to paraffin ratios of the proposed catalyst. It can be deduced from this Figure that the C2 O/P ratio was close to each other and is substantiated by a small standard deviation of 0.53. The C3 hydrocarbons O/P ratio is also close to each other owing to its standard deviation of 1.66 but not as close as the C2 O/P case. It is noteworthy to cite that the averages of C3 O/P ratio of 9.18 were slightly higher than that of 8.91, but it the C2 hydrocarbon formation rate was the highest as shown in Fig 4.12. The O/P ratio of 3.97 for C4 hydrocarbons was lower than both C2 and C3 and was expected based on the very low formation rates reported in Figure 4.15 in comparison to the C2 and C3 ones.

The Selectivity of 10% binder catalyst towards carbon dioxide, methane, C2-C4 and C5+ are displayed in the figure below and discussed to assess its catalytic performance. These selectivities represent their averages through the 130 hours on stream of proposed catalyst and is depicted in Figure 4.17 below;

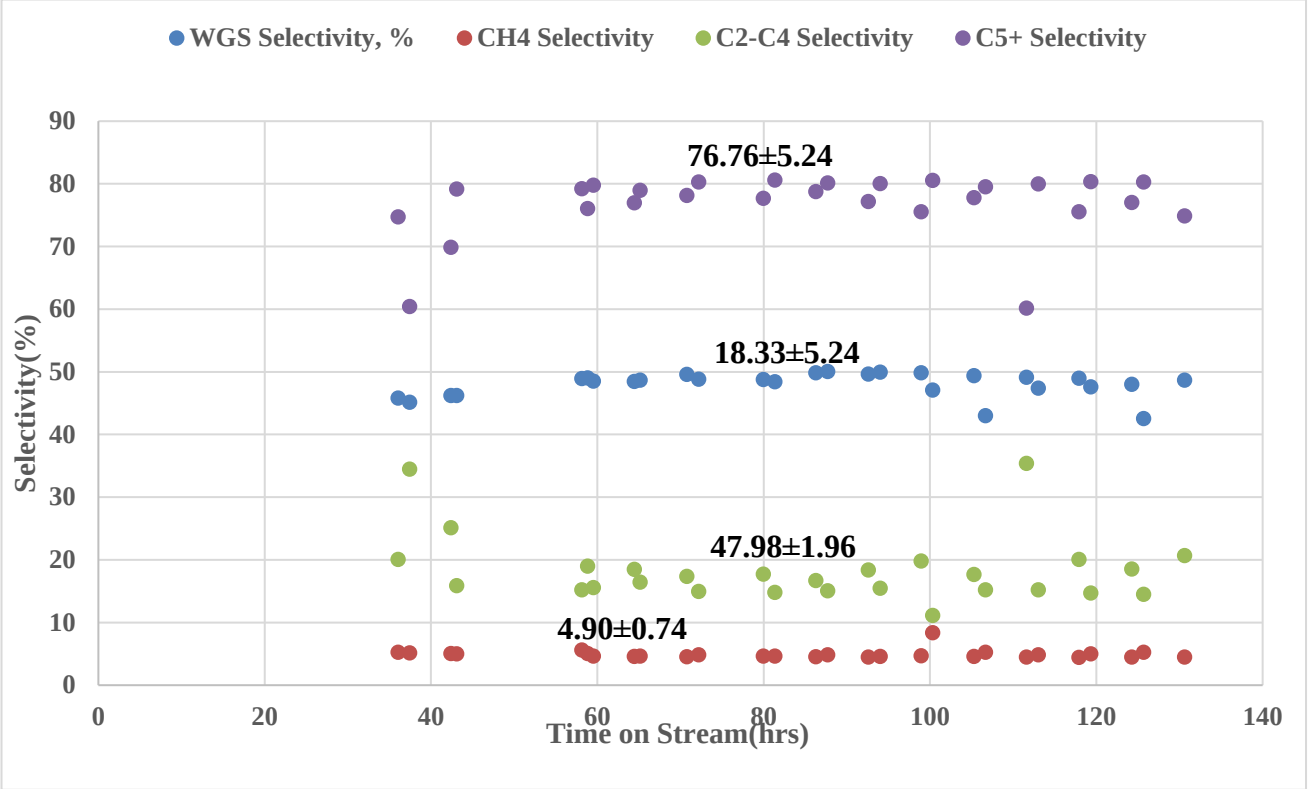

Figure 4.17: Delineates the Carbon dioxide, Methane and C5+ selectivity of 10% binder catalyst after 131h time on stream. Reaction conditions: 270ºC, 20 bar, Reduction done for 12 hours at 350ºC, GHSV of 3.6 NL/g-cat/h (H_2/CO=2.0)

The 10B CAT showed a mean Water-gas shift (CO_2) of 47.98% throughout the time on stream and was likened to other iron ore Fischer Tropsch studies reported in the literature. A better comparison is displayed in table 4.11 by considering the selectivity of other catalyst systems in literature specifically at time streams of 66-114 hrs. The C2-C4 selectivity of the modified iron ore studied in this work was reported to be 18.33%. The CH_4 and C5+ selectivity of this catalyst systems was reported to be 4.90 and 77.7% respectively; also deemed to be within the acceptable range based on other findings in the literature.

Table 4.11 summarizes the catalytic performance of the 10CAT, which was found to be most suitable for FT based on the mechanical evaluation of the shaped catalyst findings reported earlier (statistical analysis). The tabulated results represent the catalytic performance of other promoted iron ore studies reported in the literature coupled with conventional precipitated iron catalysts between 66-114 hours on stream. These findings were used to gauge the catalytic performance of the present's study iron ore shaped catalyst and validate its application in pilot-scale fixed FT operations

Table 4. 11: The FT catalysts performance and reaction conditions summary of 10B catalyst versus other iron- based catalyst reported in the literature between 66-114 hours TOS

Catalysts	Reaction conditions				Conversion	Selectivity (%)				Class
	Temp (ºC)	GHSV (NL/g-cat.h)	Pres (bar)	H_2/CO	CO (mol%)	CO_2	CH_4	C2-C4	C_{5+}(%))	
10BCAT	270	3.6	20	2.0	72.1	48.6	5.00	17.4	83.2	Present work
IO-CAT	275	2.8	15	1.0	75.4	42.6	9.05	20.0	71	Literature [3]
PFe-CAT	275	2.8	15	1.0	85.0	44.2	9.25	22.9	68	Literature [3]
PFe-CAT1	270	2.8	13	0.7	78.7	47.5	36.0	-	64	Literature [3]
PFe-CAT 2	270	2.0	13	0.7	74.7	47.7	5.8	21.7	72	Literature [3]

IO-CAT denotes promoted ore prepared by slurry phase impregnation with no binder and PFe denotes conventional low temperature Fischer Tropsch catalysts prepared by precipitation.

The current proposed iron ore catalyst had a lower selectivity towards undesirable methane which was found to be 5.00 % which is very similar to the 5.8% of a conventional precipitated iron catalyst that operated at analogous process conditions (Table 4.11) reported in the literature [3]. Moreover, low methane selectivity favoured the total selectivity towards C_{5+} hydrocarbons and was evident in this study, 10% Binder catalyst (present study) recorded a high of 83.2% in comparison to the iron ore catalyst [IO-CAT] which was reported to 71% [3] between 66-114 hours. The same work reported their conventional iron-based catalyst to have a C_{5+} hydrocarbons selectivity of 68% [3] which lower than the one that the present study catalyst yielded. The C_{5+} hydrocarbon selectivity of 83.2% is consistent with the ones reported by Sandeep et al,.2017 who also used bentonite as a binder for shaping an iron-based catalyst into spherical pellets with similar binder ratios [4]. Their C_{5+} hydrocarbon selectivity was in the range of 80-85% after 70 hours and which suggest that bentonite(binder) has a positive effect on the C_{5+} hydrocarbon selectivity of iron-based FT catalysts. The C2-C4 selectivity of the proposed catalyst was very similar to other iron ore and precipitated iron catalyst as showed in the Table 4.11.

The present study reported an average of 17.4% selectivity towards C2-C4 hydrocarbons between 66-114 hours on stream as shown above.

Conversely, the high selectivity towards CO_2 is normally associated with a high water- gas shift reaction which characteristic to iron-based catalysts in general and this study was not an exception. The current pelletized promoted iron ore catalysts exhibited a CO_2 selectivity within the range of 42-48% which agreed with other iron-based LT-FTS catalyst reported in the literature [3, 4]; recording of CO_2 selectivity of 48.6%.

REFERENCES

1. Huve, J (2017). Highly selective, active and stable Fischer-Tropsch catalyst using entrapped ironnanoparticles in silicalite-1. Catalysis. Université de Lyon; English. <NNT : 2017LYSE1042>.<tel-01721319>
2. Hensen E. J. M., Wang P, Xu W. (2016). Research trends in Fischer-Tropsch catalysis for coal to liquids technology. Frontiers of Engineering management, 3(4), 321-330. DOI: 10.15302/J-FEM-2016051
3. Bae, J.-S., Hong, S. Y., Chan Park, J., Bae Rhim, G., Youn, M. H., Jeong, H., … Chun, D. H. (2018). Eco-friendly prepared iron-ore-based catalysts for Fischer-Tropsch synthesis. Applied Catalysis B: Environmental. doi:10.1016/j.apcatb.2018.11.082

4. Badgoga S, Vosough V, Dalai A.K(2018). Performance of promoted Iron/CNT for catalyst for Fischer Tropsch Synthesis: Influence of pellet shape and binding loading; *Energy Fuels 31*, 11, p 12633-12644[Online] DOI: 10.1021/acs.energyfuels.7b01318.

5. Seo, J.H., Chae, H.J., Tae, W.K., Kwang-Eun, J., Chul-Ung, K., Sang-Bong, L., Soon-Yong, J., (2011). Influence of Binder on Fe-based Extrudate as Fischer-Tropsch Catalysts. *Korean Chem. Eng. Res.*, Vol. 49, No. 6, December, 2011, pp. 726-731

6. Gorimbo, J., Lu, X., Liu, X., Hildebrandt, D., Glasser, D. (2017). A long-term study of the gas phase of low pressure Fischer-Tropsch products when reducing an iron catalyst with three different reducing gases. *Applied Catalysis A: General*, 534, 1–11. doi:10.1016/j.apcata.2017.01.013

7. Abernethy, R. B (2006).The New Weibull Handbook- Reliability and Statistical Analysis for Predicting Life, Safety, Supportability, Risk, Cost and Warranty Claims. 5 th ed. Abernethy, R. B .North Palm Beach, Florida , pp 1.1-4.25.

8. Weaver, K.F; Morales, V.C; Dunn. S.L; Godde, K; Weaker, P.F(2018). An Introduction to Statistical Analysis in Research: With Applications in the Biological and Life Sciences**;** John Wiley & Sons, *First Edition;* NW, USA; pg 353-392. DOI:10.1002/9781119454205

9. E.David (2015).Mechanical strength and reliability of the porous materials used as adsorbents/ catalysts and the new development trends', *Archives of Materials Science and Engineering*, 73(1), pp. 5–17.

10. Zakeri, M., Samimi, A., Afarani, M. S., & Salehirad, A. (2017). Interaction between Weibull parameters and mechanical strength reliability of industrial-scale water gas shift catalysts. *Particuology*, 32, 160–166.doi:10.1016/j.partic.2016.08.006

11. Gorimbo J, Muleja A.A, Liu X, Hildebrandt D (2018). Fischer-Tropsch: product distribution, operating conditions, iron catalyst deactivation and catalyst speciation. *International Journal of Industrial Chemistry*. https://doi.org/10.1007/s40090-018-0161-4

12. Nilsson, A (2016). Wet Granulation of carbonized bio-ash, Master's thesis. Department of Civil, Environmental and Natura l Resources Engineering, Lulea University of Technology. Available on: https://www.semanticscholar.org/paper/MASTER'S-THESIS-Wet-Granulation-of-Carbonised-Nilsson/262beb2bc0b0b6d784cef844f118cd97691d9a41

5. CONCLUSIONS

The present study proposes a facile and cost effect FT catalyst development method, which is scalable and suited for fixed-bed operations. Moreover, this investigation exhibits a more comprehensive mechanical evaluation of the pellets using Weibull statistics, which is more convenient to pre-emp the mechanical performance of a solid catalyst for laboratory and pilot-scale scenarios. This approach to Fischer Tropsch catalysts development is a promising alternative to conventional precipitation Fischer Tropsch catalyst preparation. The main results of this work can be summarized in the following ways;

- The mechanical evaluation using single pellet crushing strength data with varying binder loading produced values of1833kPa, 1069 kPa and 1213 kPa that were by far more than the recommended alumina spherical pellets and a good indication that the proposed catalysts were suitable for upscale fixed bed operations.
- Weibull statistics gave a better insight into the interpretation of the single scattered pellet crushing strength data for each binder loading and introduced the element of mechanical reliability, which is crucial for pilot and industrial fixed-bed operations. Additionally, Kruskal Wallis and Post hoc Dunn tests can help bolster the selection of an appropriate catalyst system during the catalyst design and development phase, as shown in this investigation. The Weibull distribution, Kruskal Wallis and Post hoc Dunn tests found that 10% binder iron ore catalyst was the best for micro-scale fixed operation while the Weibull plots which calculate the mechanical reliability of solid catalysts found that the 20 % binder iron ore was a better choice for upscaled fixed operations. These parameters are useful for FT Practitioners scaling up existing laboratory catalyst formulations. This approach could help alleviate some of the operational problems such as plant shutdowns which cost FT practitioners a lot of money and start to compete with conventional petrochemical plants.
- An inexpensive iron ore FTS catalyst was successfully formulated and despite having inferior physio-chemical qualities than other promoted ore and conventional precipitated iron-based FT catalyst still had comparable FT catalytic performance. The proposed iron ore catalyst yielded CO conversion 72 mol% with an FT and CO rate of 2.75 E-04 mol/g-cat.min and 5.68E-04 mol/g-cat.min. The same catalyst recorded CO_2, CH_4 and C_{5+} hydrocarbon selectivity of 48.6%, 5.00% and 83.2% respectively between 66-114 time on stream. Since these findings were comparable to the catalytic performance of other iron catalysts reported in the literature, the developed iron ore catalyst was deemed as a viable catalyst option for pilot-scale fixed bed operations.

6. RECOMMENDATIONS

Based on the promising laboratory results of mechanical and catalytic performance of the proposed catalyst, we suggest that future works investigate the following;

- Conducting reaction studies of all the pelletized catalysts on a pilot-scale fixed bed reactor and visibly observe if their mechanical strength is maintained throughout the reaction studies and link it to the calculated mechanical reliability of the solid catalysts. This will be a significant step towards commercialization of this work;
- Utilizing a wide range of binder additions to the iron ore catalyst to get more insight into how the binder affects the mechanical strength of this catalyst. These findings will, in turn, facilitate the study of parameters such as moisture, size of particle size. These findings could help ascertain the initial moisture content and particle size that would yield the strongest pellets during pelletization for this catalyst system. Moreover, also optimizing the pelletization process could be useful and can be achieved by pelletizing on a smaller rotating drum before going to the pilot scale and optimizing process variables such as rotating speed of the drum and angle of inclination as oppose to keeping constant as was done for this work would offer interesting insights to the study ;
- Investigating the effect of varying copper and potassium as dopants for iron ore catalysts and linking to its catalytic activity and selectivity. This result will pave the way for an optimized promoter combination that yields the best catalytic performance of the proposed catalyst and improve the overall economics of the study;
- Evaluating the FT catalytic performance of all the developed catalysts (10B, 15B & 20B) and study how the binder variations influence its activity and selectivity. Also running the FT experiments for longer times on streams would be attractive in evaluating the catalyst stability of these pelletized catalysts, which is crucial during upscaling laboratory catalyst formulations. These results would facilitate the study of internal mass transfer limitations during the FT reaction and elucidate the initial and steady-state kinetics of pelletized catalysts. Furthermore, conducting a more detailed characterization of the developed catalysts by using techniques such Steady-state Isotopic transient kinetics analysis (SSITKA) to study kinetics on a molecular level would complement the results obtain from the internal mass transfer limitation and improve kinetic modelling of this catalyst system;

APPENDICES

Pressure Drop Calculations

Pressure drop is a significant factor in reactor design especially for scalable operations and this study considered the Ergun's equation to evaluate the pressure drop for the reactor design of fixed beds. Furthermore, huge pressure drop will instigate mechanical stress on a catalyst system and other operational problems extensively covered in the chapter 2 and was accounted for this work. Pressure drop calculations are shown below for the pilot plant fixed bed reactor at NECSA;

Ergun's Equation

$$\frac{dP}{dz} = -\frac{(1-\varepsilon)}{d\text{p}\, A\, \varepsilon^3}\,\frac{(150(1-\varepsilon)\mu}{d\text{p}} + \frac{1.75\, m)}{A}\,\text{Q} \qquad \textbf{3.6}$$

Where dP is the total pressure drop across the bed (Pa); dz is the height of the bed (m); ε is voidage of the bed (Dimensionless), *d*p is the particle diameter(m); A is the cross-sectional area of the bed (m^2); m is the mass flow rate ($\frac{Kg}{S}$); Q is the volumetric flow rate ($\frac{m^3}{s}$)

Assumptions Made

- Wall effects are small provided the ratio of the diameter of bed to particle diameter is a minimum of 8:1 to 10:1 [33]
- Heat and Mass transfer resistance is negligible [34]
- The packed is isothermal and Ideal gas correlations are valid [33,34,35]
- Mass is conserved; [33,34,35]
- Pressure Calculation is done before the Fischer Tropsch Reaction; thus, Mass and energy balance expressions are not considered. [33]

Packed Bed Information and Operating Conditions

Diameter of the bed, D =0.025m
ε=0.6
Height of Bed, z =3m
Height of catalyst Bed= 2.5 m
In let Temperature, T_1 =270°C
Inlet Pressure, P_1=20 bar
Syngas Velocity (v) = 0.250 m/s
Syngas Density, ρ=13.2 $\frac{Kg}{m^3}$
Particle Density; *d*p= 2mm
Syngas Viscosity, μ = $1.8x10^{-5}$Pa.s
Iron ore particle Density=2100$\frac{Kg}{m^3}$

$Q = vA$ (2) $A = \frac{\pi D^2}{4}$ (3) $m = \rho Q$ (4) F=$\frac{PQ}{RT}$ (5) F is the molar flow rate ($\frac{mol}{s}$)

$A_{bed} = \frac{\pi(0.025)^2}{4}$ = 4.908 $x10^{-4}m^2$

Q = (0.250 m/s) (4.908 $x10^{-4}m^2$) = 1.227 $x10^{-4}\frac{m^3}{s}$

m= (13.2 Kg/m^3) = 1.6196 $x10^{-3}\frac{kg}{s}$

F=$\frac{(20x10^5 Pa)(1.227\ x10^{-4}\frac{m^3}{s})}{(8.314\ Pa\ m^3 mol^{-1}K^{-1})543K}$

= 0.54 mol/s

According to the ideal Gas, Q can be expressed in terms of Pressure as;

Q=$\frac{FRT}{P}$ (6) ; substituting eq6 into equation gives the expression below:

$\int P\frac{dP}{dz} = -\frac{(1-\varepsilon)}{dp\ A\ \varepsilon^3}\frac{(150(1-\varepsilon)\mu}{dp} + \frac{1.75\ m)}{A}\ (FRT\ )$

$\int P\frac{dP}{dz} = -\frac{(1-0.6)}{2x10^{-3}\ x\ 4.908\ x10^{-4}\ x\ 0.6^3}\frac{(150(1-0.6)1.8X10^{-5}}{2x10^{-3}} + \frac{1.75x\ 1.6196\ x10^{-3}\ )}{4.908\ x10^{-4}}$ (0.54 x 8.314 x 543)

$\int_{20bar}^{P} P\ dp$ =-(4.598 $x10^9$) $\int_0^{2.5} dz$

Right-hand side of EQ Units is Pa^2 Must be consistent with Left-hand side .

For Homogeneity on both sides this relation is used bar = $10^5\ Pa$;So $1bar^2 = 10^{10}Pa^2$

$\frac{P^2}{2} - \frac{20^2}{2}$ =-40598 $x10^9$)(2.5)

$\frac{P^2}{2} - \frac{20^2}{2}$ =-(1.1495 $x10^{11}$ solving for P Substituting boundaries, we can rewrite the term

$1.1495\ x10^{11}\ in\ bar$

$P^2 - 400$ =-11.495

$P^2 = 385.48$; P= 19.71 bar

Pressure Drop = 20-19.71

= 0.29 bar

MECHANICAL TESTING RESULTS

Table 7. 1: Single pellet crushing strengths (SPCS) Results

SAMPLE NO.	DRY STRENGTH (N/PELLET)		
	10% Binder Addition	15% Binder Addition	20%Binder Addition
1	25.7	22.35	22.40
2	30.95	15.80	31.20
3	47.95	17.25	18.05
4	47.95	19.00	16.60
5	17.10	23.35	18.95
6	15.30	12.65	32.30
7	21.75	18.40	21.30
8	31.00	21.20	20.70
9	23.20	26.15	22.00
10	30.65	15.80	22.95
11	45.05	13.40	15.95
12	36.05	7.10	18.65
13	53.35	20.30	19.00
14	39.40	29.95	22.75
15	33.50	22.65	21.35
16	29.25	24.05	27.45
17	42.00	17.35	19.65
18	32.60	19.05	23.65
19	27.15	19.20	21.35
20	28.10	18.30	19.25
Standard Deviation, σ	**10.43**	**5.01**	**4.30**
Variance, σ^2	**108.75**	**25.60**	**18.46**
Mean, X	**32.90**	**19.17**	**21.78**

Average Single Pellet Crushing test conversion into Kilopascals (Kpa)

10% Binder loading Single pellet crushing strength

$$\tau_s = \frac{2.8 \times 32.9}{(\pi)\ 0.004^2} = 1832.67 \text{ kPa}$$

15% Binder loading Single pellet crushing strength

$$\tau_s = \frac{2.8 \times 19.19}{(\pi)\ 0.004^2} = 1068.96 \text{ kPa}$$

20% Binder loading Single pellet crushing strength

$$\tau_s = \frac{2.8 \times 21.78}{(\pi)\ 0.004^2} = 1213.24 \text{ kPa}$$

Porosity Calculations

Porosity (%) $= (Density\ X\ single\ pore\ volume)\ x\ 100$

10% Binder loading porosity

$$\text{Porosity}(\Phi) = \frac{0.0033 \times 4329}{1000} \text{ X } 100$$

$= 1.43\%$

15% Binder loading porosity

$$\text{Porosity}(\Phi) = \frac{0.044 \times 4210}{1000} \text{ X } 100$$

$= 1.85\%$

20% Binder loading porosity

$$\text{Porosity}(\Phi) = \frac{0.045 \times 4133}{1000} \text{ X } 100$$

$= 1.86\ \%$

Table 7. 2: Weibull Distribution parameters calculated using estimators

Failure probability (P) =(i-0.5)/n	Single Pellet crushing strengths for 10B(N/Pellet)	Single Pellet crushing strengths for 15B (N/Pellet)	Single Pellet crushing strengths for 20B (N/Pellet)
0.025	15.3	7.1	15.95
0.075	17.1	12.65	16.6
0.125	21.75	13.4	18.05
0.175	23.2	15.8	18.65
0.225	25.7	15.8	18.95
0.275	27.15	17.25	19
0.325	28.1	17.35	19.25
0.375	29.25	18.3	19.65
0.425	30.65	18.4	20.7
0.475	30.95	19	21.3
0.525	31	19.05	21.35
0.575	32.6	19.2	21.35
0.625	33.5	20.3	22
0.675	36.05	21.2	22.4
0.725	39.4	22.35	22.75
0.775	42	22.65	22.95
0.825	45.05	23.35	23.65
0.875	47.95	24.05	27.45
0.925	47.95	26.15	31.2
0.975	53.35	29.95	32.3